

Copyright © 2001, by the author(s).
All rights reserved.

Permission to make digital or hard copies of all or part of this work for personal or classroom use is granted without fee provided that copies are not made or distributed for profit or commercial advantage and that copies bear this notice and the full citation on the first page. To copy otherwise, to republish, to post on servers or to redistribute to lists, requires prior specific permission.

**CHARACTERIZING THE SENSITIVITY
OF SCATTEROMETRY**

by

Weng Loong Foong

Memorandum No. UCB/ERL M01/14

21 February 2001

**CHARACTERIZING THE SENSITIVITY
OF SCATTEROMETRY**

by

Weng Loong Foong

Memorandum No. UCB/ERL M01/14

21 February 2001

ELECTRONICS RESEARCH LABORATORY

College of Engineering
University of California, Berkeley
94720

Characterizing the Sensitivity of Scatterometry

by

Weng Loong Foong

Research Project

Submitted to the Department of Electrical Engineering and Computer Sciences,
University of California at Berkeley, in partial satisfaction of the requirements for the
degree of **Master of Science, Plan II.**

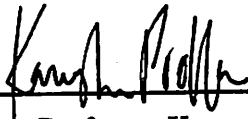
Approval for the Report and Comprehensive Examination:

Committee:



Professor Costas J. Spanos
Research Advisor

2/21/01



Professor Kameshwar Poolla
Second Reader

2/21/00

Abstract

Characterizing the Sensitivity of Scatterometry for Sub-100nm Technologies

by

Weng Loong Foong

Master of Science in Electrical Engineering

University of California, Berkeley

Professor Costas J. Spanos, Chair

The shrinking of device sizes has resulted in a tremendous increase in the number of transistors being patterned per unit area on a wafer. The complexity of process steps employed in manufacturing wafers today has resulted in finished wafers that are very expensive. As such, there is increasing focus and concern on the yield achievable through these manufacturing processes.

Smaller device sizes have also meant smaller device tolerances. This has put a premium on the precision of the metrology technique being employed. In order to increase yield, one must perform more measurements per wafer, which highlights the necessity of throughput. There is therefore a strong need for accurate, high-throughput in-line metrology solutions.

Scatterometry appears to be a suitable candidate. It uses broadband light for internal profiling of semiconductor device structures. Its non-destructive nature and high-throughput appear to be well-suited for integrated metrology.

This report introduces a rigorous method of characterizing the sensitivity of scatterometry for sub-100nm technology generations. Developed using a Sopra GESP5 DUV ellipsometer and based on Jones' vectors, this method can also be used to characterize the noise functions and hence the sensitivity of other ellipsometers to be used for scatterometry.

Table of Contents

Chapter 1.....	1
Introduction.....	1
1.1 <i>Motivation.....</i>	<i>1</i>
1.2 <i>Report Organization.....</i>	<i>2</i>
<i>References for Chapter 1.....</i>	<i>4</i>
Chapter 2.....	5
Background.....	5
2.1 <i>Thin Film Ellipsometry.....</i>	<i>5</i>
2.2 <i>Profilometry.....</i>	<i>7</i>
2.2.1 SEM.....	7
2.2.2 CD-AFM.....	8
2.2.3 Scatterometry.....	8
<i>References for Chapter 2.....</i>	<i>10</i>
Chapter 3.....	11
Sensitivity Analysis.....	11
3.1 <i>Methodology.....</i>	<i>11</i>
3.2 <i>Sensitivity Analysis.....</i>	<i>11</i>
3.3 <i>Conclusion.....</i>	<i>55</i>
<i>References for Chapter 3.....</i>	<i>56</i>
Chapter 4.....	57
Ellipsometric Detection Limits.....	57
4.1 <i>Jones vectors.....</i>	<i>58</i>
4.1.1 Nulling ellipsometer.....	58
4.1.2 Modulation by Rotating Element.....	60
4.2 <i>Signal-to-Noise Ratio for Sopra Ellipsometer.....</i>	<i>61</i>
4.2.1 Sopra Ellipsometer Measurement Technique.....	62
4.2.2 Noise function.....	64
4.3 <i>Sensitivity Analysis for 100nm Technology Node.....</i>	<i>70</i>
4.4 <i>Conclusion.....</i>	<i>82</i>
<i>References for Chapter 4.....</i>	<i>83</i>

Chapter 5.....	84
Sub-100nm Scatterometry	84
5.1 <i>Sub-100nm Technology Node.....</i>	<i>84</i>
5.2 <i>Sub-240nm Wavelength Analysis</i>	<i>89</i>
5.3 <i>Conclusion.....</i>	<i>91</i>
Chapter 6.....	93
Conclusion.....	93
6.1 <i>Report Summary.....</i>	<i>93</i>

List of Figures

Figure 2.1 Spectroscopic Ellipsometry Measurements	6
Table 3.1 Feature CDs Projected by ITRS Roadmap.....	12
Figure 3.2 Illustration of profile parameters used for sensitivity analysis	14
Figure 3.3 (a)-(j) Scatterometric Response for 100nm Line / 230nm Pitch.....	15
Figure 3.4 (a)-(j) Scatterometric Response for 65nm Line / 230nm Pitch.....	20
Figure 3.5 (a)-(j) Scatterometric Response for 70nm Line / 160nm Pitch.....	25
Figure 3.6 (a)-(j) Scatterometric Response for 45nm Line / 160nm Pitch.....	30
Figure 3.7 (a)-(j) Scatterometric Response for 50nm Line / 110nm Pitch.....	35
Figure 3.8 (a)-(j) Scatterometric Response for 30nm Line / 110nm Pitch.....	40
Figure 3.9 (a)-(j) Scatterometric Response for 35nm Line / 80nm Pitch.....	45
Figure 3.10 (a)-(j) Scatterometric Response for 20nm Line / 80nm Pitch.....	50
Figure 4.1 Sopra GESP5 Signal-to-Noise Ratio	62
Figure 4.2 (a)-(d) Theoretical and measured scatterometry noise for integration times of 1 second and 10 seconds	68
Figure 4.3 (a)-(j) 100nm Linewidth / 230nm Pitch.....	71
Figure 4.4 (a)-(j) 65nm Linewidth / 230nm Pitch.....	76
Table 4.1 Matrix for test of interaction effects of profile variations.....	81
Figure 5.1 70nm Dense Lines	85
Figure 5.2 50nm Dense Lines	86
Figure 5.3 45nm Isolated Lines.....	87
Figure 5.4 30nm Isolated Lines.....	88
Figure 5.5 35nm Dense Lines	89
Figure 5.6 20nm Isolated Lines.....	90

List of Tables

Table 3.1 Feature CDs Projected by ITRS Roadmap.....	12
Table 4.1 Matrix for test of interaction effects of profile variations.....	81

Acknowledgements

This research was conducted with the help of many different people. First of all, I would like to thank my advisor, Professor Costas Spanos, for his guidance, insight, constant support, and especially for sharing his knowledge about metrology with me. I would like to thank him and Professor Kameshwar Poola for the time they spent on this thesis.

I would like to acknowledge the support that I received from the University of California, Berkeley Microlab, where I carried out the experiments for this research project.

This research was conducted with the support of Timbre Technologies, Inc., which provided me with the simulation software necessary for this research. I would especially like to thank Xinhui Niu and Nickhil Jakatdar for their support and friendship.

During my time here, I have been very privileged to be associated with the Berkeley Computer-Aided Manufacturing (BCAM) group. I would like to thank the members of BCAM, both past and present: Junwei Bao, Jason Cain, Runzi (Tiger) Chang, Tim Duncan, Scott Eitapence, Mason Freed, Anna Ison, Nickhil Jakatdar, Payman Jula, Michiel Kruger, Jae-Wook Lee, Thanh-Xuan Nguyen, Xinhui Niu, Matt Onsum, Jiangxin Wang, Haolin Zhang and Dongwu Zhao. I will always hold them in the highest regard.

A special note of appreciation goes to Junwei Bao, whose experience and advice were invaluable to me during this time.

I would like to thank my other friends in Berkeley: Martin Chai, Yong Hwee Chua, Victor Liu, Bee Kay Ng, Sue Ting Ong, Yi-Nong Peh, Steven Shih, Chin Peng Soen, Natalie Tay, Jing Li Thoh, Seggy Umboh, Leon Voon, Eric Wang, Benny Wong and

other members of the bay area Singaporean and Malaysian communities for their friendship.

Finally, I would like to express my sincere thanks to my family for their undying love and support. My father, Seng Kee Foong, and my mother, Suat Leng Teoh, have always been there for me in every endeavor. I would also like to thank my brother, Weng Keat Foong, for being a role model to me.

This research has been funded by the UC-SMART program and 16 participating companies: Advanced Energy, Advanced Micro Devices, Applied Materials, ASML, Asyst Technologies, Inc., Atmel Corporation, Cymer, Inc., Etec Systems, Inc., Intel Corporation, KLA-Tencor, Lam Research, Nikon Research Corporation of America, Novellus Systems, Inc., Schlumberger, ATE and Silicon Valley Group.

Chapter 1

Introduction

1.1 Motivation

Rapid device scaling has been the factor governing the growth of the semiconductor industry, which has produced devices with ever-better performance characteristics in terms of high speed and low power. The semiconductor industry has been experiencing an average growth rate of 15% annually over the past three and a half decades [1.1]. With this explosive growth has come a reduction in average cycle time between introductions of new technologies from the traditional 3-year cycle towards an approximate 2-year cycle. Current production (2001) is being done employing 0.15 μm technology, with 0.13 μm technology expected to be introduced in the year 2002.

With this constant push to reduce minimum feature size, the most serious challenge posed is that of achieving acceptable yield and throughput. In recent technology generations, optical steppers have often been operated at or near their resolution limit. As such, achieving high yield becomes increasingly difficult as we reduce feature size. As new technologies are employed, product failures become increasingly costly due to the increasing number of steps that a wafer has to go through in the manufacturing process. A 1nm CD variation is estimated to be equivalent to a 1MHz variation in chip-speed, which in today's terms is worth about \$3.60 in the selling price of each chip [1.2] [1.3].

In order to minimize the potential of product failures after undergoing the complete manufacturing process, there is an increasing need for more complete testing for wafers

rather than just having wafer-to-wafer inspection. However, increased testing comes at a cost of a reduction in throughput. In order to maintain throughput and minimize inspection costs, the inspection technique would have to be non-destructive, non-intrusive, as well as in-line or better yet, in-situ.

In addition, the time savings associated with in-line placement of metrology solutions, there is also the added benefit of being able to employ feedback loops that will enable closed-loop process monitoring and process control, which is becoming increasingly important in optimizing process recipes.

The technique of scatterometry appears to be a suitable candidate. With scatterometry still being a considered a “novel” technique, its full potential remains unknown. It is necessary to formalize its capabilities for the 100nm technology node as well explore its full potential with respect to the 70nm and 50nm nodes, especially in post-lithography inspection. Commercial ellipsometers have been identified as being capable of performing spectroscopic scatterometry. Hence, the focus of this study is on this type of equipment.

Spectroscopic scatterometry can also be applied to post-CMP inspection, which will be part of a future study.

1.2 Report Organization

The report begins by providing a review of thin film metrology. The concept of ellipsometry will be discussed in the context of determining thin film properties. This will be followed by a description of scatterometry, which can be applied to measure properties of periodic profiles on a wafer.

Chapter 3 introduces the methodology and experiments carried out in preparation of this report. Software simulations were conducted as part of the study of the limits of scatterometry. These are in the form of standard ellipsometric responses, $\tan \Psi$ and $\cos \Delta$, which define a particular thin film or profile.

Chapter 4 will describe the hardware experiments conducted, predominantly with a Sopra GESP5 multiple incident angle, multiple wavelength ellipsometer. A quantitative methodology will be proposed in order to characterize the measurement errors associated with a particular machine. The measurements and results of these experiments will be discussed.

Chapter 5 summarizes the results from experiments as well as offers a methodology of determining required ellipsometer specifications in order for scatterometry to be successfully implemented in future metrology applications.

Finally, a conclusion on the entire project is offered in Chapter 6, which summarizes the capabilities of spectroscopic scatterometry as well as potential improvements that might enhance its capabilities.

References for Chapter 1

- [1.1] "International Technology Roadmap for Semiconductors", 1999 Edition, Semiconductor Industry Association (SIA).

- [1.2] J. Sturtevant et al, "Characterization of CD control for sub-0.18 μ m lithographic patterning", Proceedings of the SPIE - The International Society for Optical Engineering, vol.3679, pt.1-2, (Optical Microlithography XII, Santa Clara, CA, USA, 17-19 March 1999).

- [1.3] www.pricewatch.com

Chapter 2

Background

2.1 Thin Film Ellipsometry

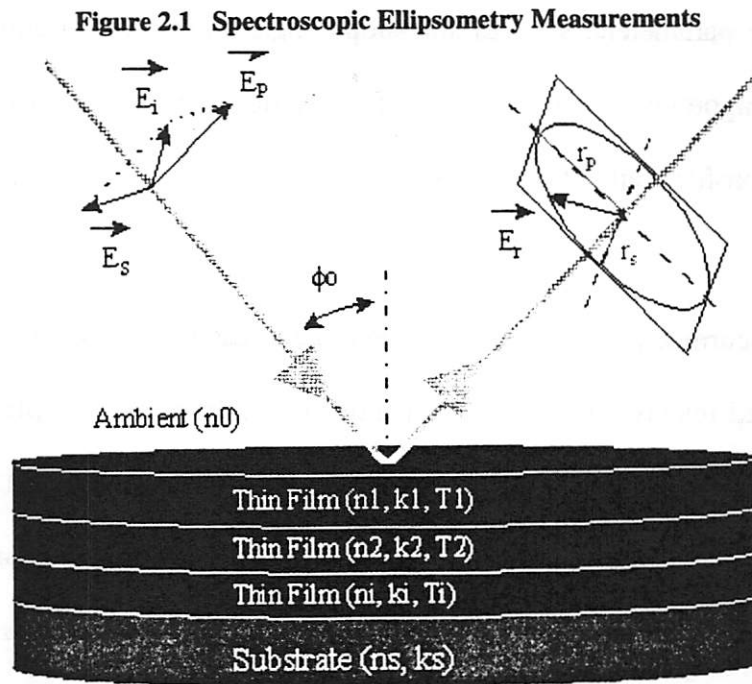
Ellipsometry has become an integral part of the metrology methods employed in the semiconductor industry. This method is based on the characteristics of light upon reflection from a surface. The component waves of light, which are linearly polarized with the electric field vibrating parallel (p or TM) or perpendicular (s or TE) to the plane of incidence, behave differently upon reflection. The component waves experience different amplitude attenuations as well as different absolute phase shifts upon reflection; as such, the overall state of polarization changes. Ellipsometry refers to the measurement of the state of polarization and intensity before and after reflection for the purpose of determining the properties of the reflecting boundary. The measurement is usually expressed in the form

$$\rho = \tan\Psi e^{j\Delta} = \frac{\tilde{R}_p}{\tilde{R}_s}, \quad (2.1)$$

where \tilde{R}_p and \tilde{R}_s are the complex reflection coefficients for TM and TE waves respectively.

Ellipsometry derives its increased sensitivity over non-polarized reflectometry from the fact that the polarization-altering properties of the reflecting boundary are modified significantly even when ultra-thin films are present. Consequently, ellipsometry has

become the *de rigueur* method of characterizing thin films. An illustration of the basics of ellipsometry is presented in Figure 2.1.



Ellipsometry analyzes the polarization-state-in and polarization-state-out of light incident on a thin film. Typically light with wavelength in the visible range is used; however, virtually any polarizable wave can be used to produce an ellipsometric measurement.

The advantage of ellipsometry over reflectometry is its accuracy. Firstly, ellipsometry measures the polarization state of light by looking at the ratio of values rather than the absolute intensity of the reflected light. This property is especially useful in the DUV wavelength range, where very little light is typically available. Second, ellipsometry can gather the phase information in addition to plain magnitude reflectivity information. Phase information provides more sensitivity to thin-film variations.

2.2 Profilometry

With feature sizes being scaled down at a rapid pace, tolerances become smaller and the tight of profile parameters, such as side-slope angle and profile footing, are becoming increasingly important. There is a need for profilometry to fully extract the various parameters of profiles rather than just the CD alone.

2.2.1 SEM

The SEM is currently the workhorse instrument used in production for measuring submicron-sized features because of its nanometer-scale resolution, precision as well as high throughput. The SEM is divided into two types: cross-sectional and top-down.

Cross-sectional SEM can provide profile information for structures on a wafer in the form of a direct image. This image can be used immediately for process characterization. However, obtaining a cross-sectional SEM image requires breaking a wafer and is also time-consuming, and there is the possibility of the presence of systematic profile errors dependent upon the image processing technique being employed.

The top-down SEM, more commonly referred to as the CD-SEM, measures the CD of a profile at a somewhat arbitrary height and does not take into account the slope associated with the profile that results in a constantly changing profile CD. Another problem associated with this method is the build-up of charge in the sample under the electron beam. The CD-SEM, being a surface scanning technique, is also unable to provide information on underlying layers or undercut features. The state-of-the-art KLA-Tencor 8250-R has a resolution in the order of 2nm.

2.2.2 CD-AFM

Atomic force microscopy provides a resolution between 0.1nm and 5nm, depending on the hardness of the material being scanned. For typical semiconductor profiles, this translates into exceptionally high vertical and lateral resolutions, which combine to provide information about a patterned structure's width, sidewall slope and thickness. However, the AFM has difficulty tracking undercut features. Also, current AFM scan rates are very slow, and measurement accuracy and precision are highly dependent upon the tip shape and stability. At present, the AFM is too slow to be used for real-time imaging as well as CD measurements.

2.2.3 Scatterometry

Scatterometry is the metrology that relates the geometry of a sample to its light scattering effects. In the same way that ellipsometry analyzes polarization-state-in and polarization-state-out of light incident on thin film, scatterometry adopts the same theory and measures the polarization-state-in and polarization-state-out of light, incident not on a thin film, but rather on periodic surface structures. The $\tan \Psi$ and $\cos \Delta$ values are measured after reflection and matched to the responses of known profiles.

Much work has previously been done which has led to the advancement of scatterometry. Moharam and Gaylord developed the Rigorous Coupled-Wave Analysis [2.1], which uses Maxwell's equations and boundary conditions to solve for the electric fields in the various regions of a sample. They subsequently used it to explore the diffraction characteristics of photoresist surface-relief gratings [2.2].

McNeil et al have explored the idea of variable-angle scatterometry, which uses angle-resolved diffracted light analysis to measure etched samples with linewidth dimensions as small as 150nm, and poly-Si thicknesses on the order of 250nm [2.3].

Niu et al have explored the idea of spectroscopic scatterometry, in which the responses for multiple wavelengths are taken into account [2.4]. This method consists of measurements taken at a fixed incident angle as opposed to variable-angle scatterometry, and requires a less-complicated mechanism. The lack of external moving parts, and hence simpler implementation, gives spectroscopic scatterometry the potential of being employed in in-line or in-situ process control loops.

Niu et al also developed an efficient simulation engine, known as the *gtk* (Grating Tool Kit) based on the Rigorous Couple-Wave Analysis [2.5]. It was demonstrated that the simulated and measured diffracted light responses based on this technique correspond with profiles that closely match those obtained through the AFM.

Spectroscopic scatterometry, when implemented with a library of generated profiles, is about a factor of 100 faster than the CDSEM and the speed advantage is even more significant when compared with the AFM. Another advantage of scatterometry is the ability to determine the properties of underlying layers depending on the libraries generated, which would not be possible with the CDSEM or AFM.

References for Chapter 2

- [2.1] M. G. Moharam, T. K. Gaylord, "Rigorous coupled-wave analysis of planar-grating diffraction," *J. Opt. Soc. Am.*, vol. 71, 811-818, 1981.
- [2.2] M. G. Moharam, T. K. Gaylord, G. T. Sincerbox, H. Werlich, B. Yung, "Diffraction characteristics of photoresist surface-relief gratings," *Applied Optics*, vol. 23, no. 18, 3214-3220, 15 Sept 1984.
- [2.3] C. J. Raymond, S. S. H. Naqvi, J. R. McNeil, "Scatterometry for CD measurements of etched structures," *Proceedings of SPIE*, vol. 2725, 720-728, March 1996.
- [2.4] X. Niu, N. Jakatdar, J. Bao, C. Spanos, S. Yedur, "Specular spectroscopic scatterometry in DUV lithography," *Proceedings of the SPIE - The International Society for Optical Engineering*, vol.3677, pt.1-2, (Metrology, Inspection, and Process Control for Microlithography XIII, Santa Clara, CA, USA, 15-18 March 1999.
- [2.5] X. Niu, "An integrated system of optical metrology for deep sub-micron lithography," Ph.D Dissertation, U.C. Berkeley, 1999.

Chapter 3

Sensitivity Analysis

3.1 Methodology

The semiconductor industry is expected to be operating at the 100nm technology node in the very near future, and at the 50nm technology node by 2011 [3.1]. In this research project, the focus is to determine the sensitivity and effectiveness of spectroscopic scatterometry in sub-100nm technology. To this effect, electromagnetic simulations as well as noise analysis associated with commercial ellipsometers were carried out. This approach is depicted in Figure 3.1.

3.2 Sensitivity Analysis

Sensitivity analysis was carried out using Timbre Technology's *gtk* simulation engine. This simulation engine uses the Rigorous Coupled-Wave Analysis [3.2] theory to solve for the reflected TE and TM wave responses over multiple layers. These responses are then used to obtain the $\tan \Psi$ and $\cos \Delta$ spectrum.

Under the guidelines of the technology roadmap for the 100nm technology node, microprocessors will have features of 65nm gate length and 115nm half-pitch. For ASICs, gate length would be approximately 100nm, with a half-pitch of 115nm. The relevant feature sizes for the various technology nodes are summarized in Table 3.1 below.

Figure 3.1 Sensitivity Analysis Framework

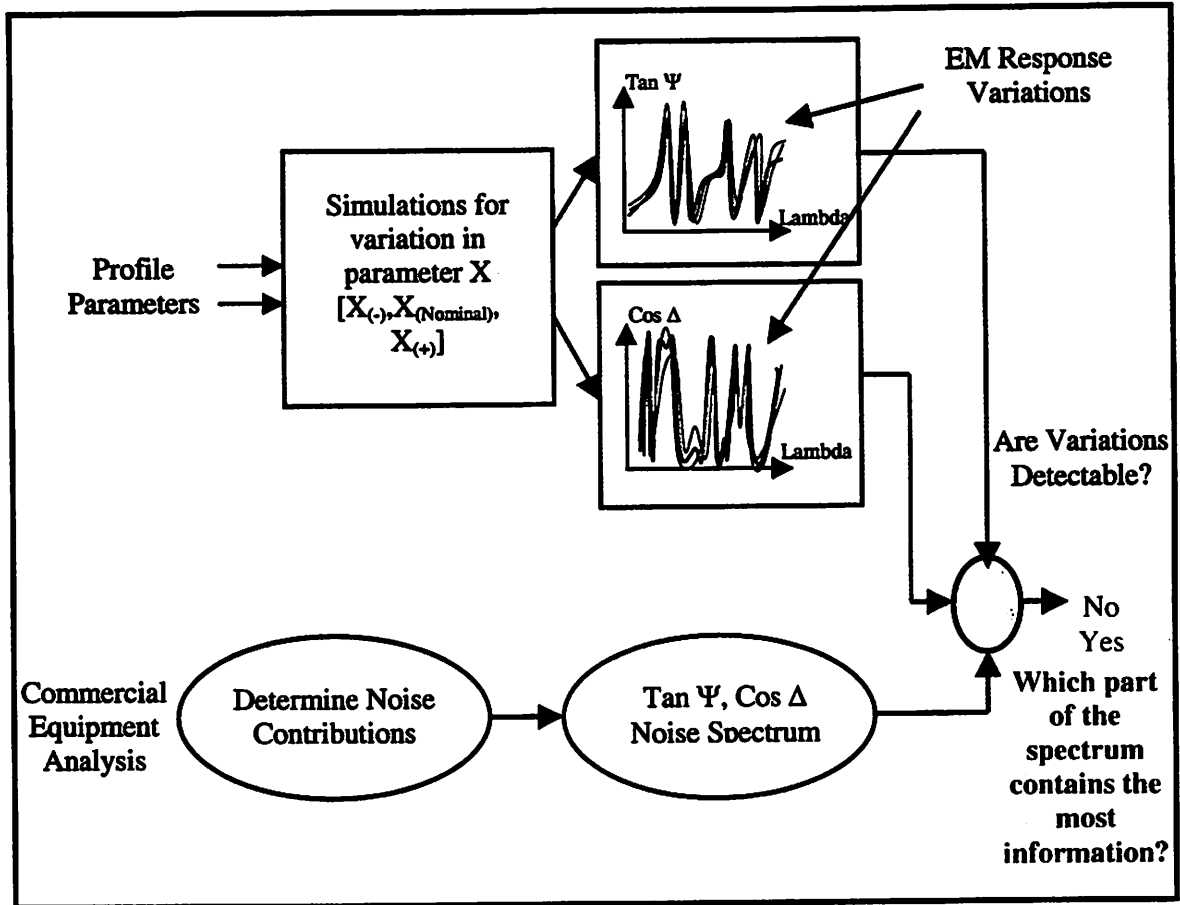


Table 3.1 Feature CDs Projected by ITRS Roadmap

Technology Node	Feature Sizes	
	MPU (Gate Length / Half Pitch)	ASIC (Gate Length/Half Pitch)
100nm	65nm / 115nm	100nm / 115nm
70nm	45nm / 80nm	70nm / 80nm
50nm	30nm / 55nm	50nm / 55nm
35nm	20nm / 40nm	35nm / 40nm

Due to various lithography process variations such as beam intensity, exposure time, development time, bake temperature, bake time, development time as well as developer properties, various profile variations are produced as a result.

These profile variation parameters are the critical dimension of the gate (CD), the stack height, the sidewall angle of the profile, the rounding curvature of the top edges, as well as the footing curvature at the bottom of the profile.

For the simulations, the number of retained orders for the simulation was chosen to be 31 for both TM and TE response. The rate of convergence with respect to the number of orders retained is such that, for a grating with 30nm CD and 55nm half-pitch, the difference in the simulated response between retaining 31 orders and 61 orders is less than 0.03% for $\tan \Psi$ and 0.1% for $\cos \Delta$. There is a factor of 7 time savings when retaining only 31 orders against retaining 61 orders. Software coding was done using Tcl/Tk [3.3]

Figure 3.2 illustrates the various profile parameters being considered. Figures 3.3-3.10 show the expected scatterometric response for the profiles with nominal feature sizes given in Table 3.1 with the response spectrum due to variations incorporated to demonstrate the sensitivity of the electromagnetic simulations.

Figure 3.2 Illustration of profile parameters used for sensitivity analysis

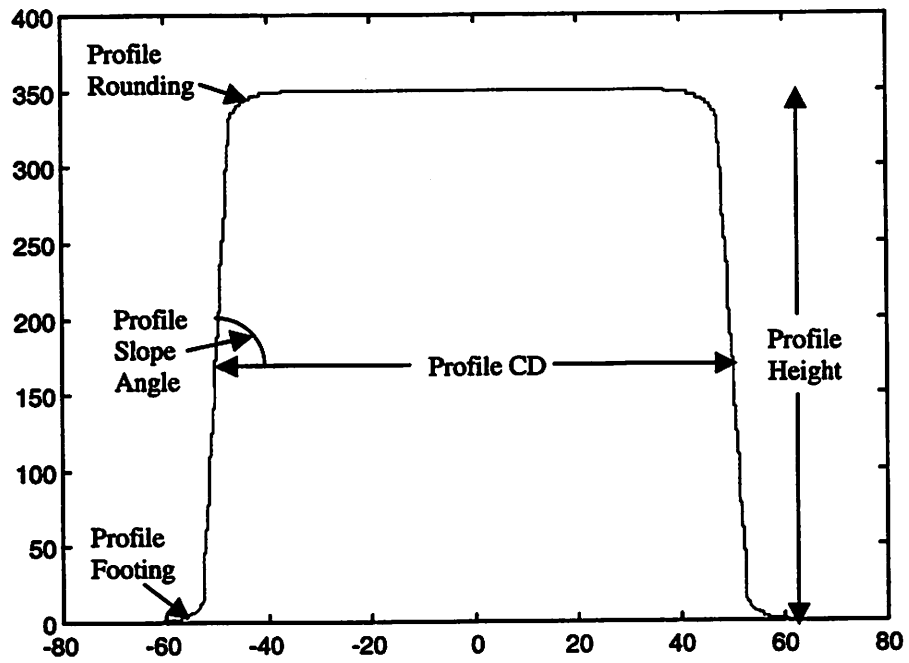
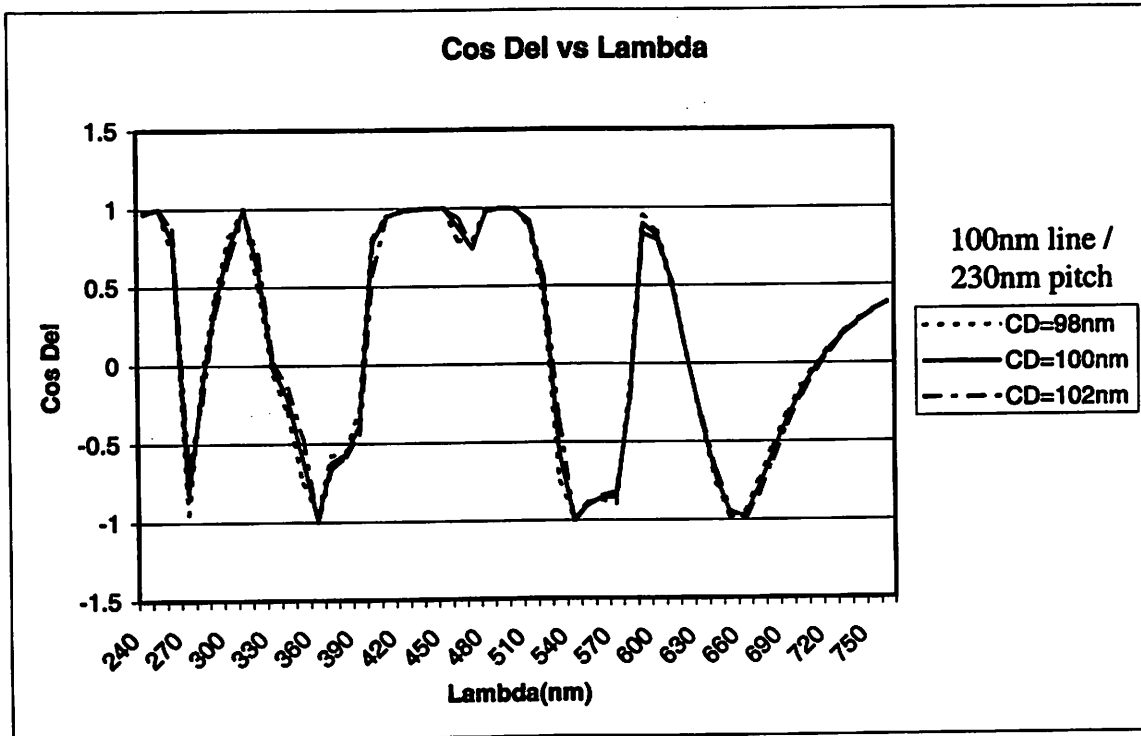
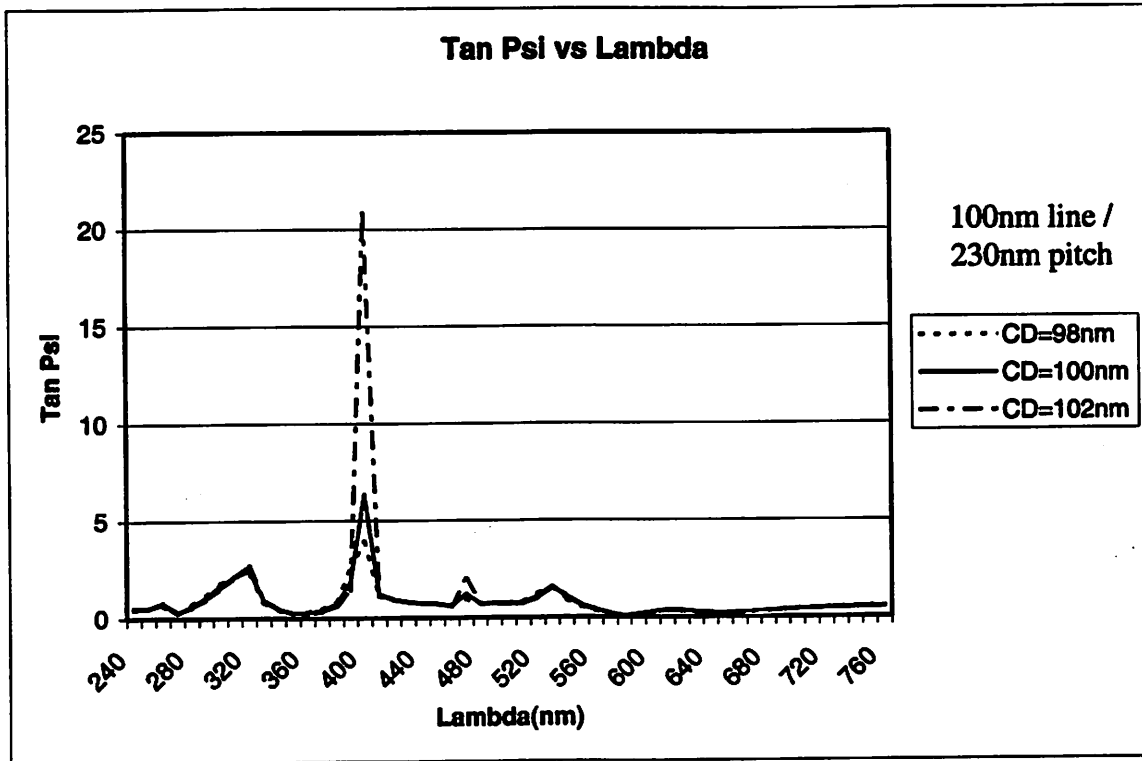
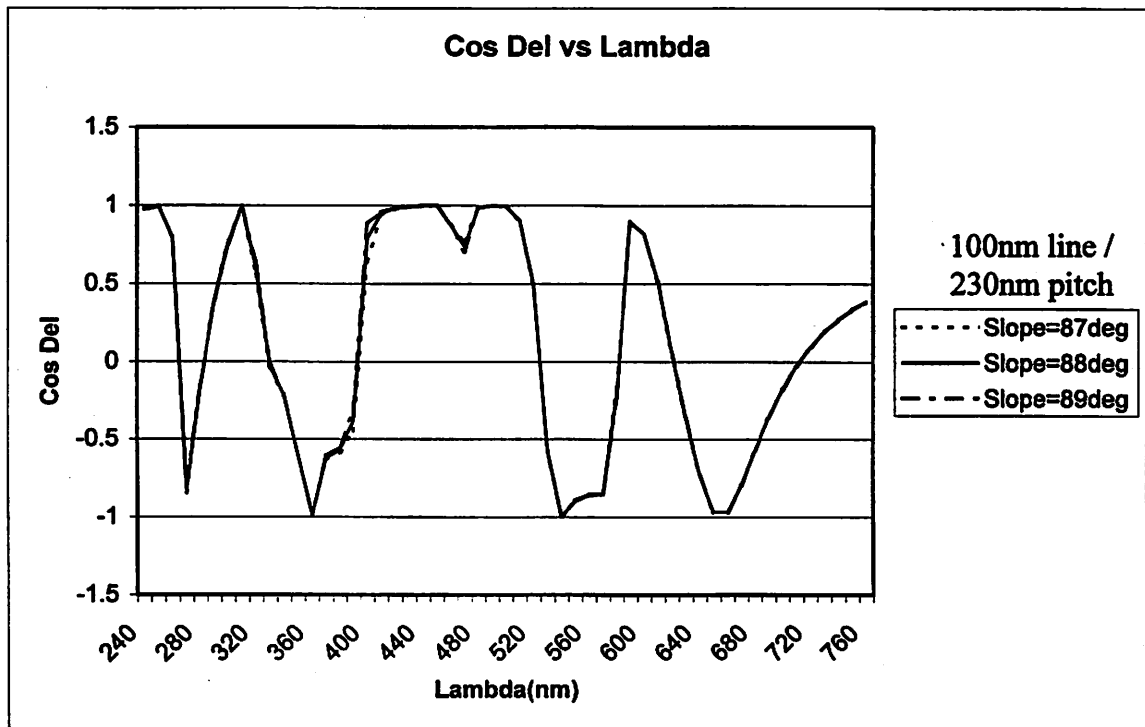
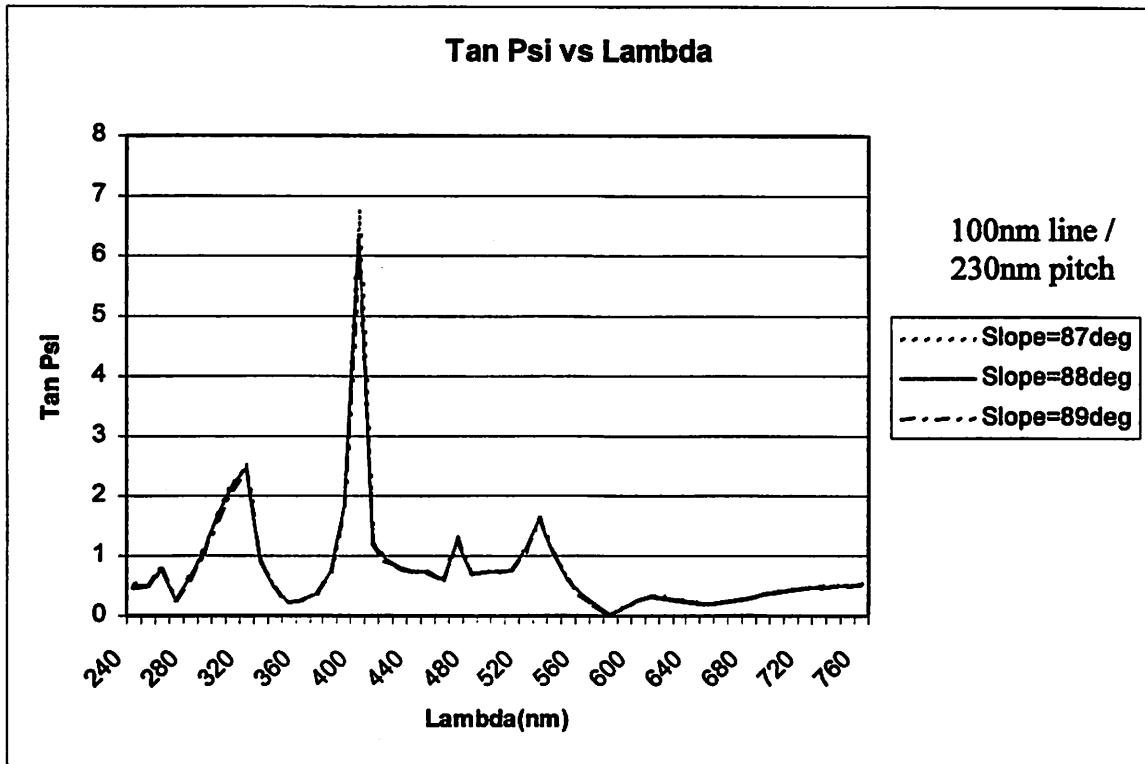
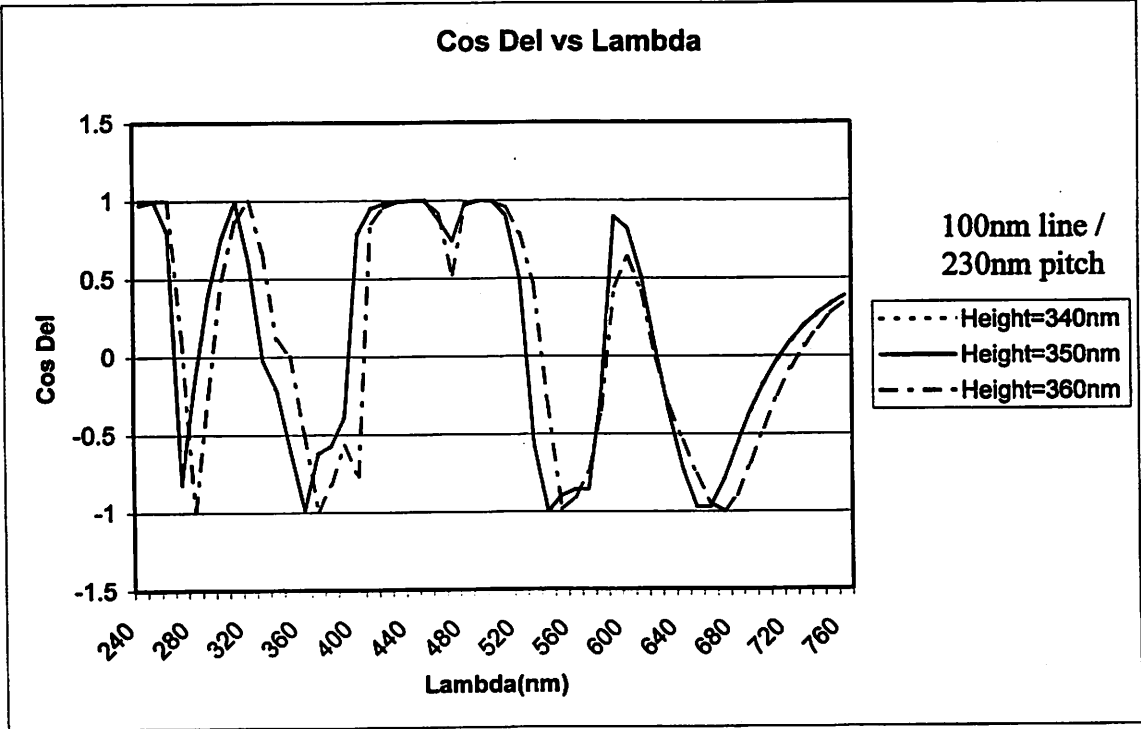
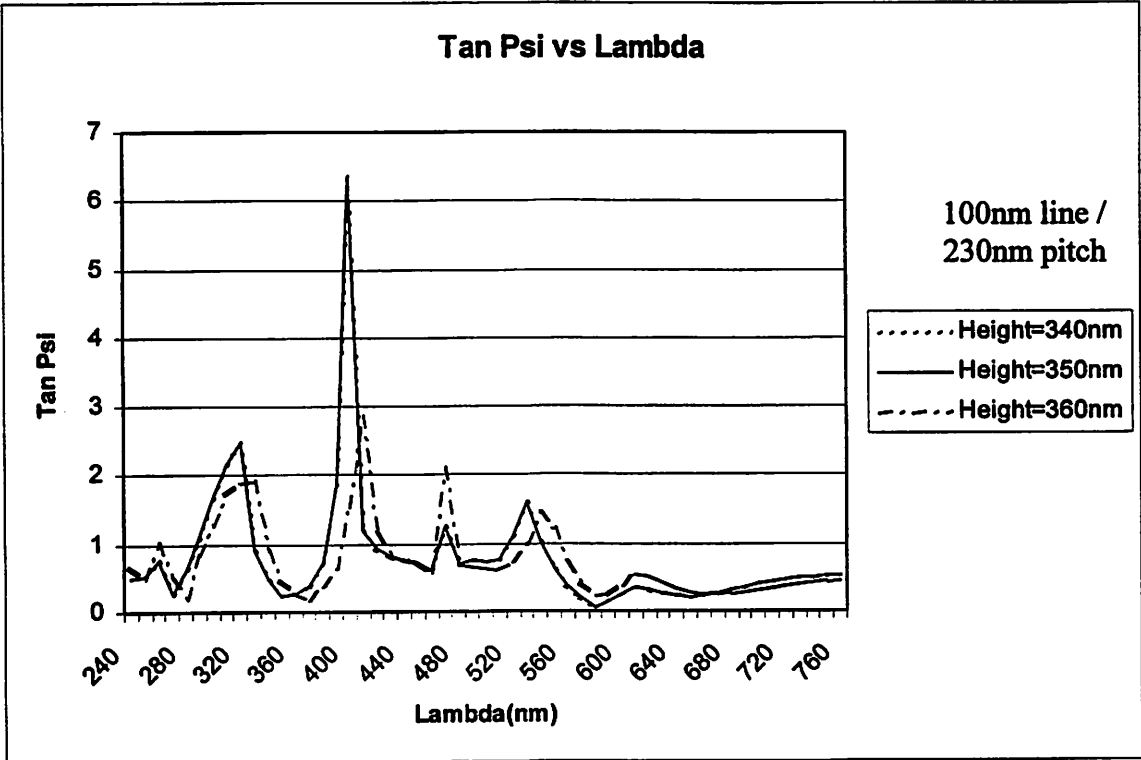
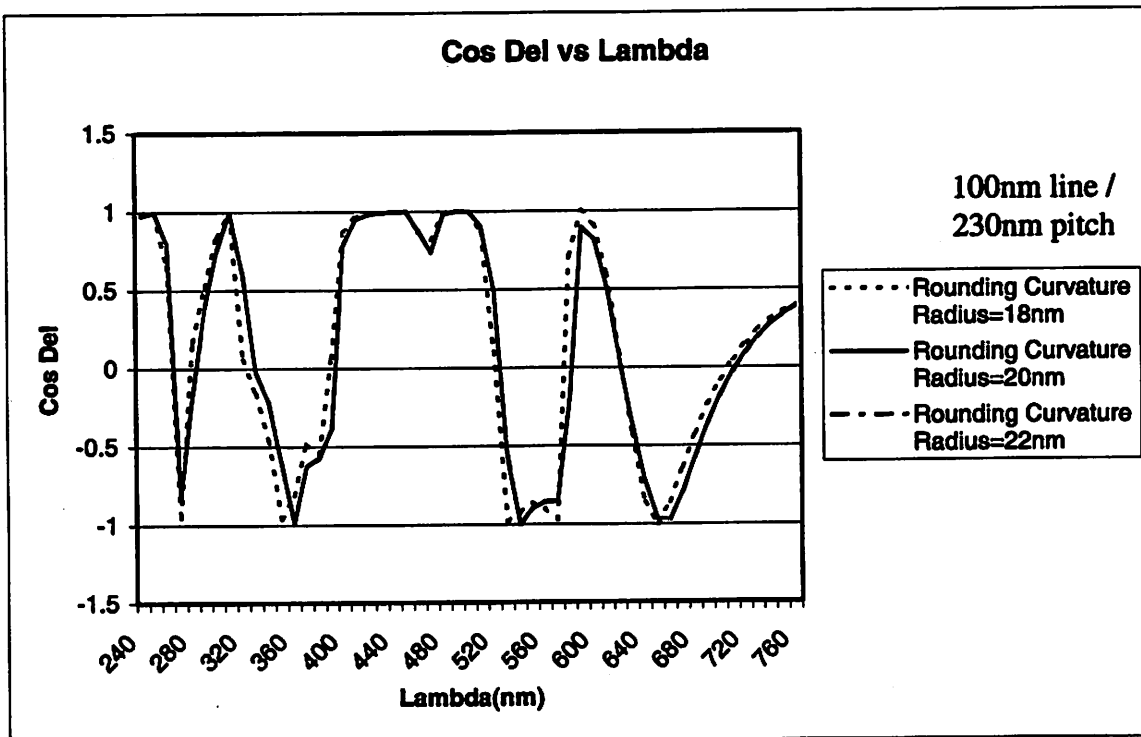
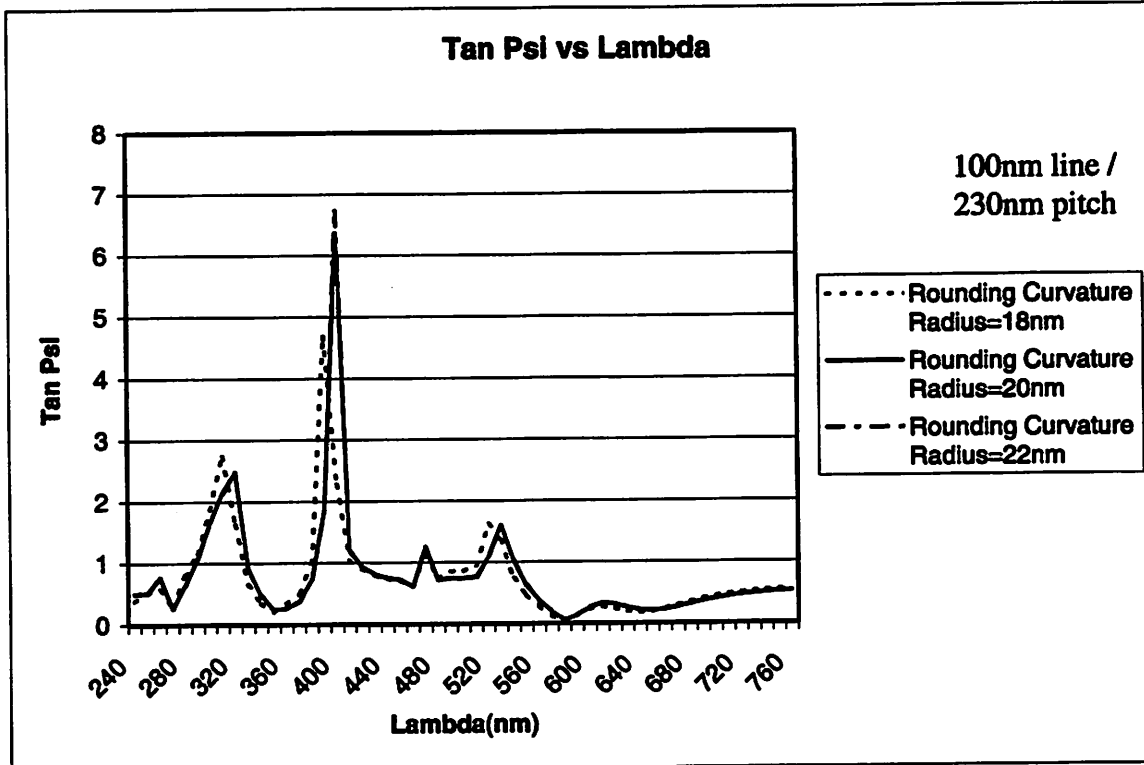


Figure 3.3 (a)-(j) Scatterometric Response for 100nm Line / 230nm Pitch









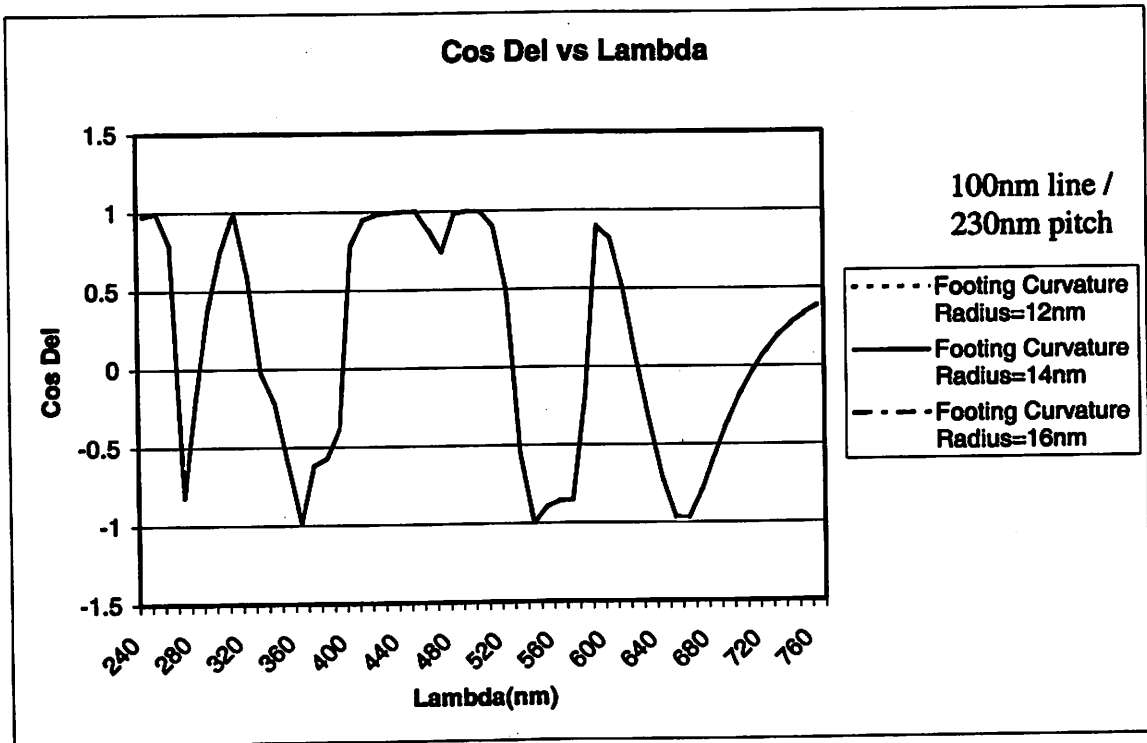
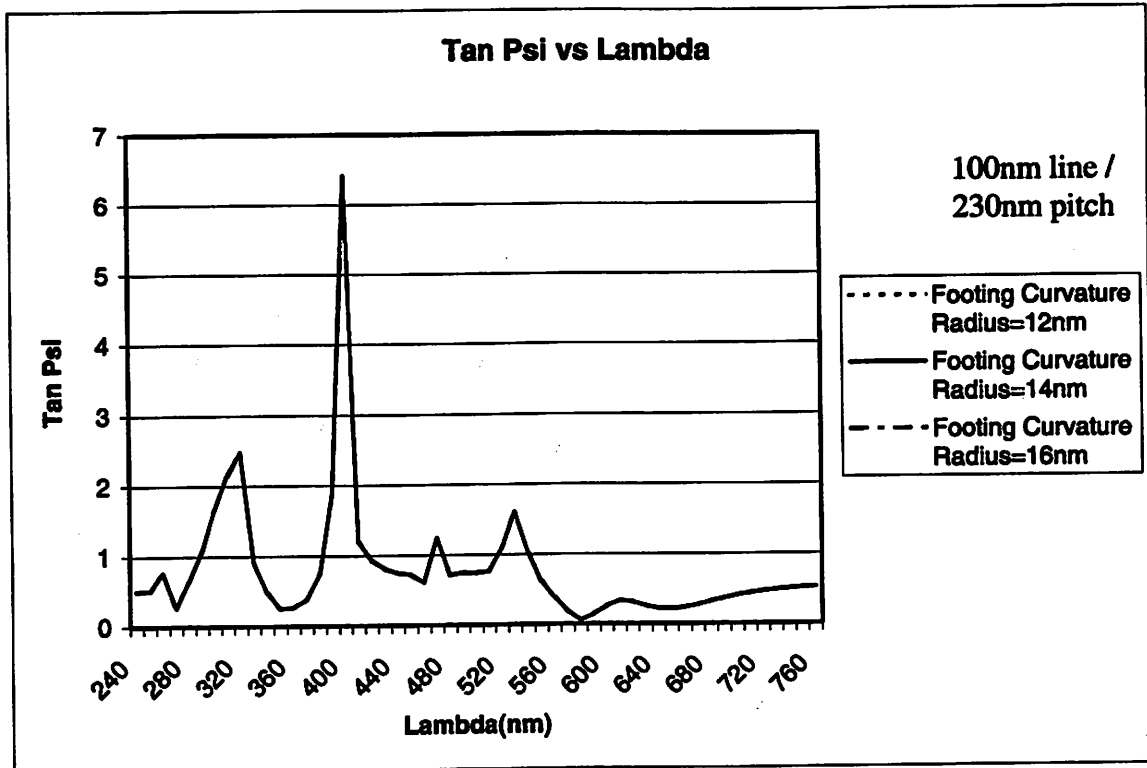
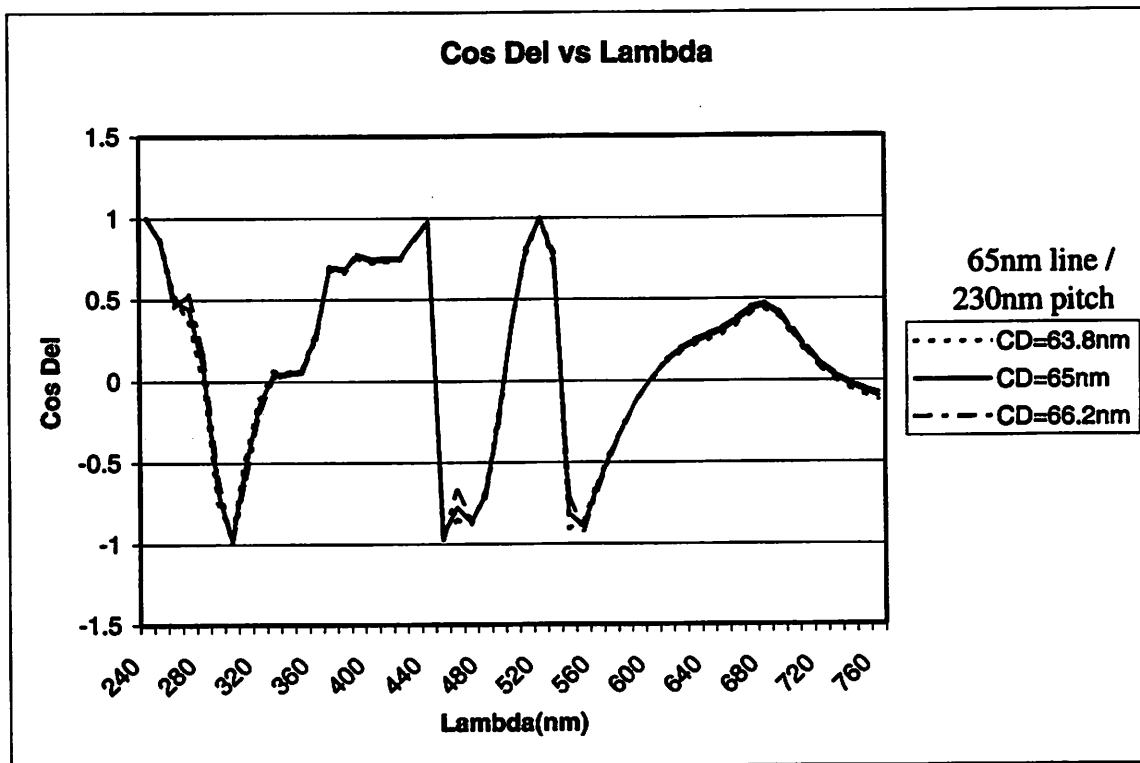
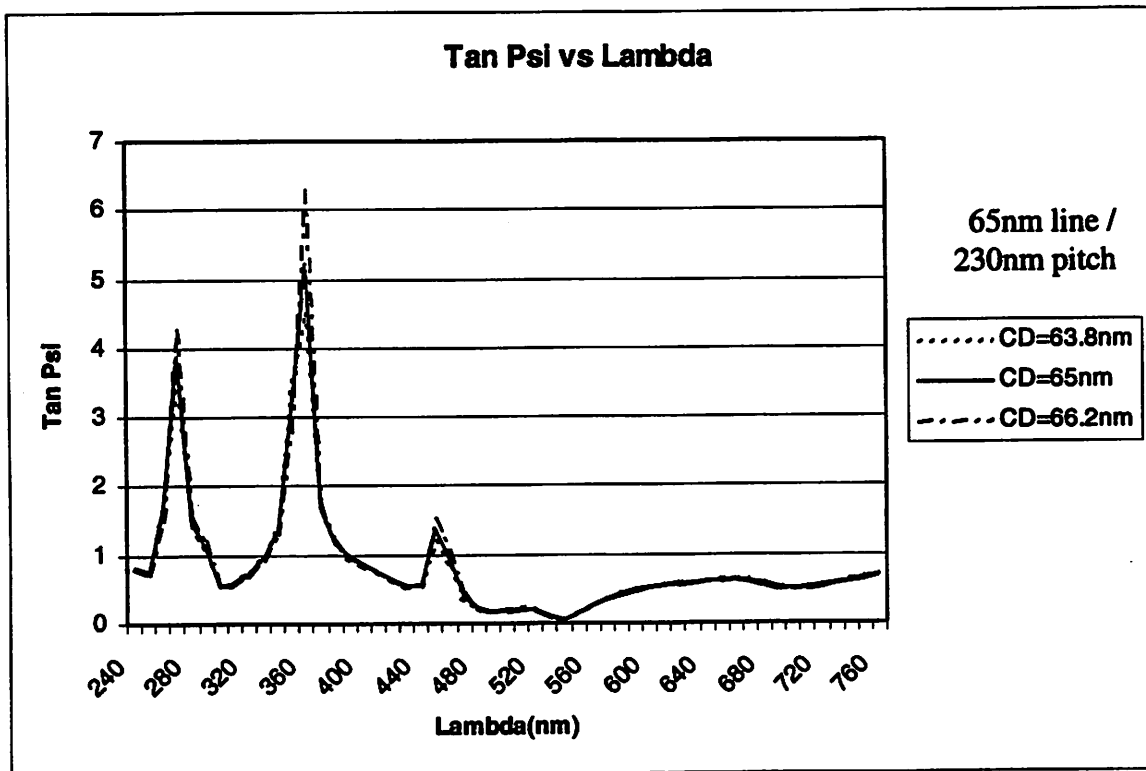
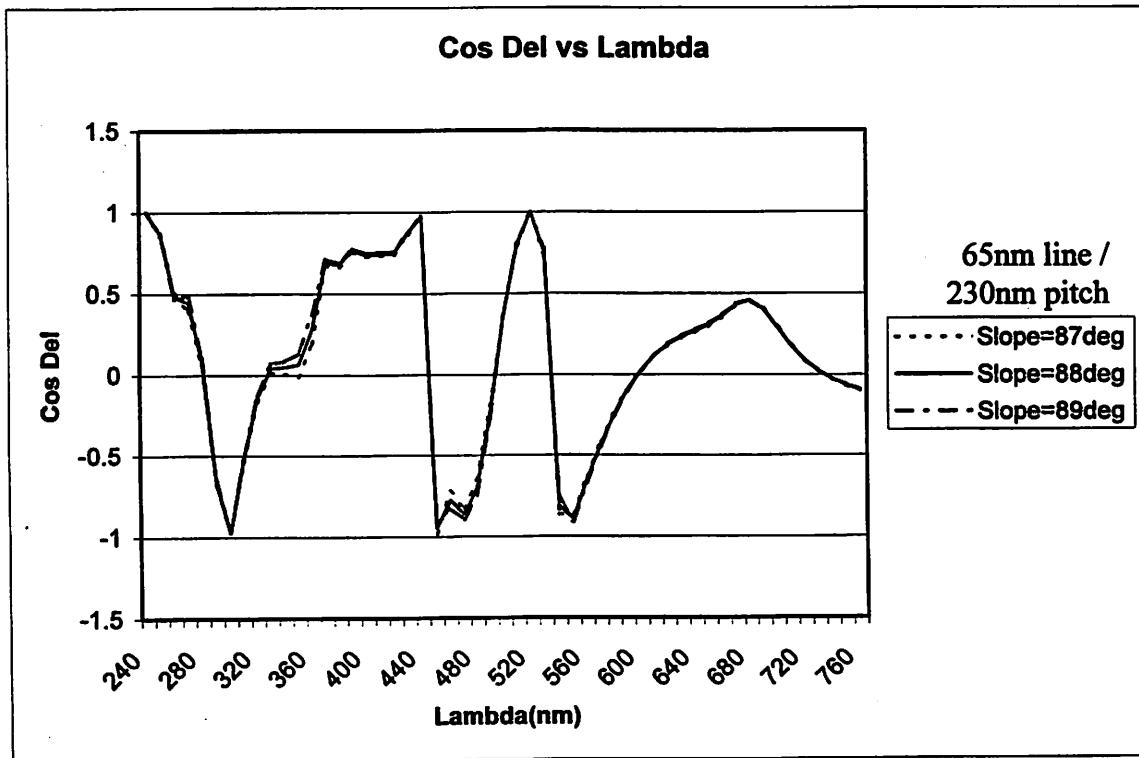
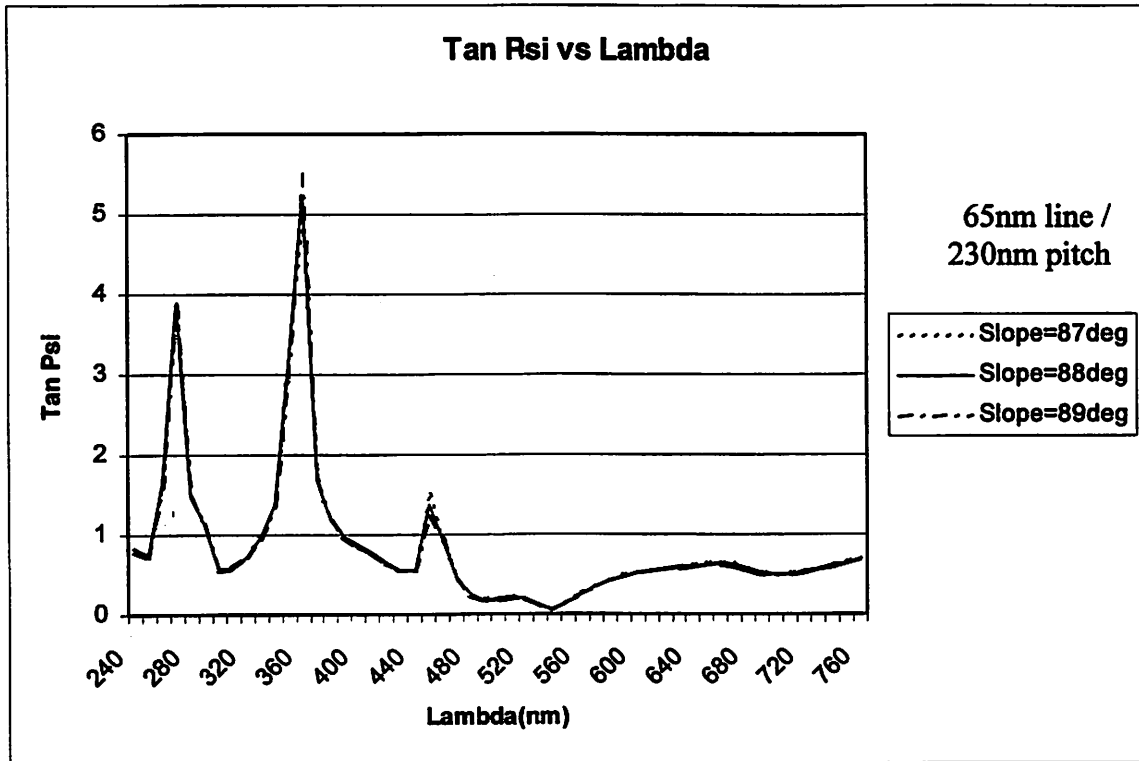
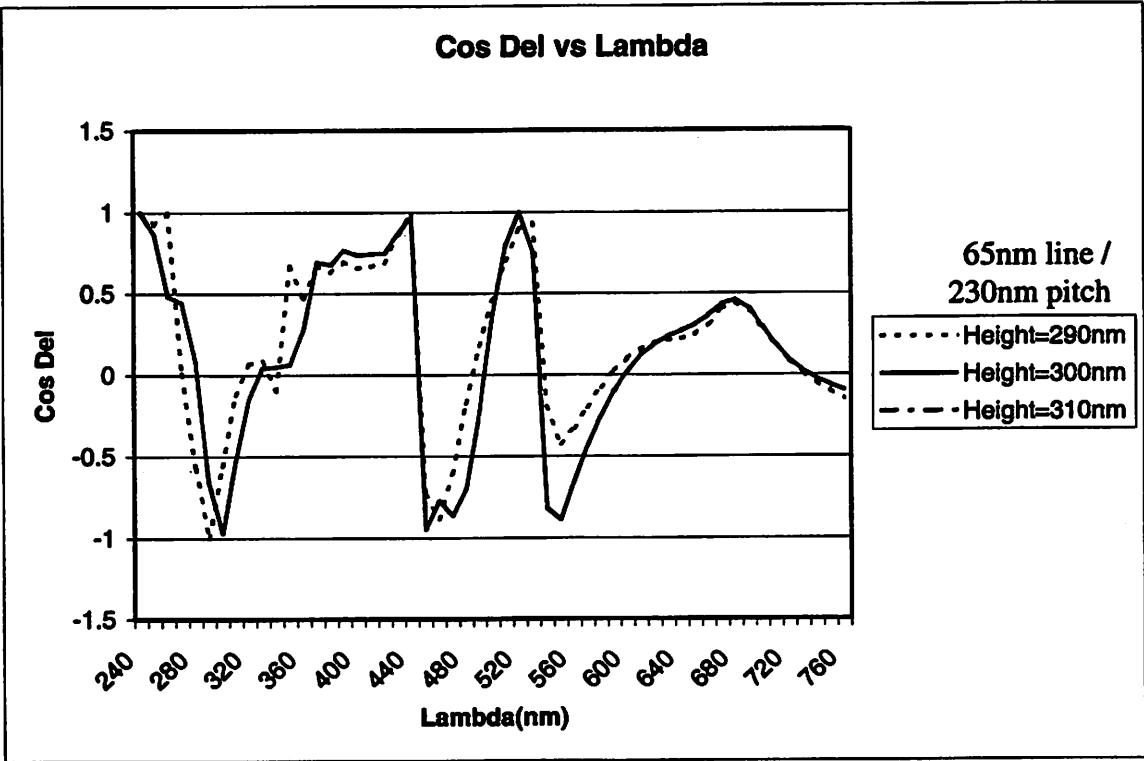
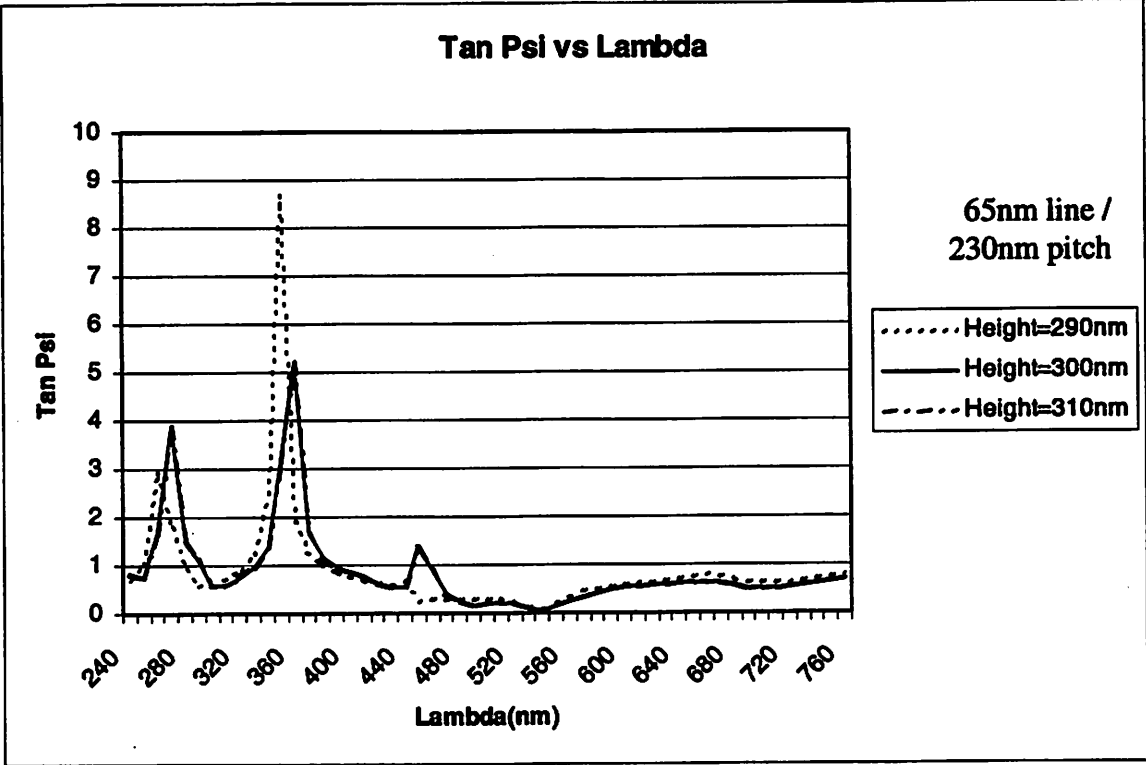
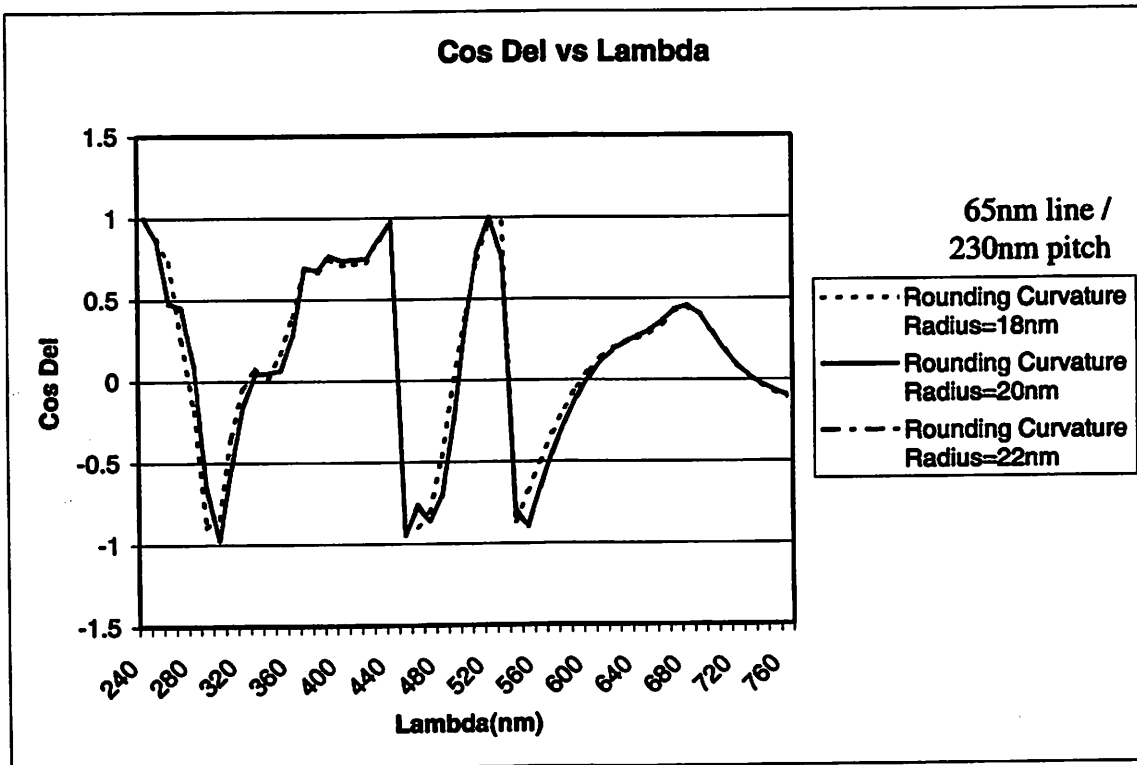
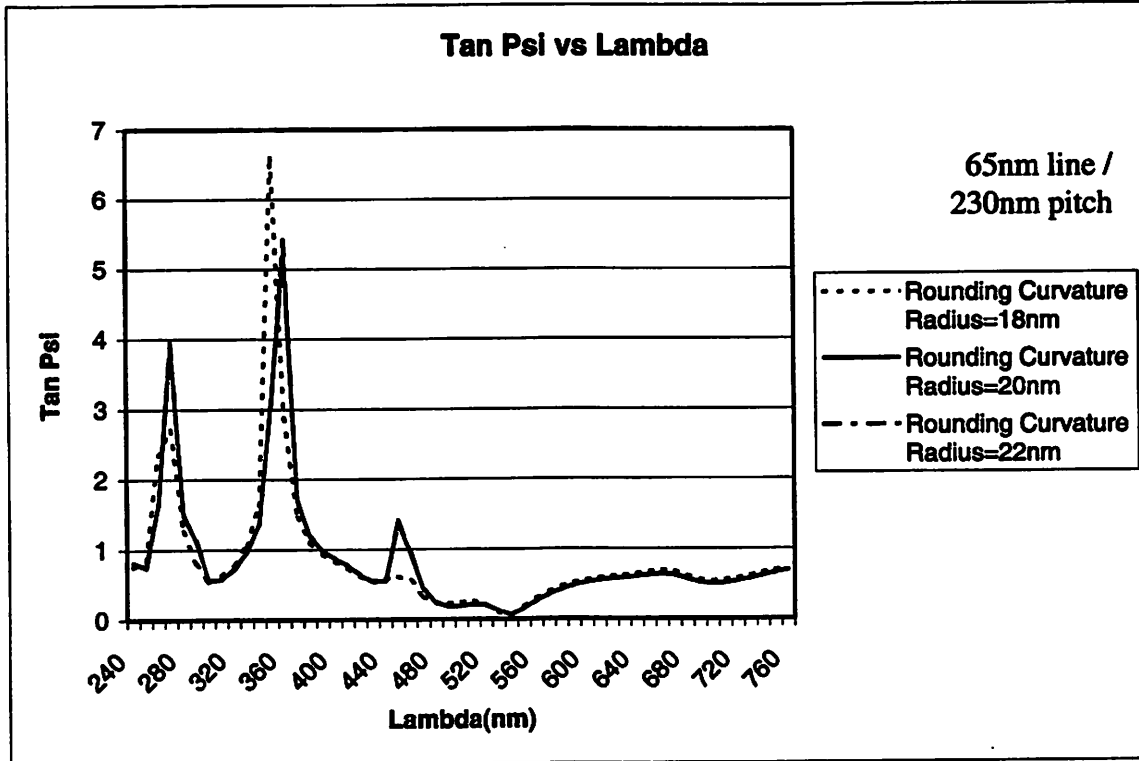


Figure 3.4 (a)-(j) Scatterometric Response for 65nm Line / 230nm Pitch









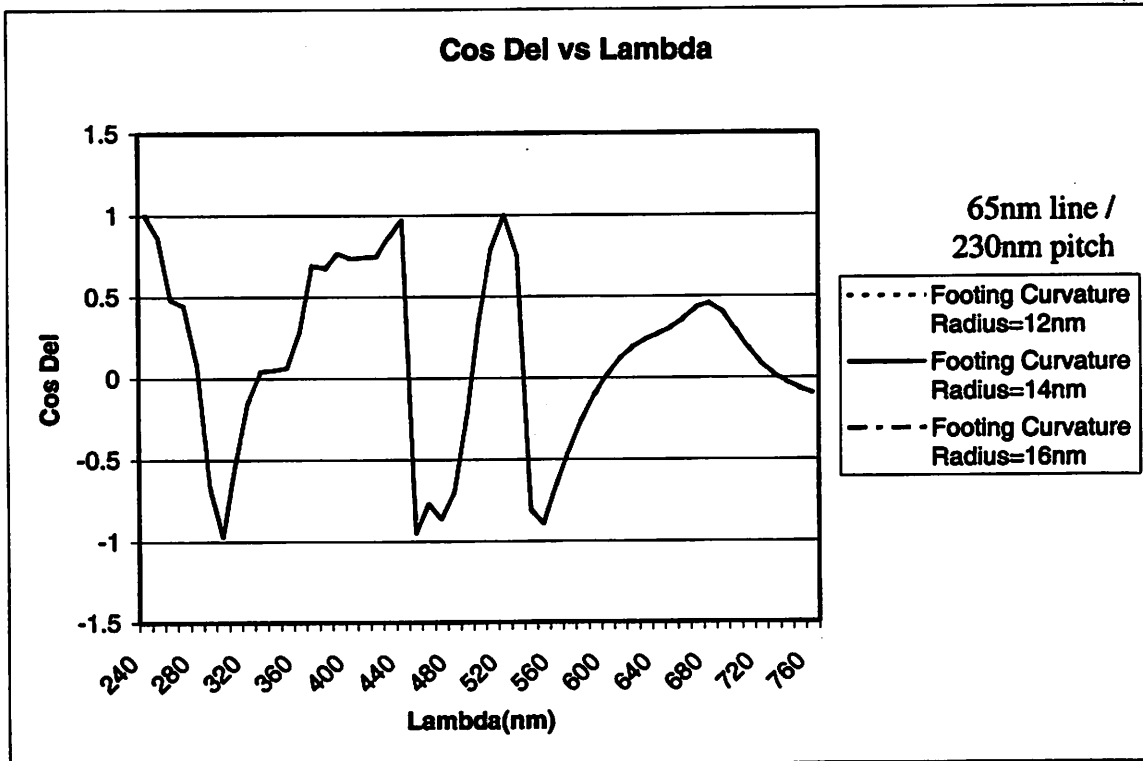
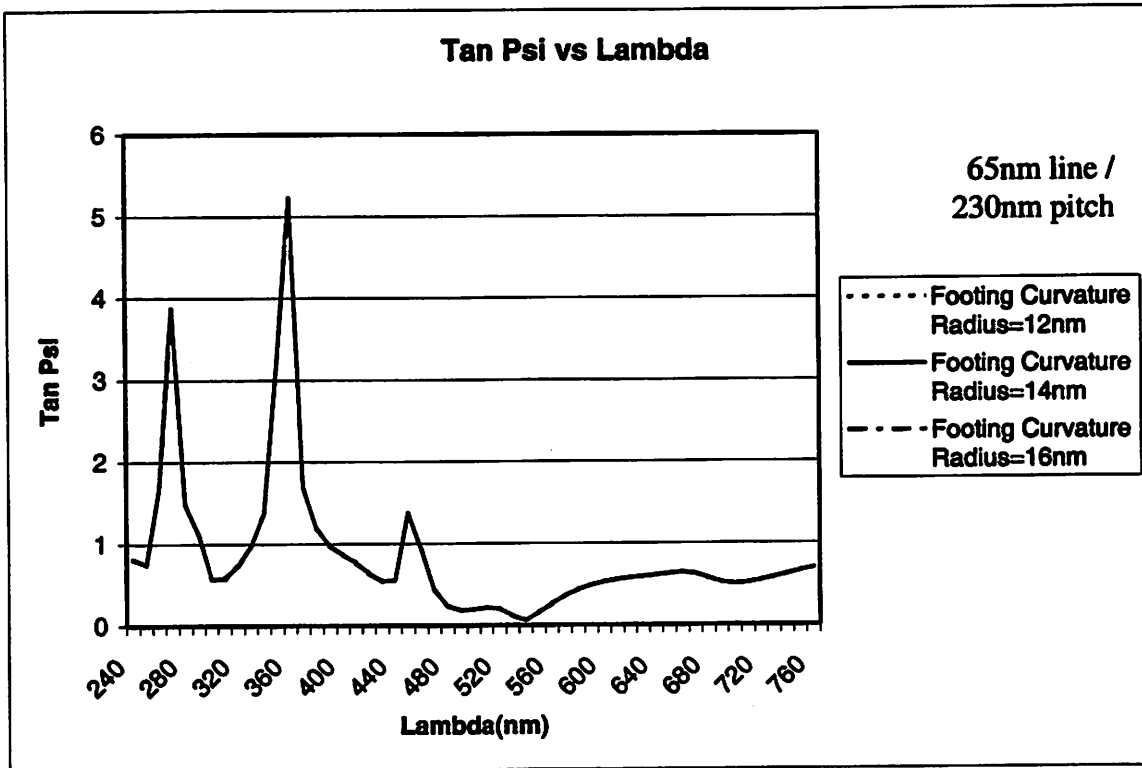
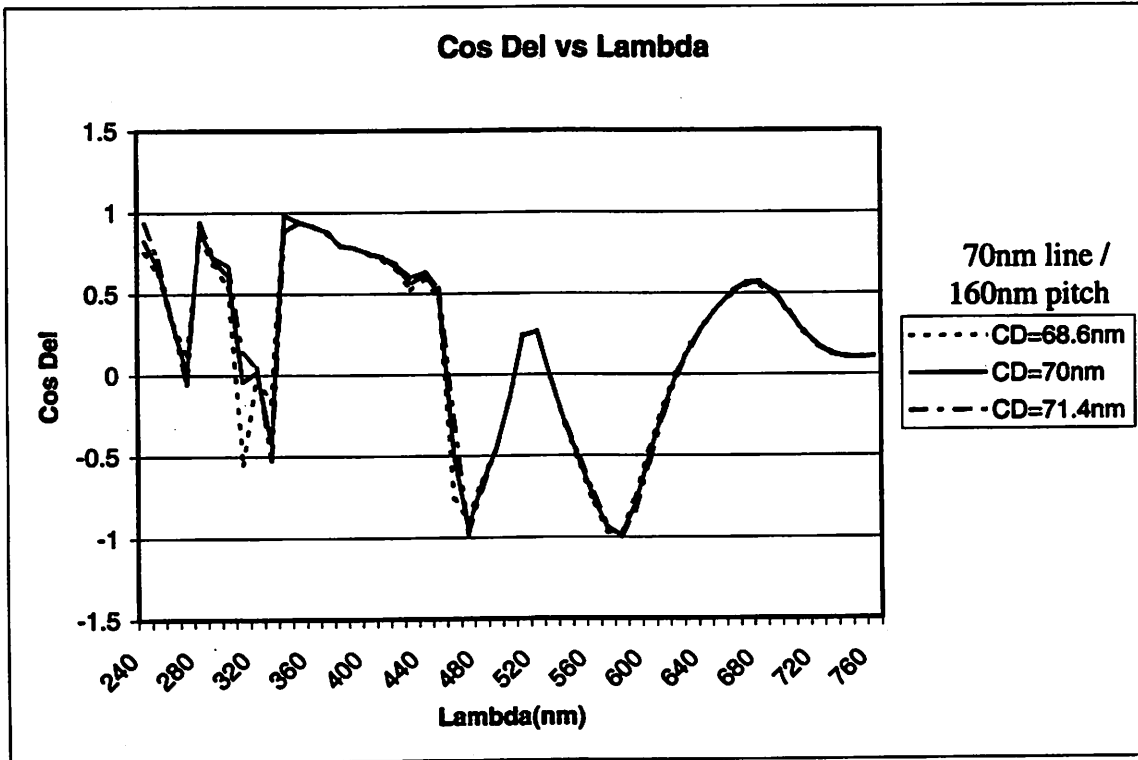
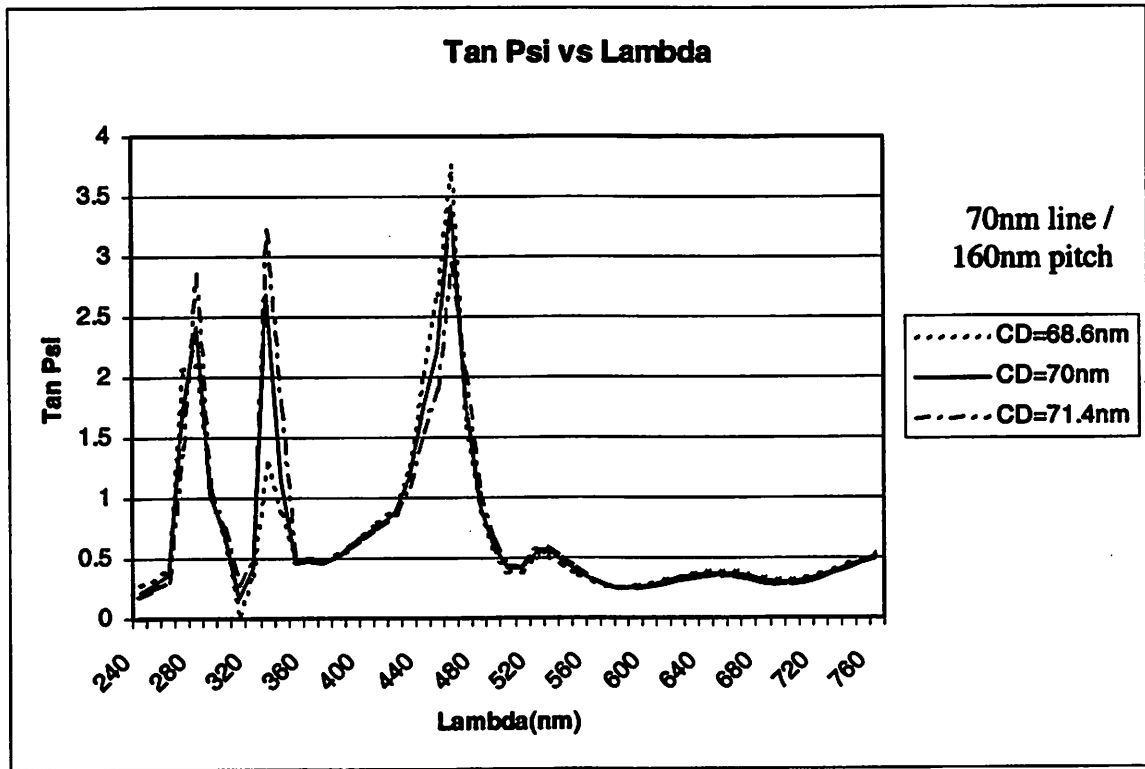
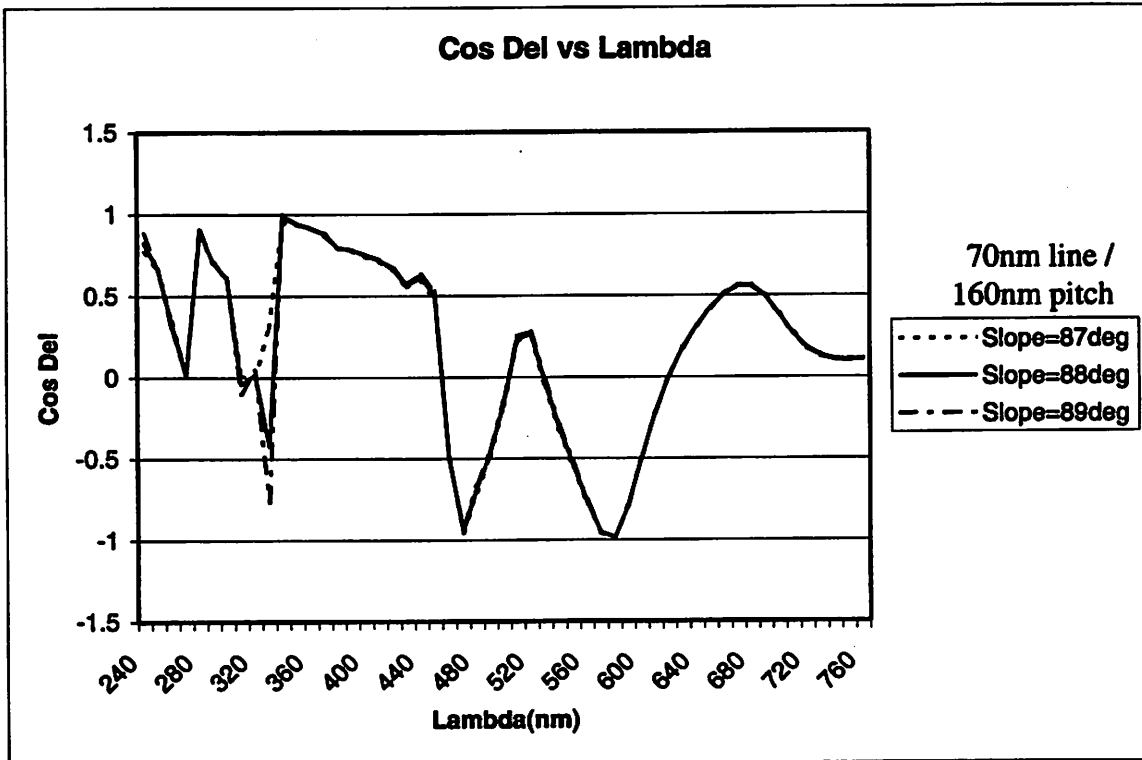
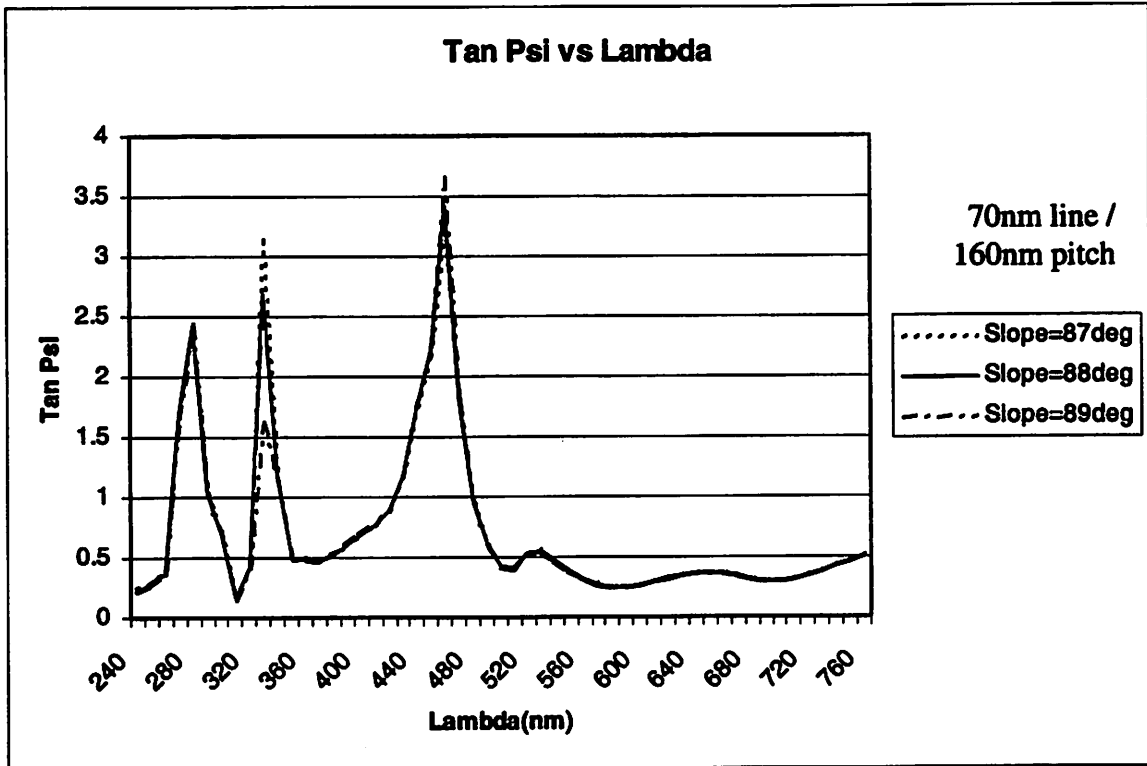
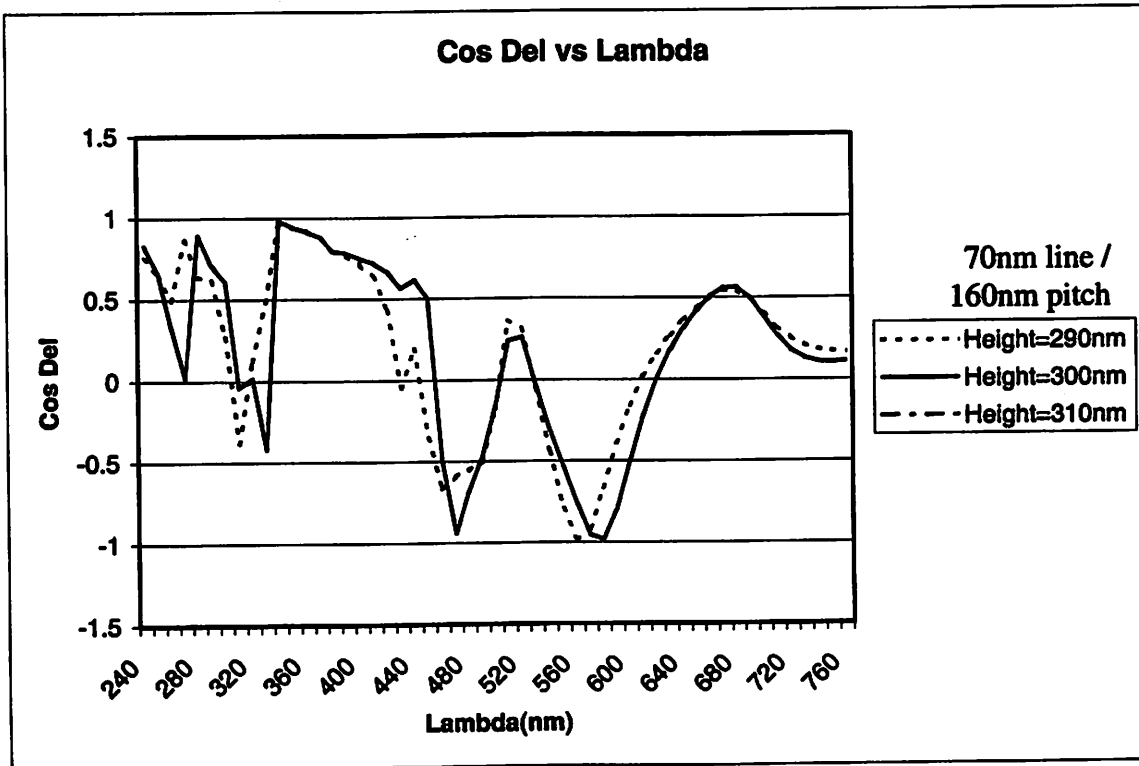
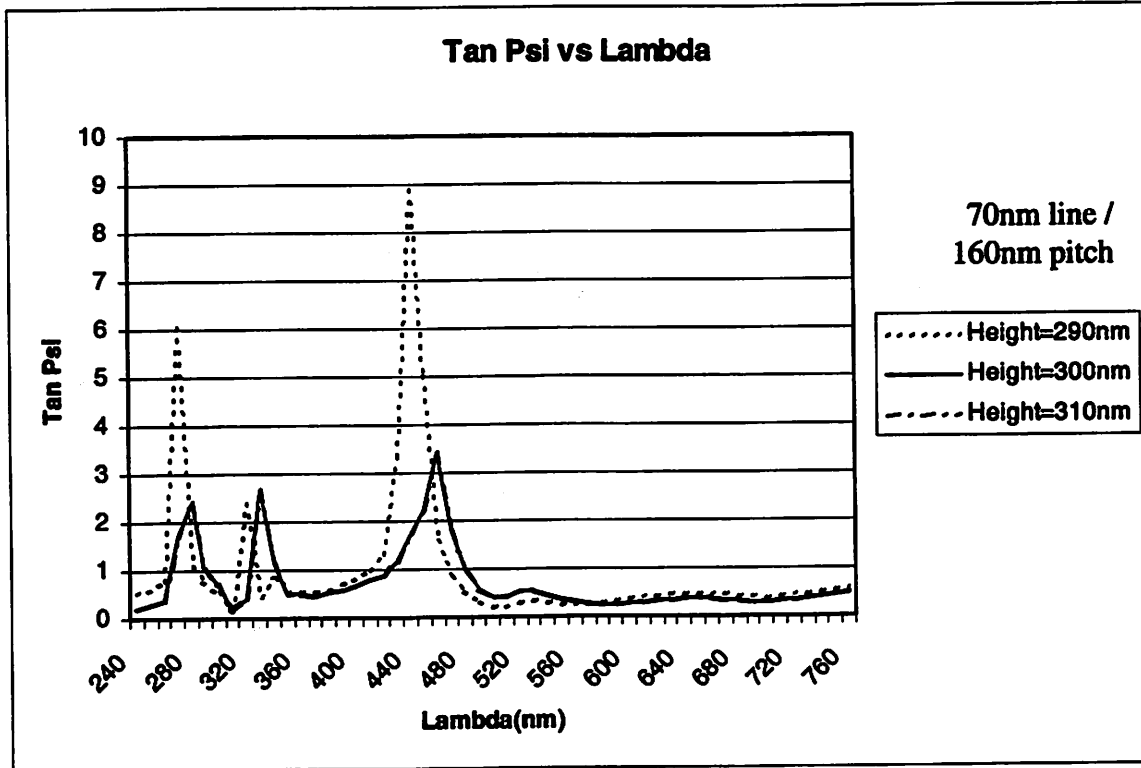
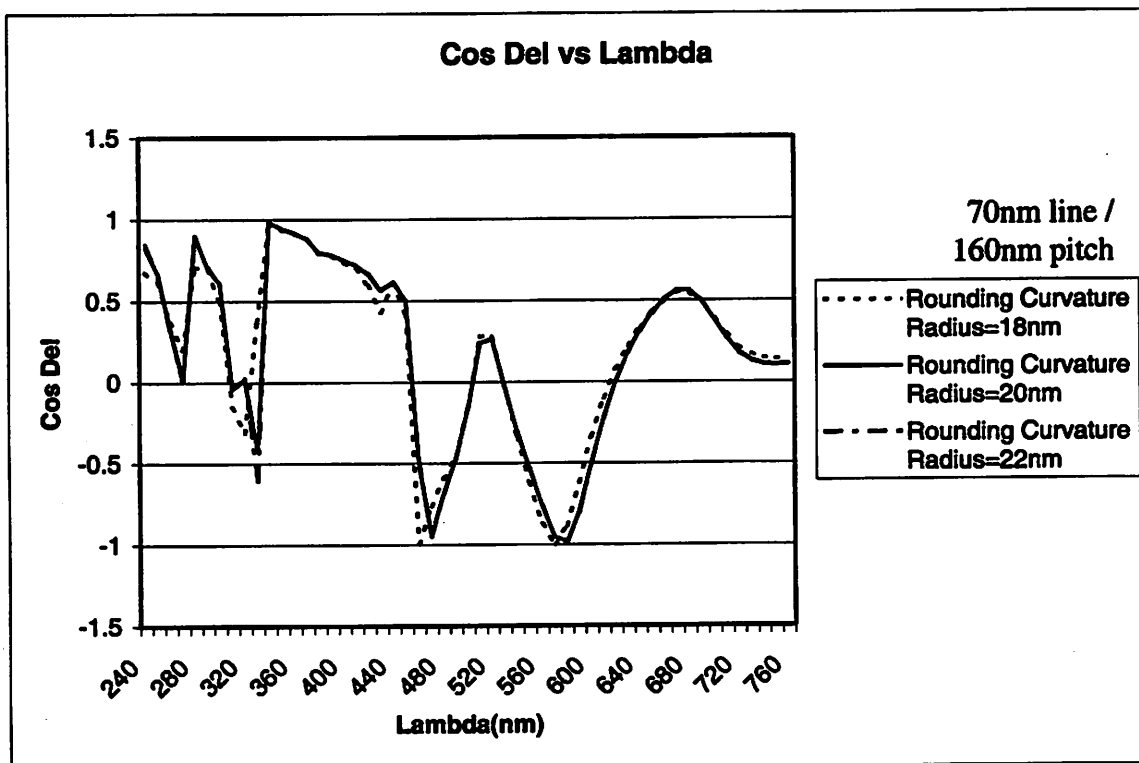
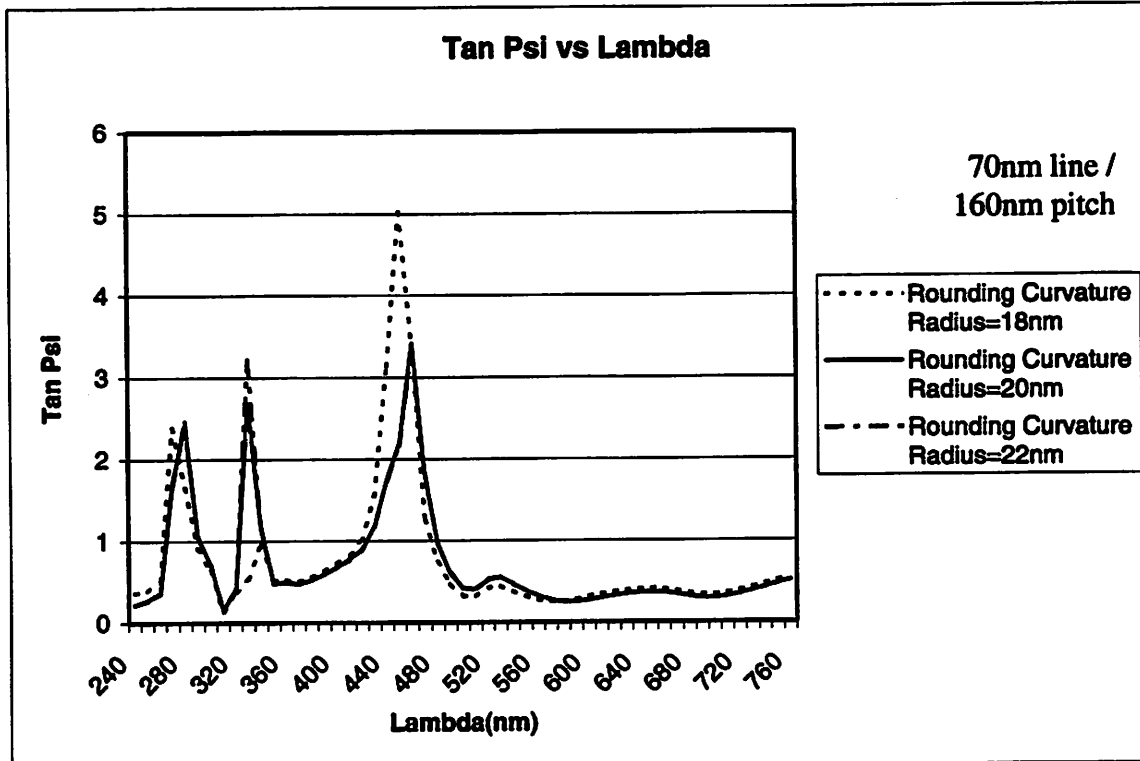


Figure 3.5 (a)-(j) Scatterometric Response for 70nm Line / 160nm Pitch









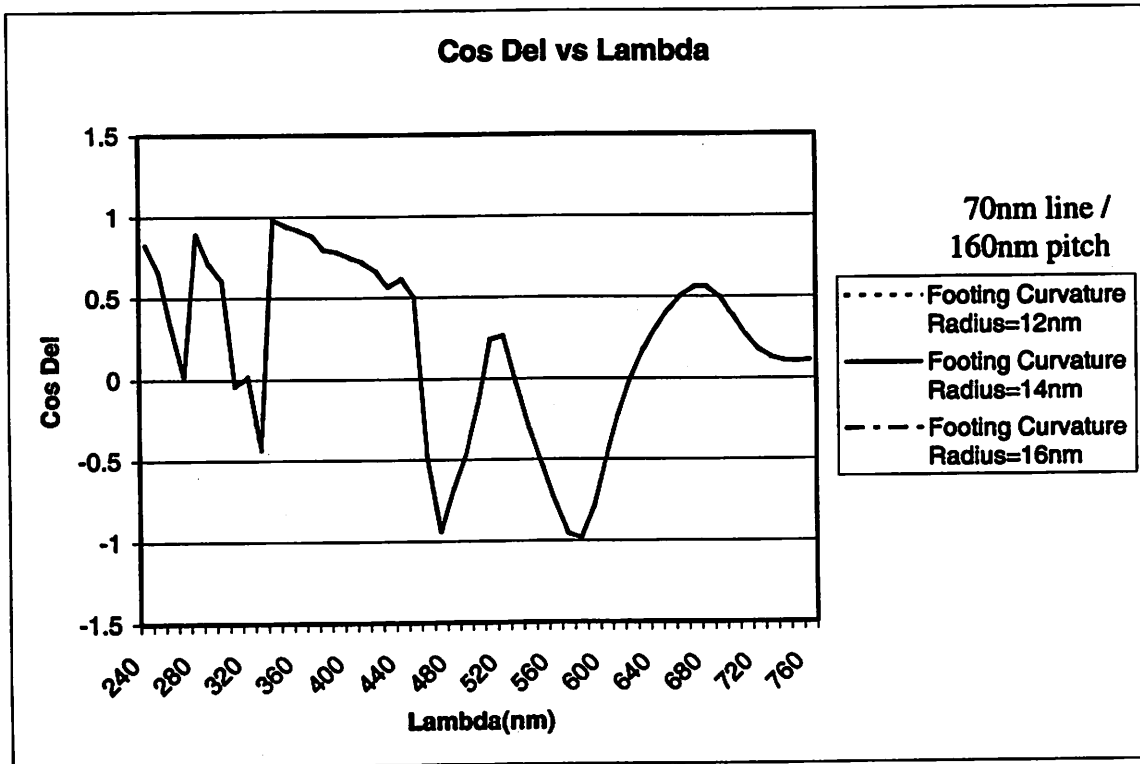
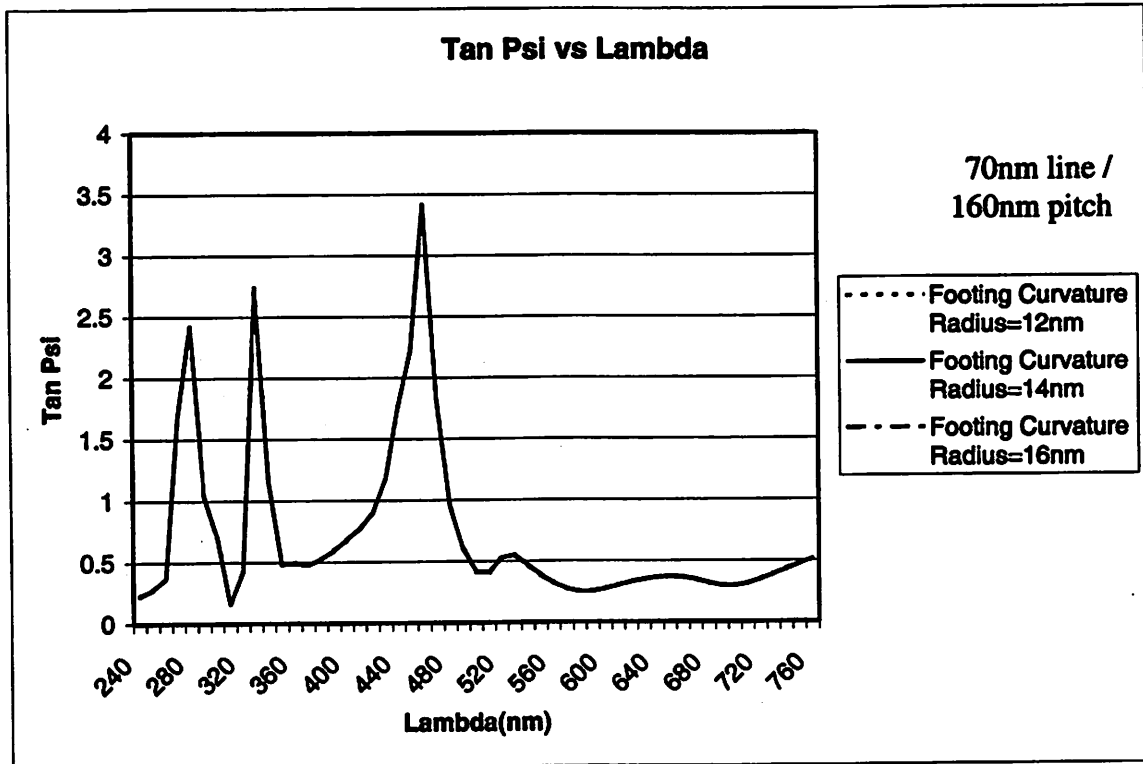
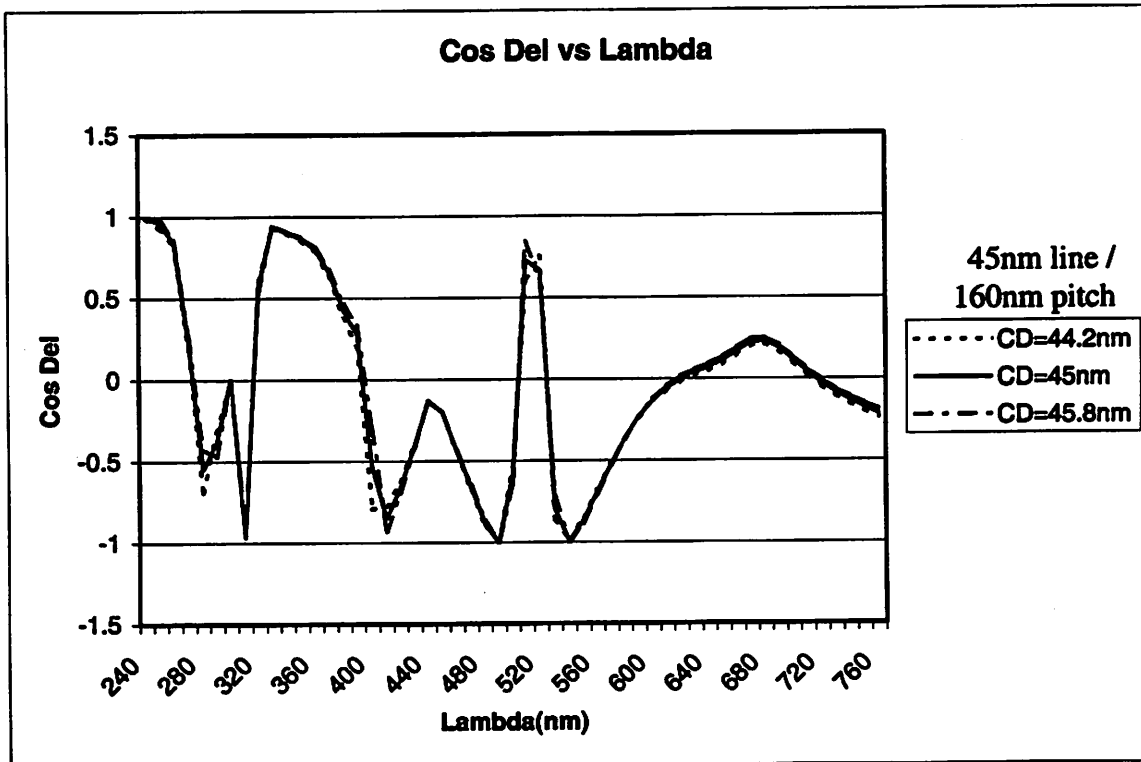
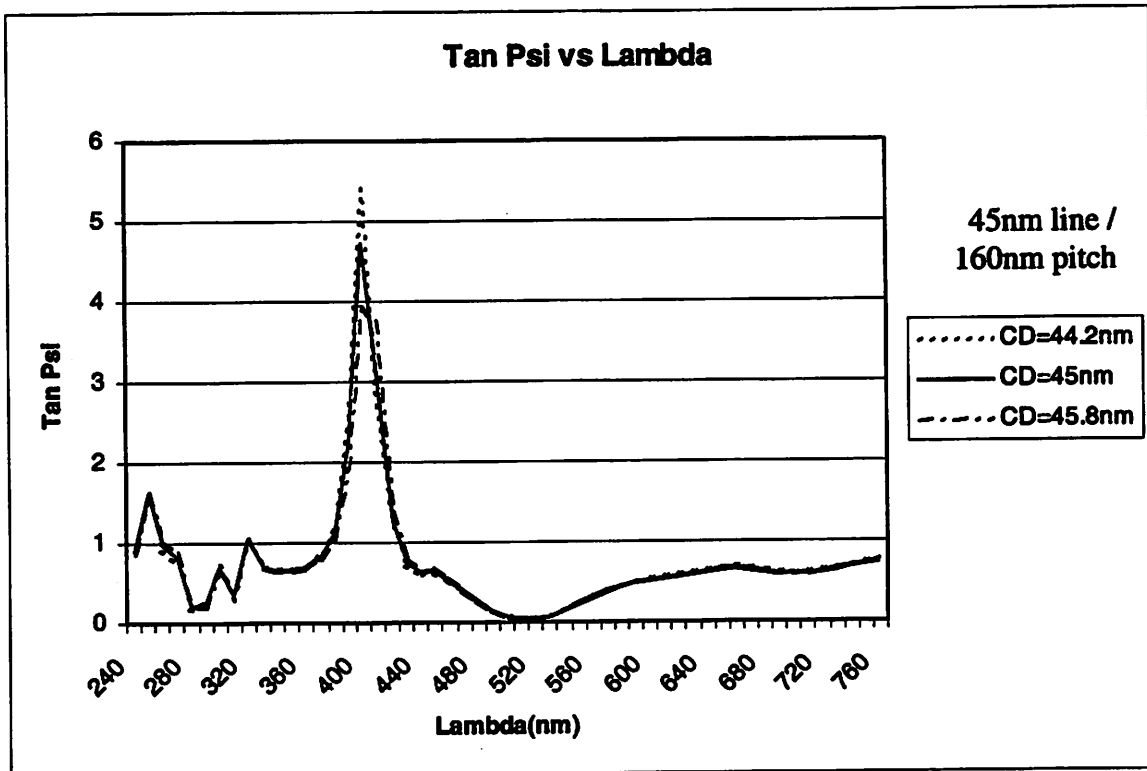
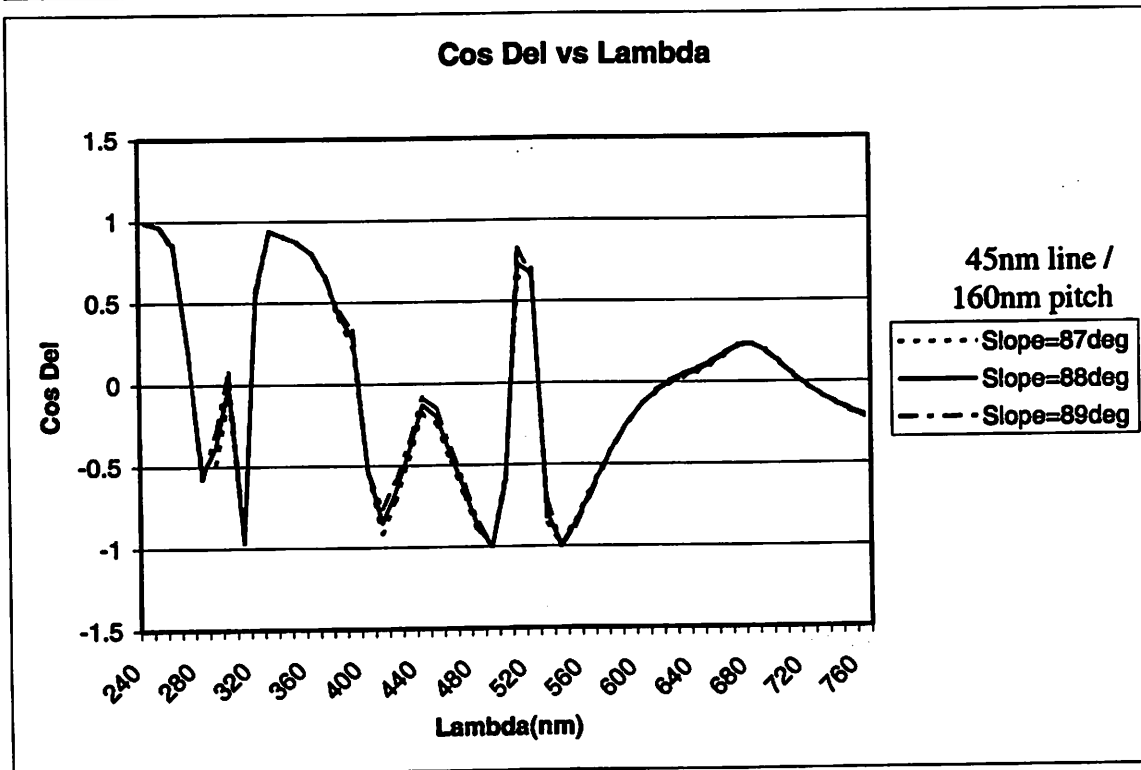
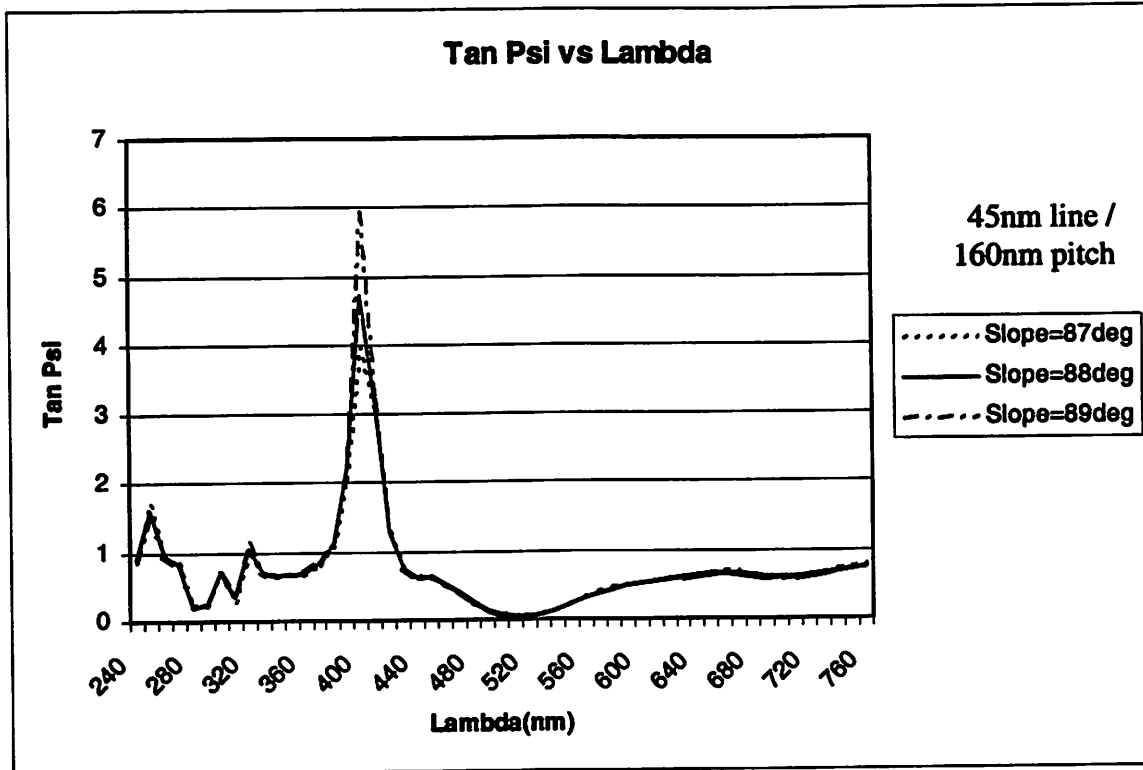
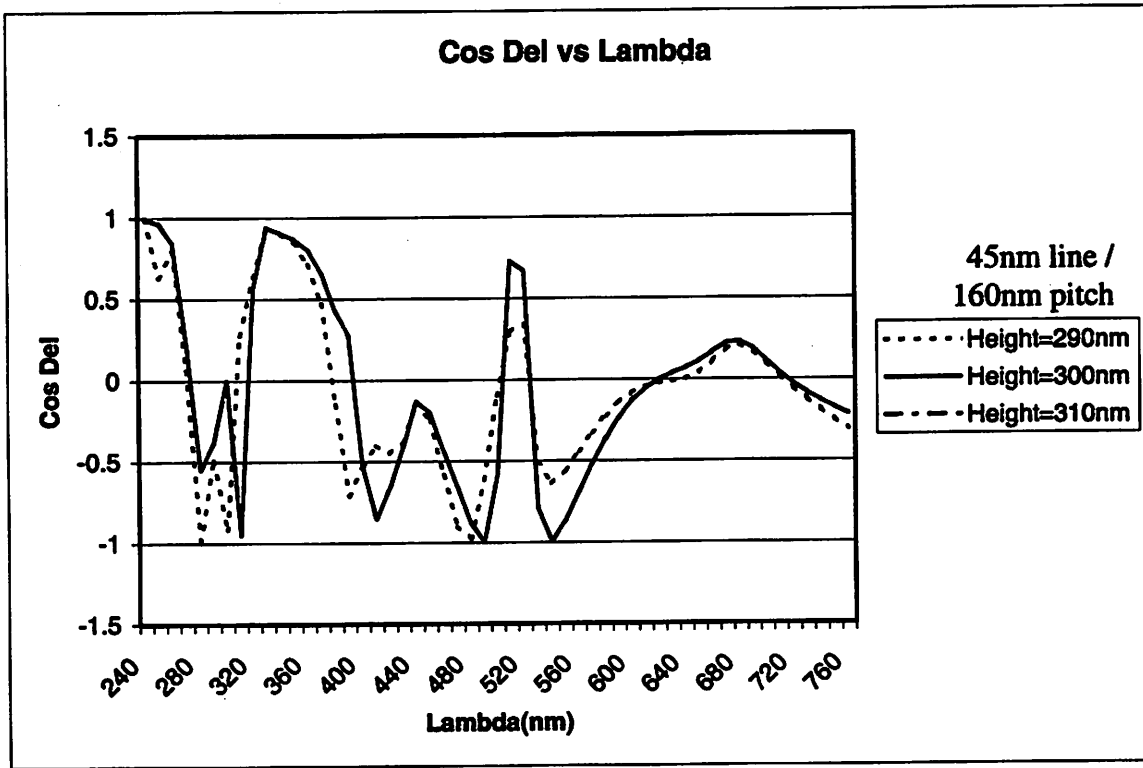
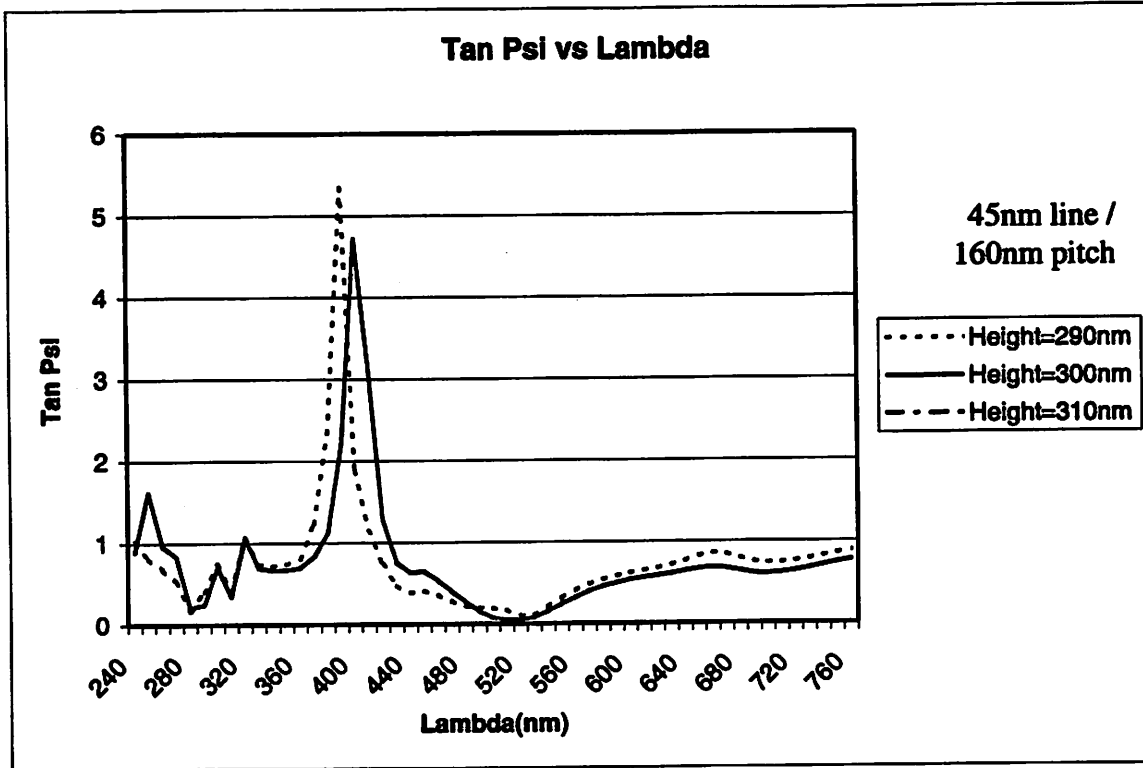
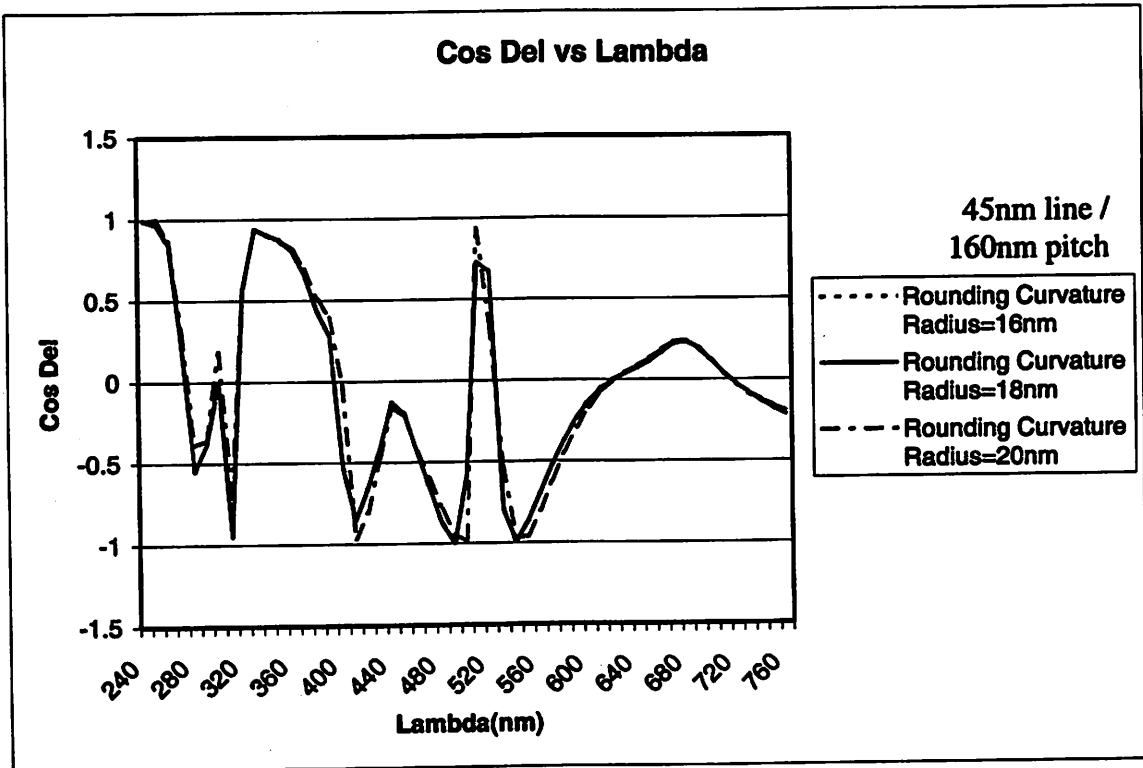
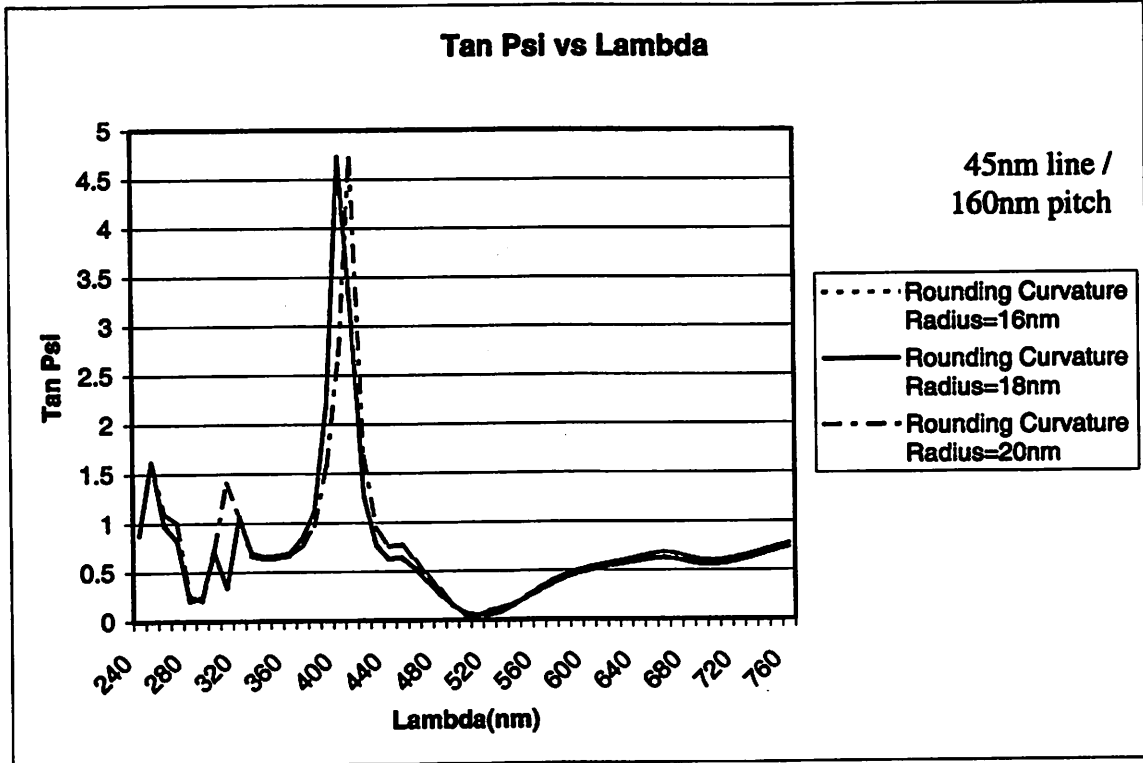


Figure 3.6 (a)-(j) Scatterometric Response for 45nm Line / 160nm Pitch









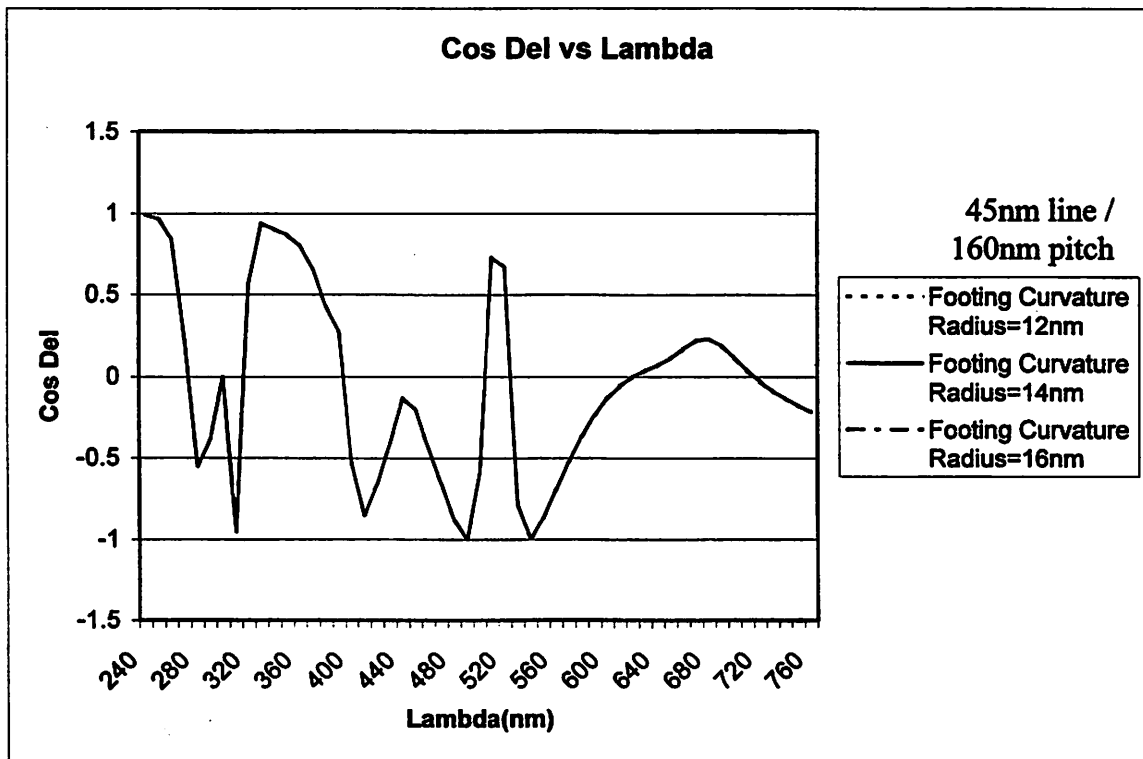
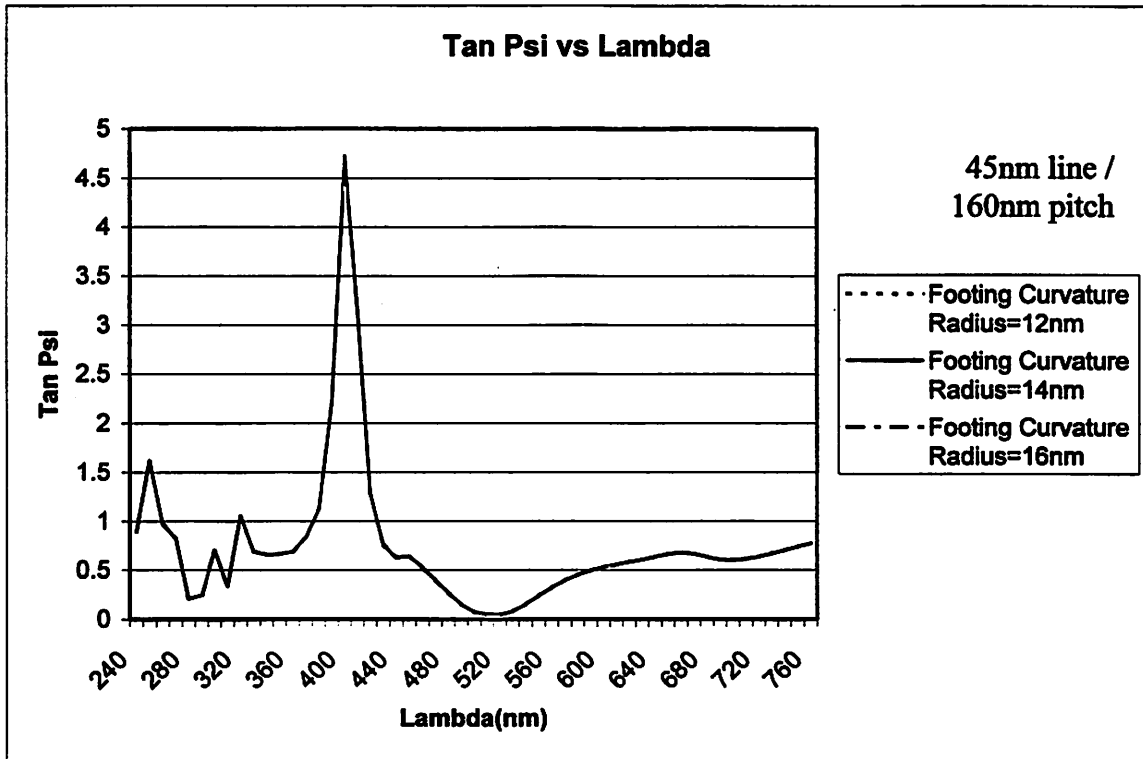
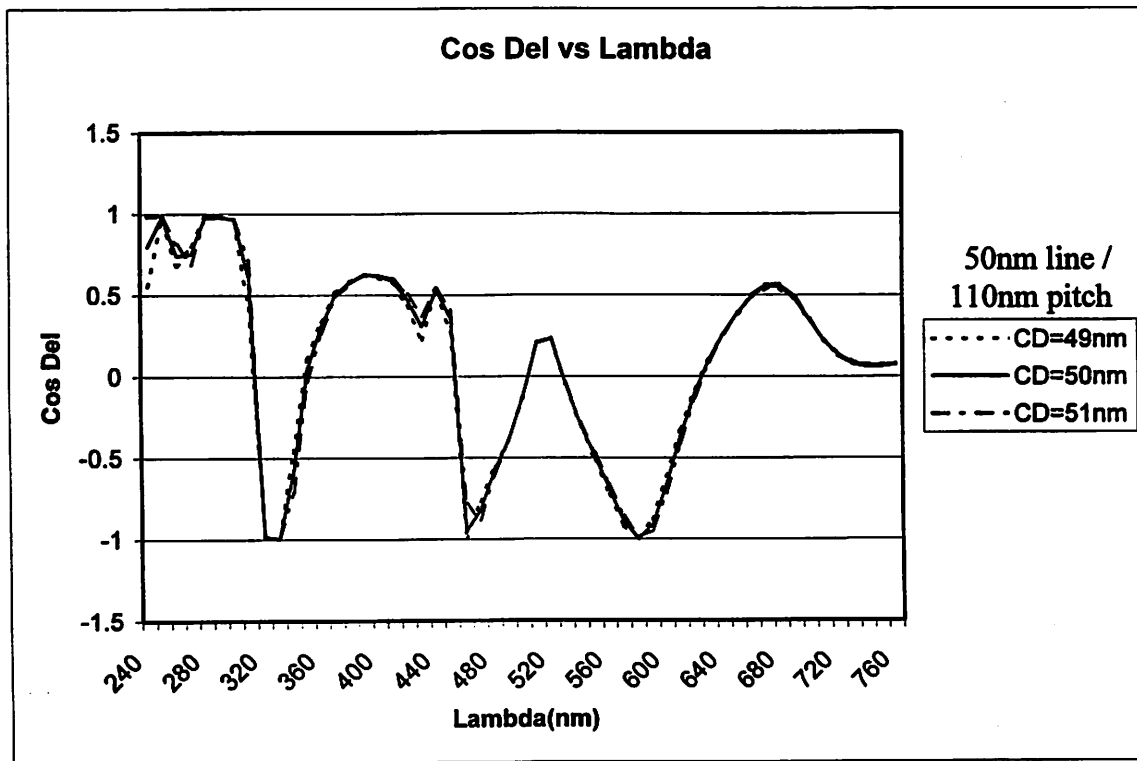
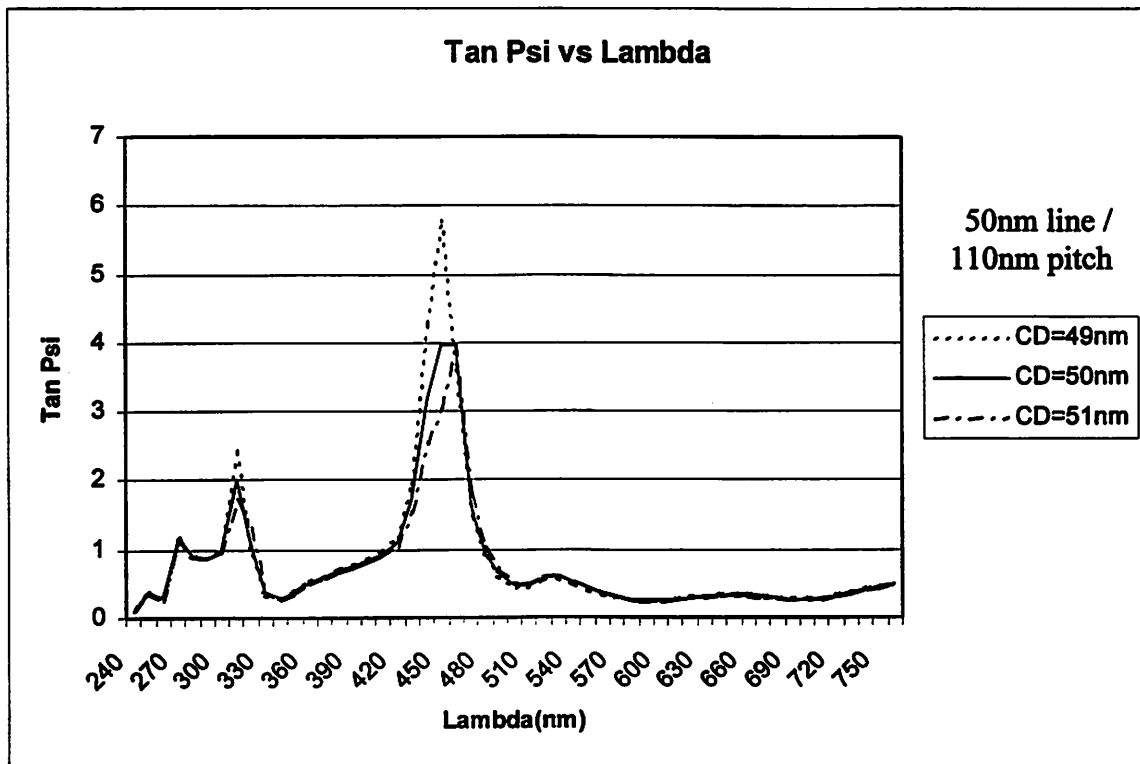
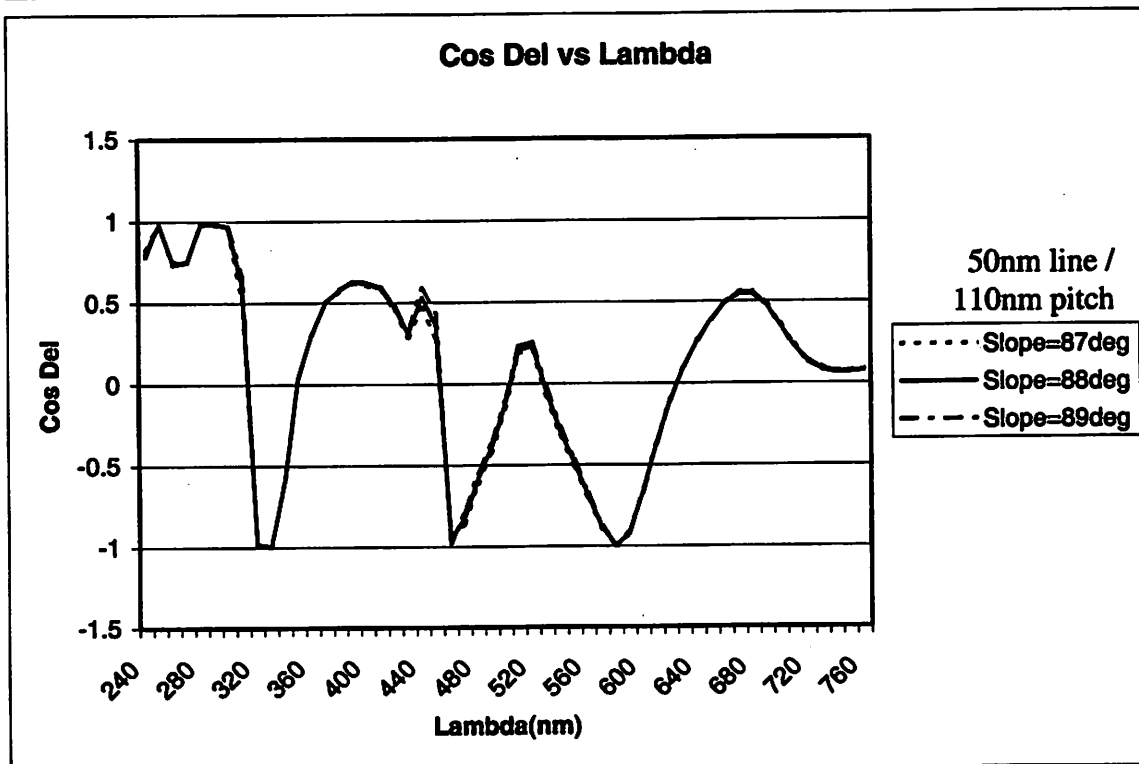
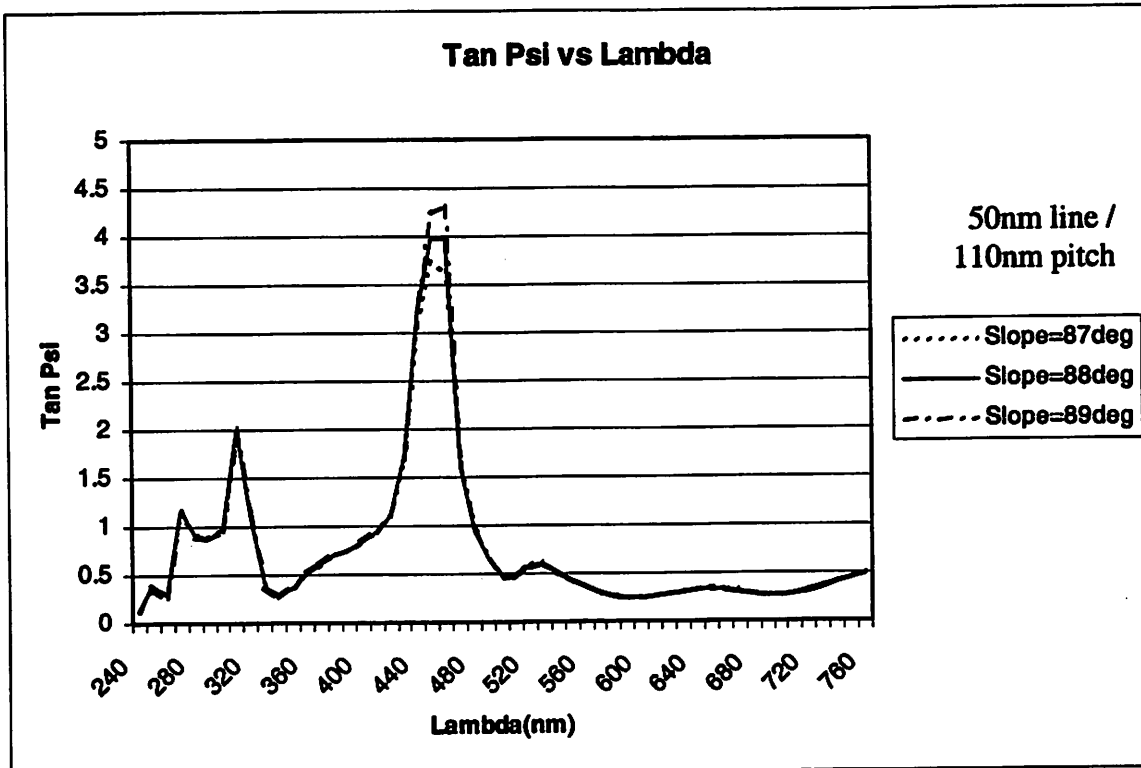
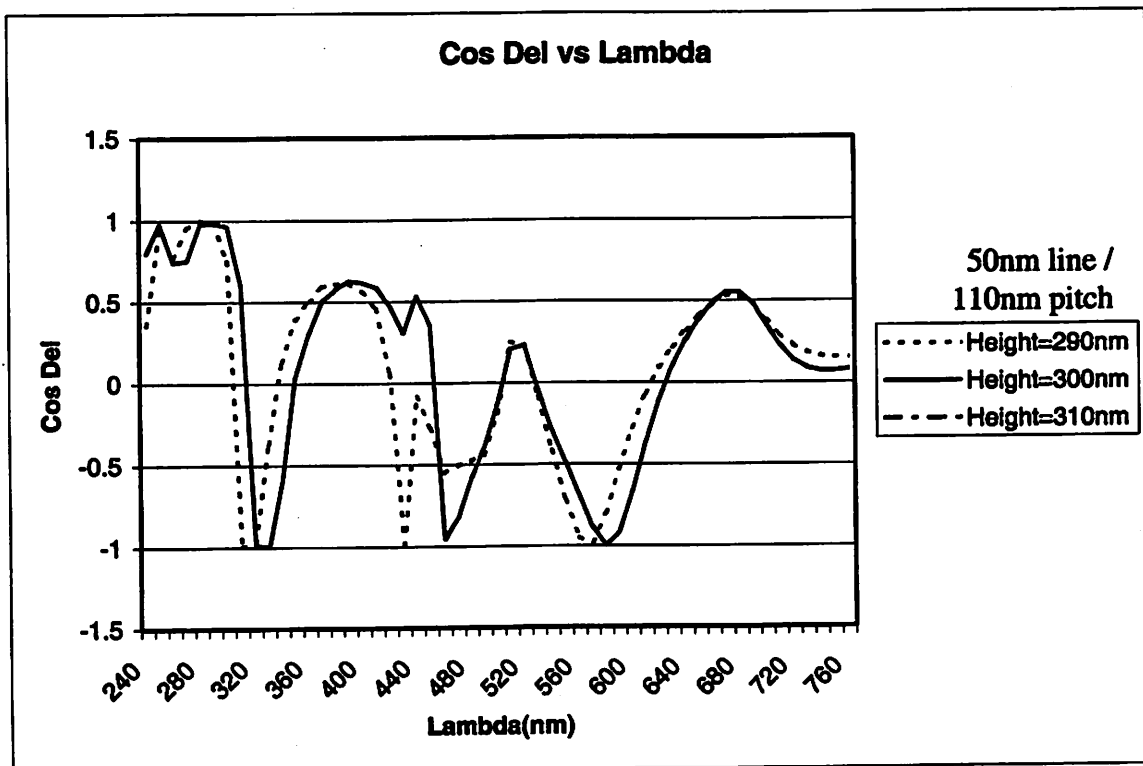
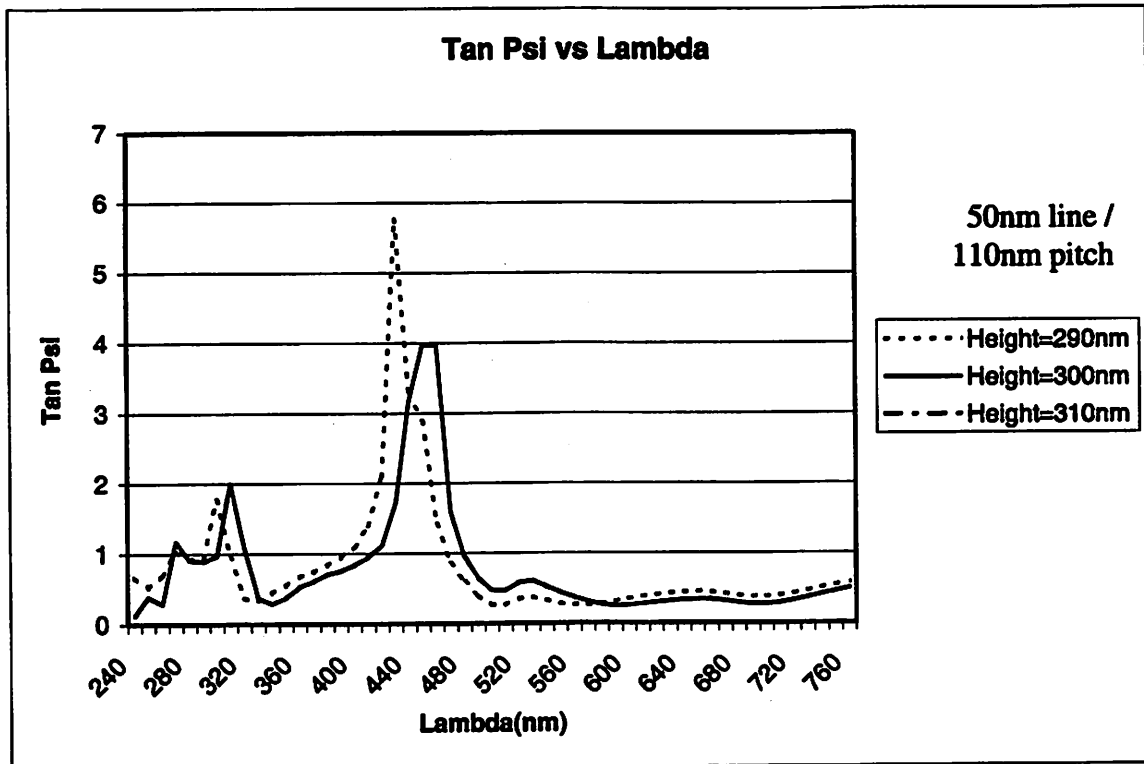
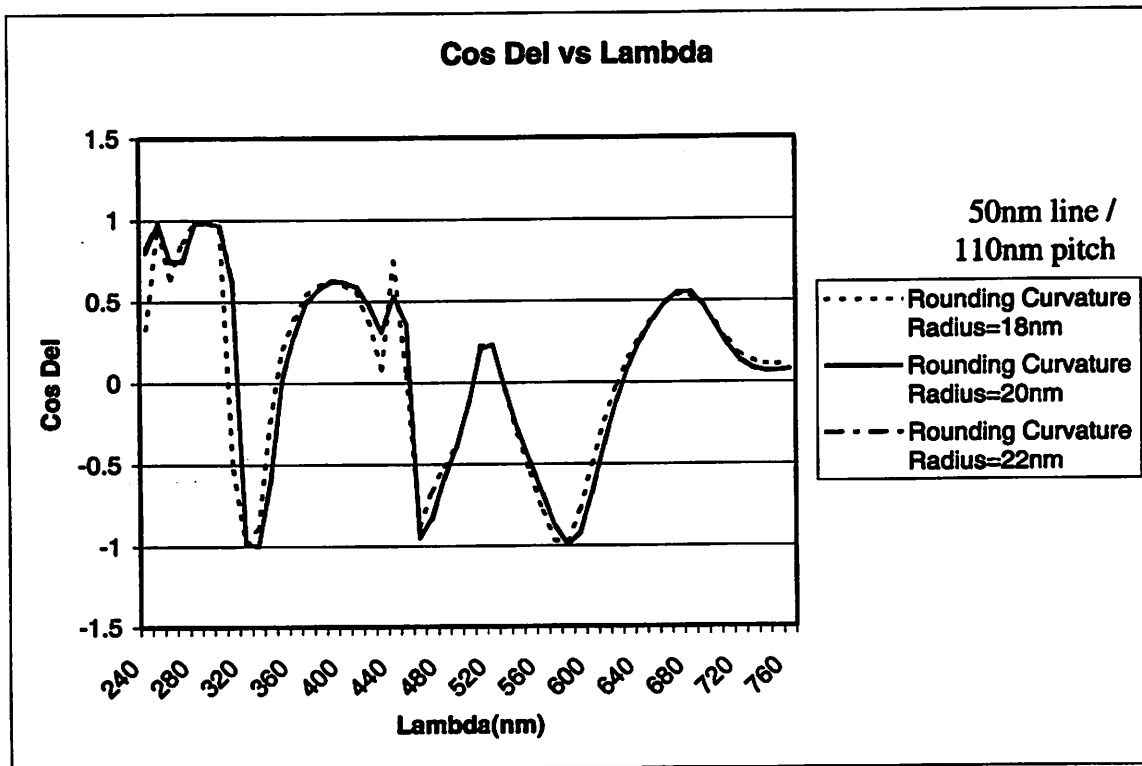
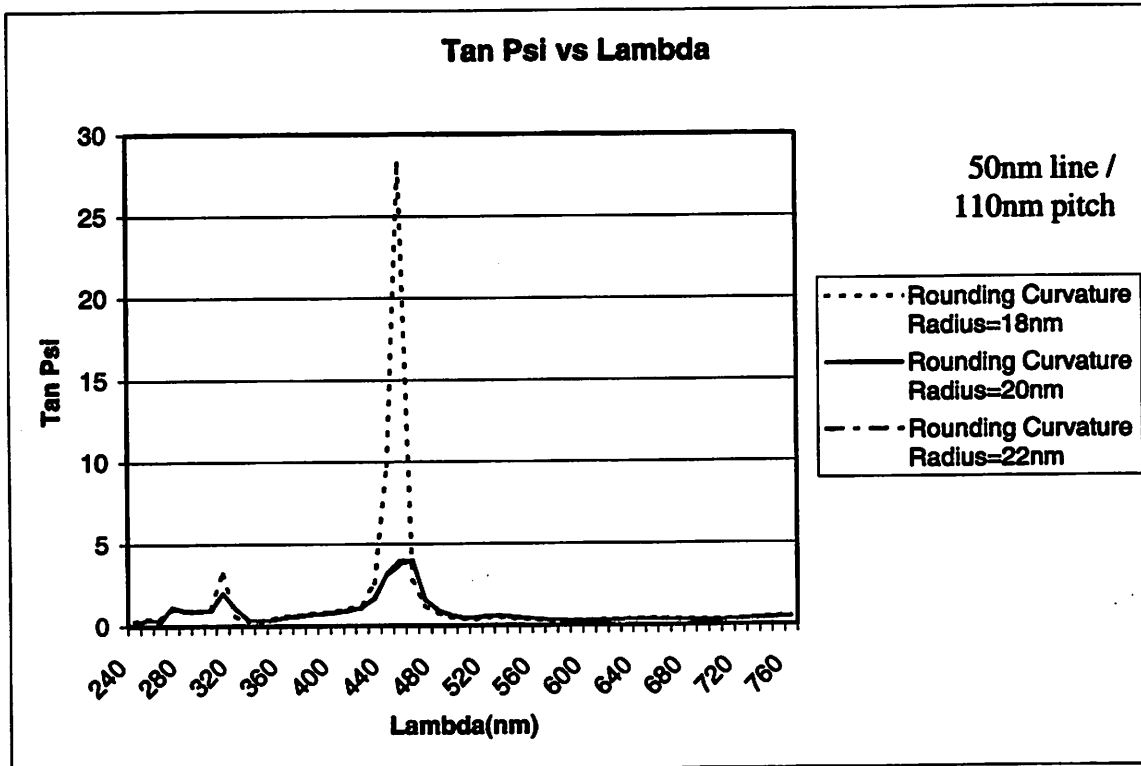


Figure 3.7 (a)-(j) Scatterometric Response for 50nm Line / 110nm Pitch









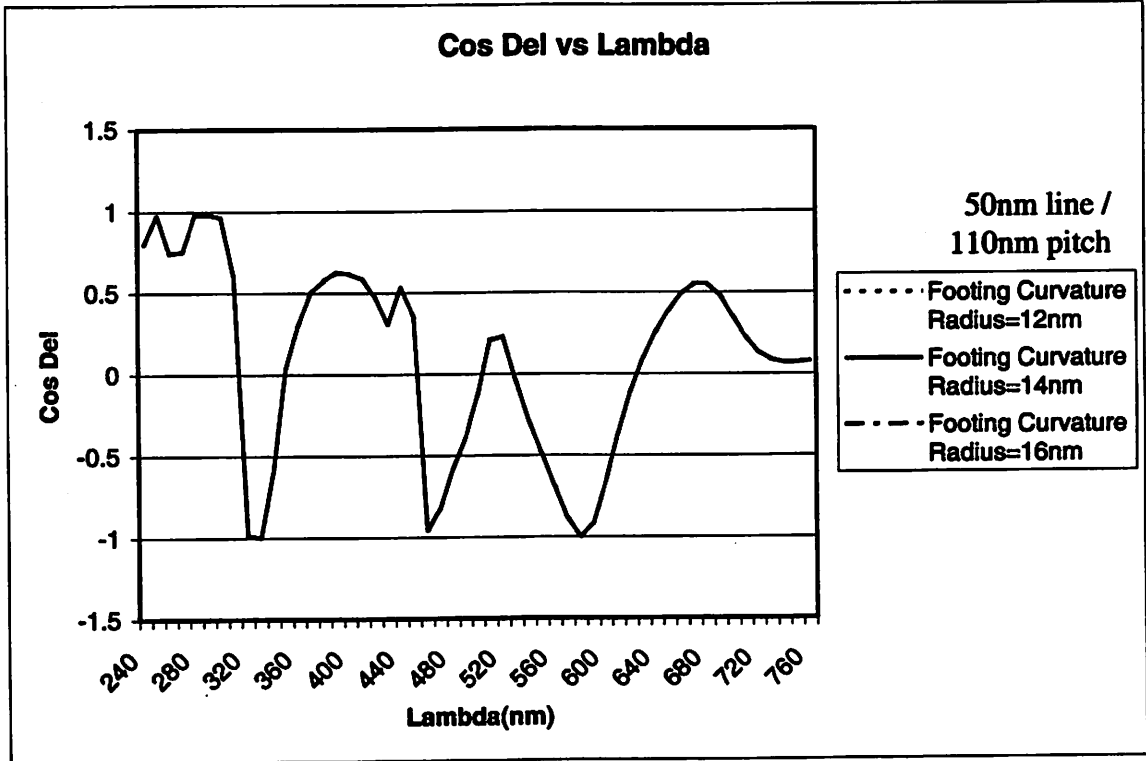
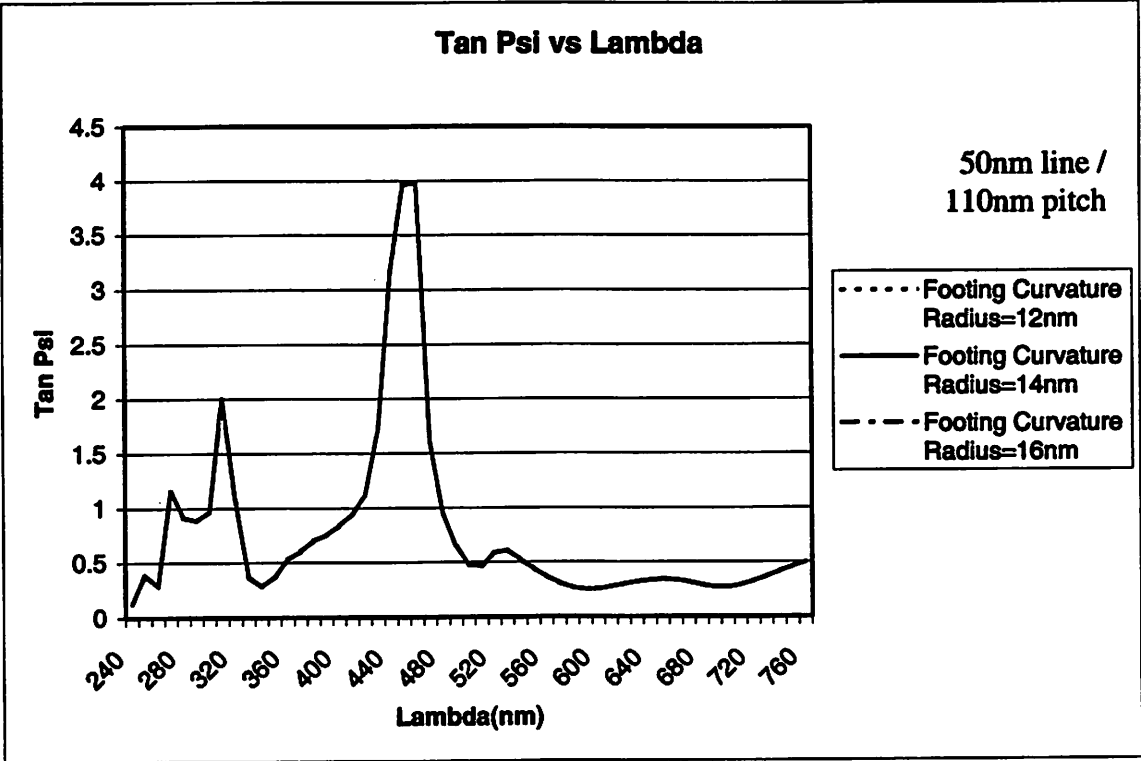
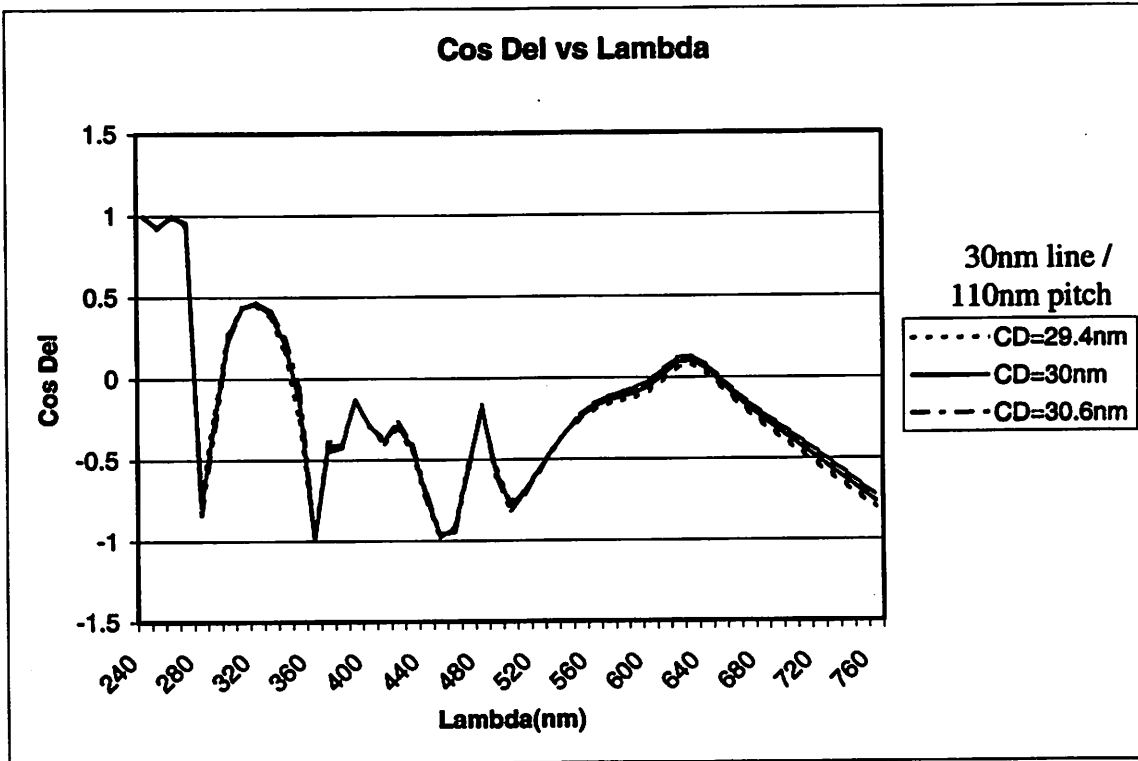
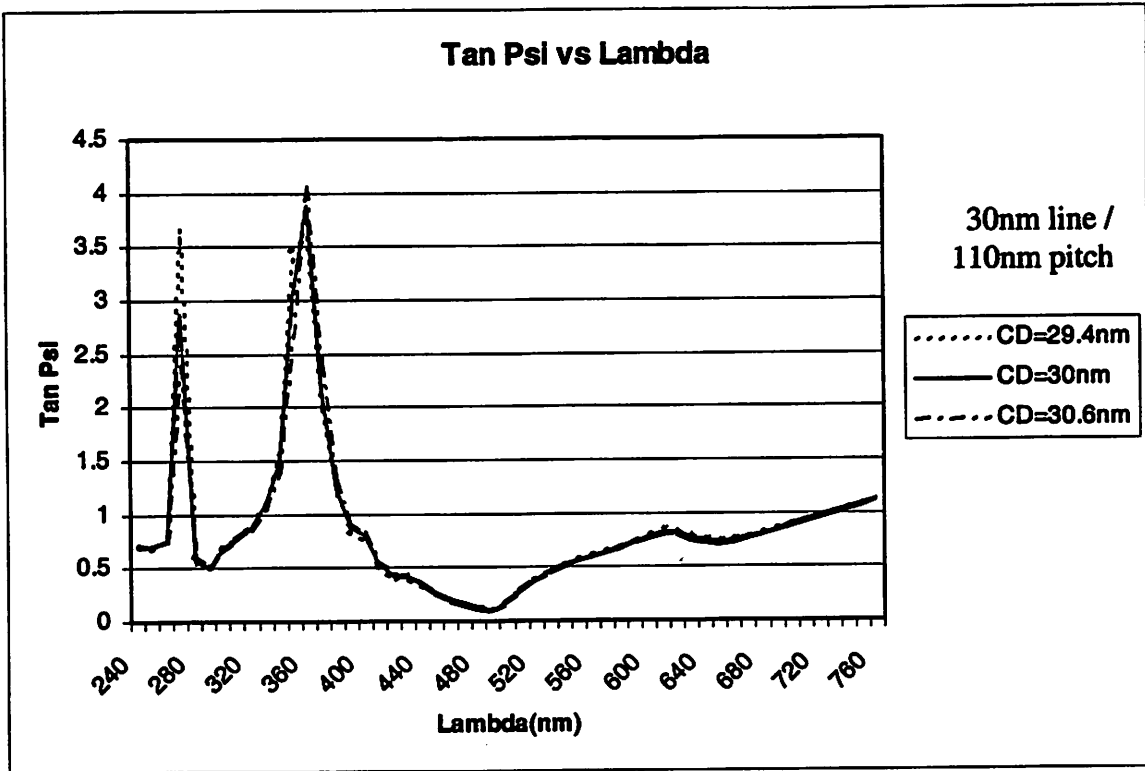
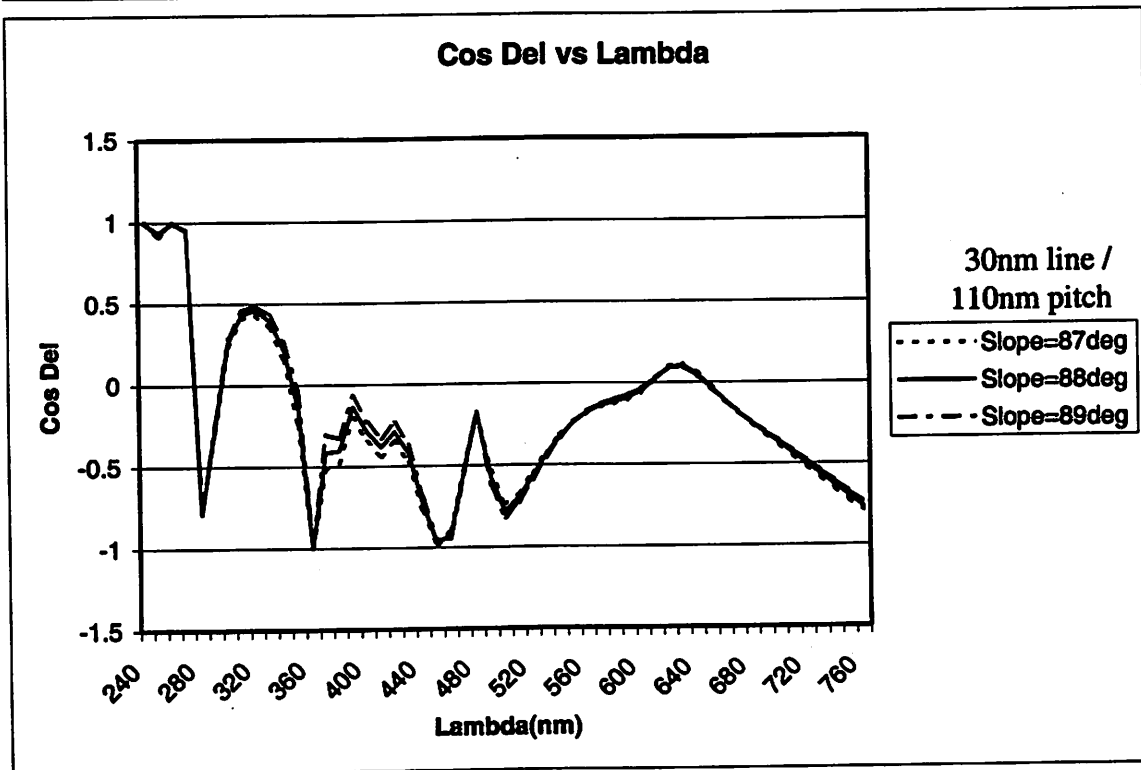
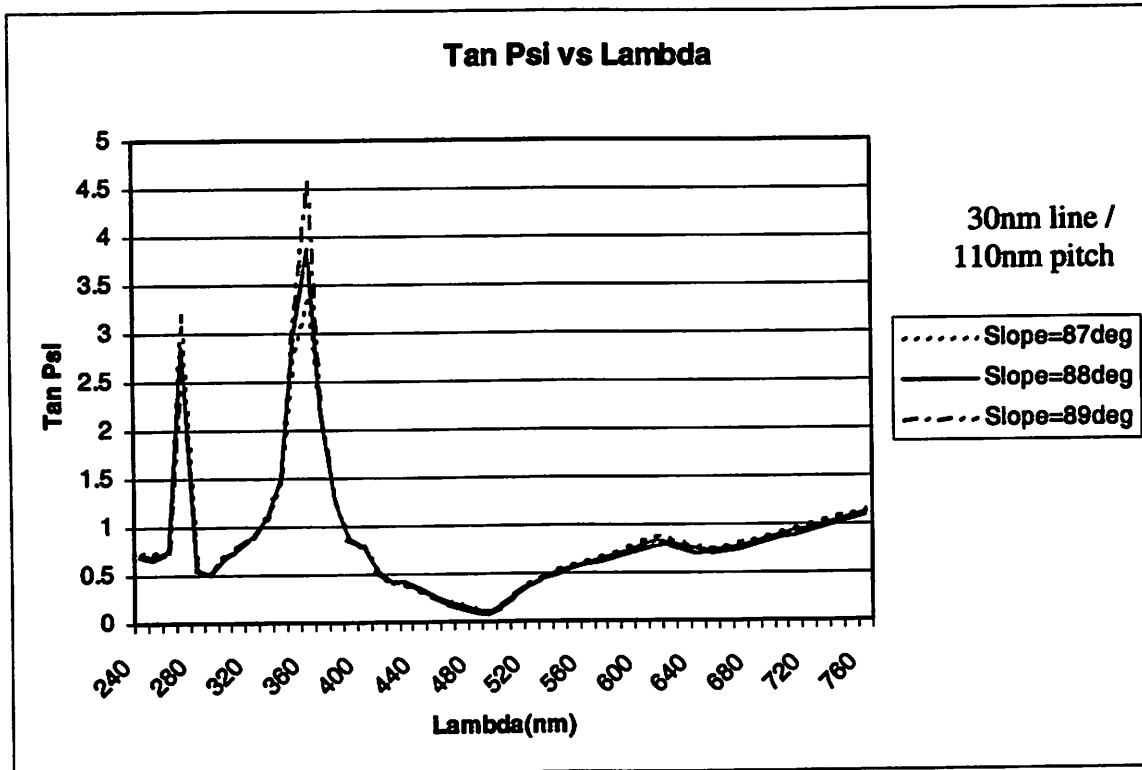
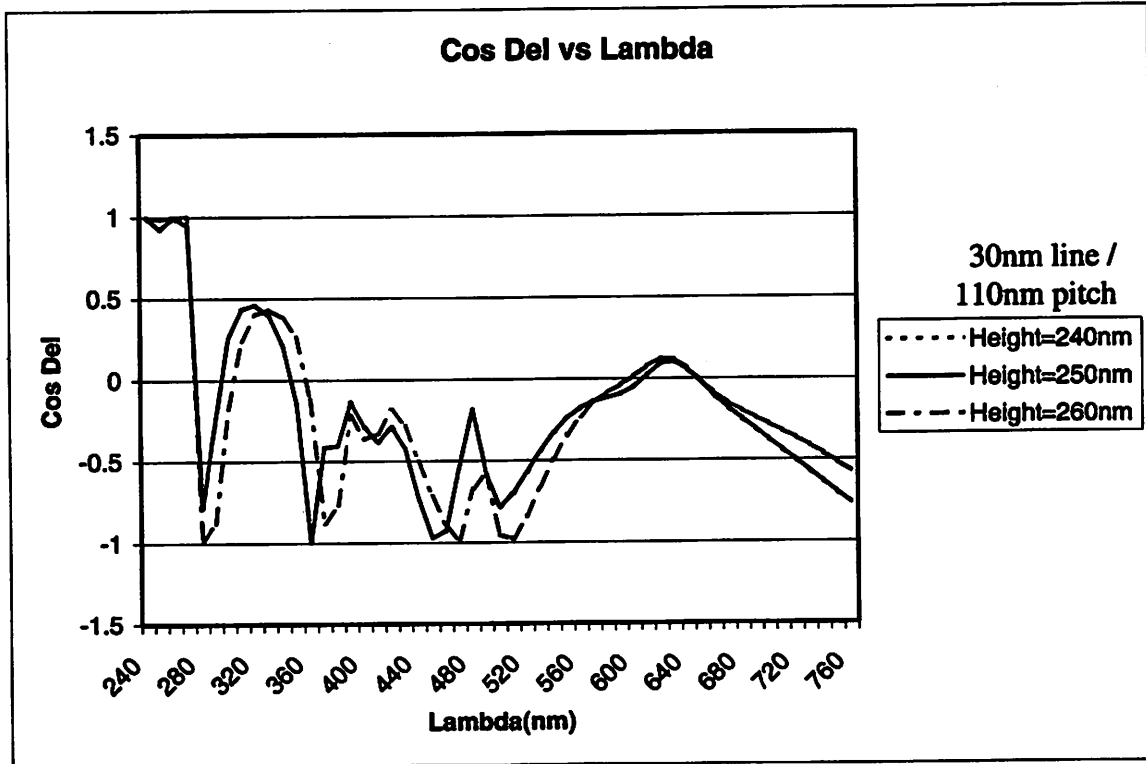
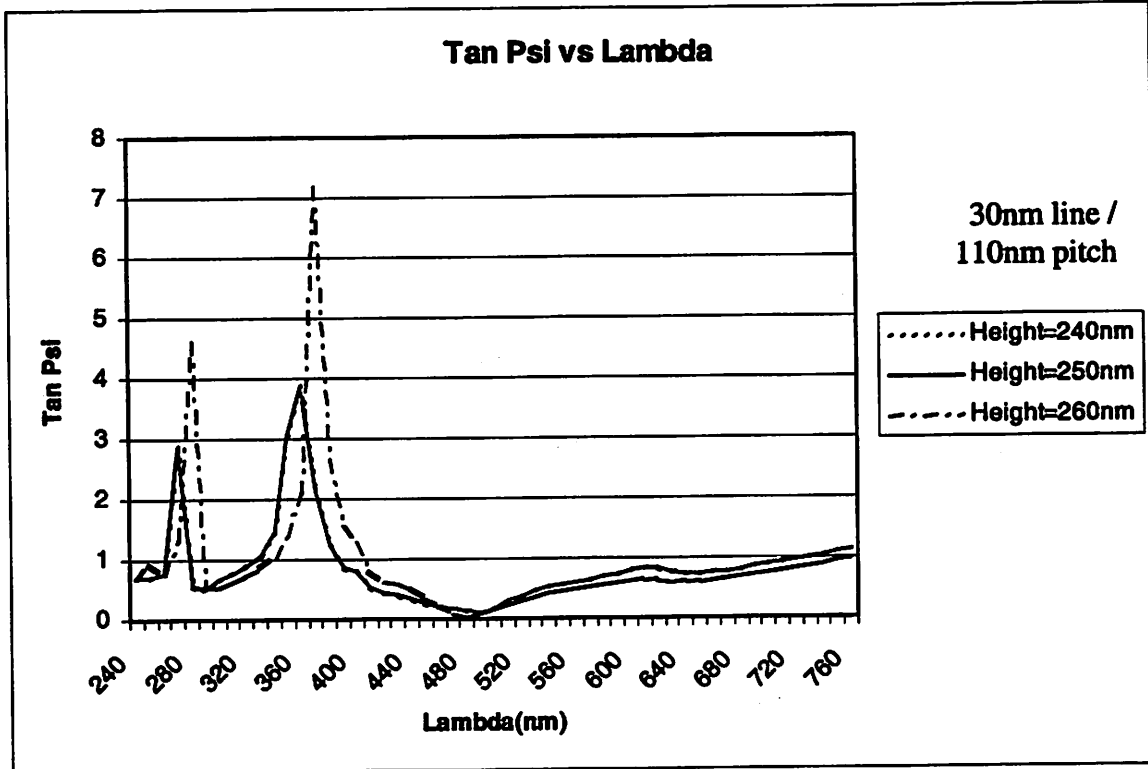
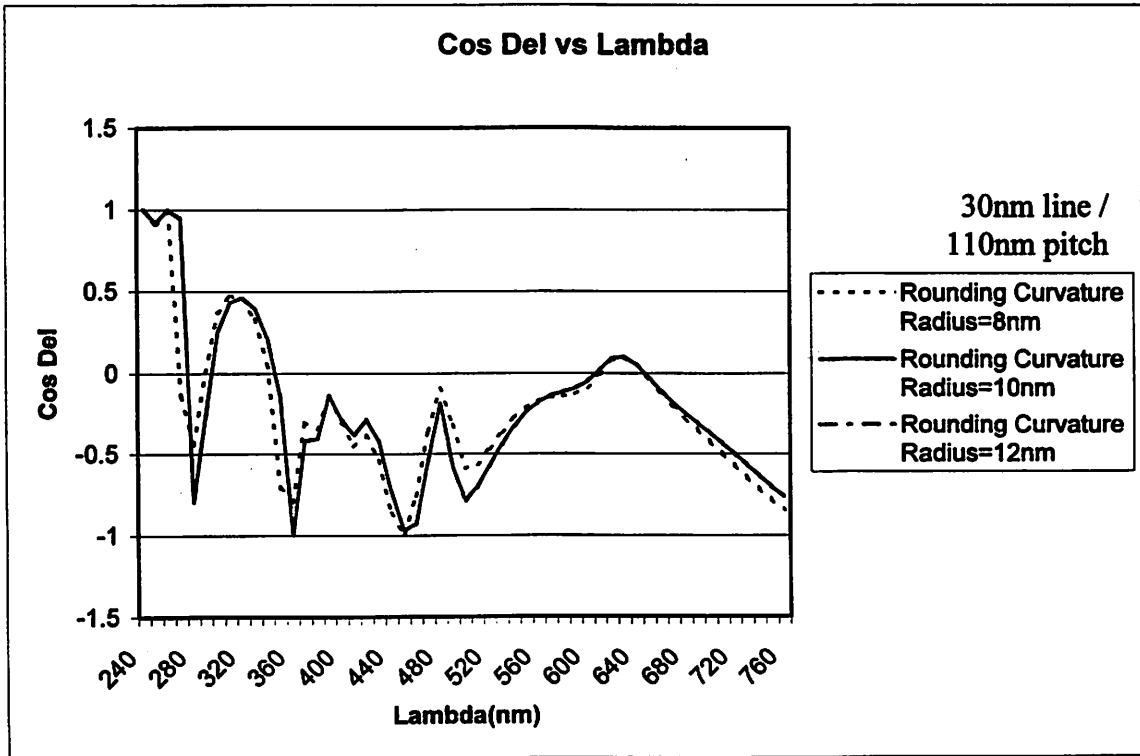
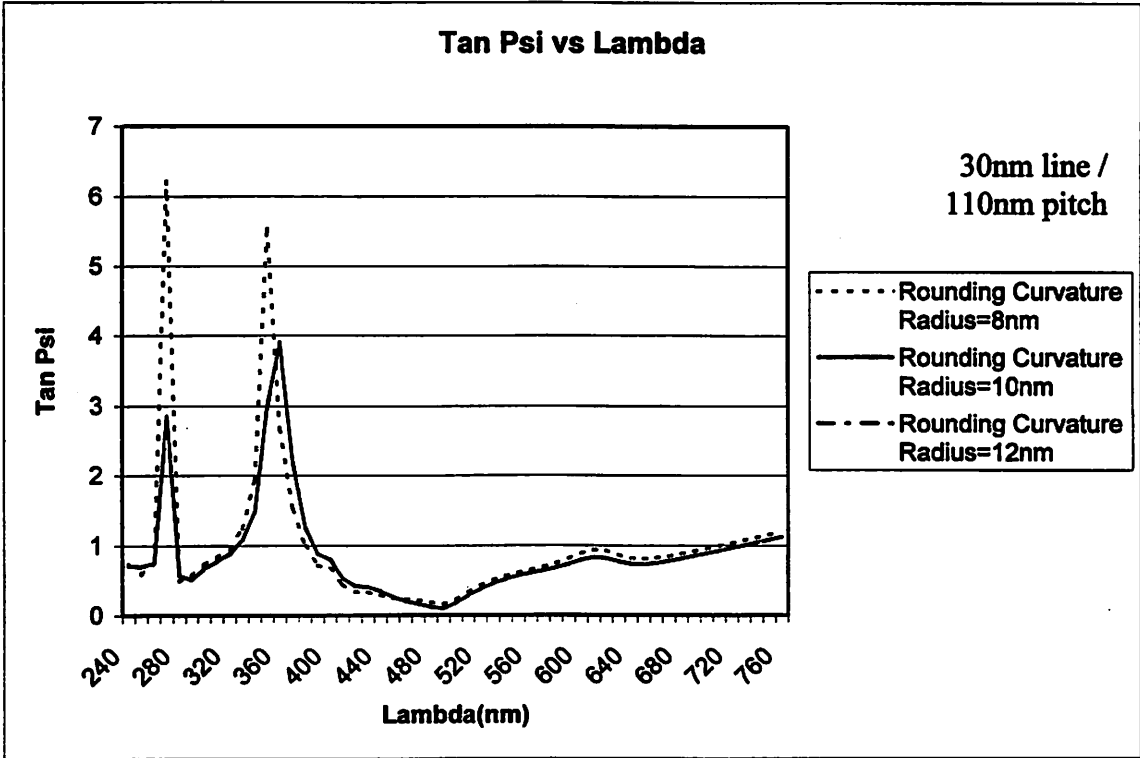


Figure 3.8 (a)-(j) Scatterometric Response for 30nm Line / 110nm Pitch









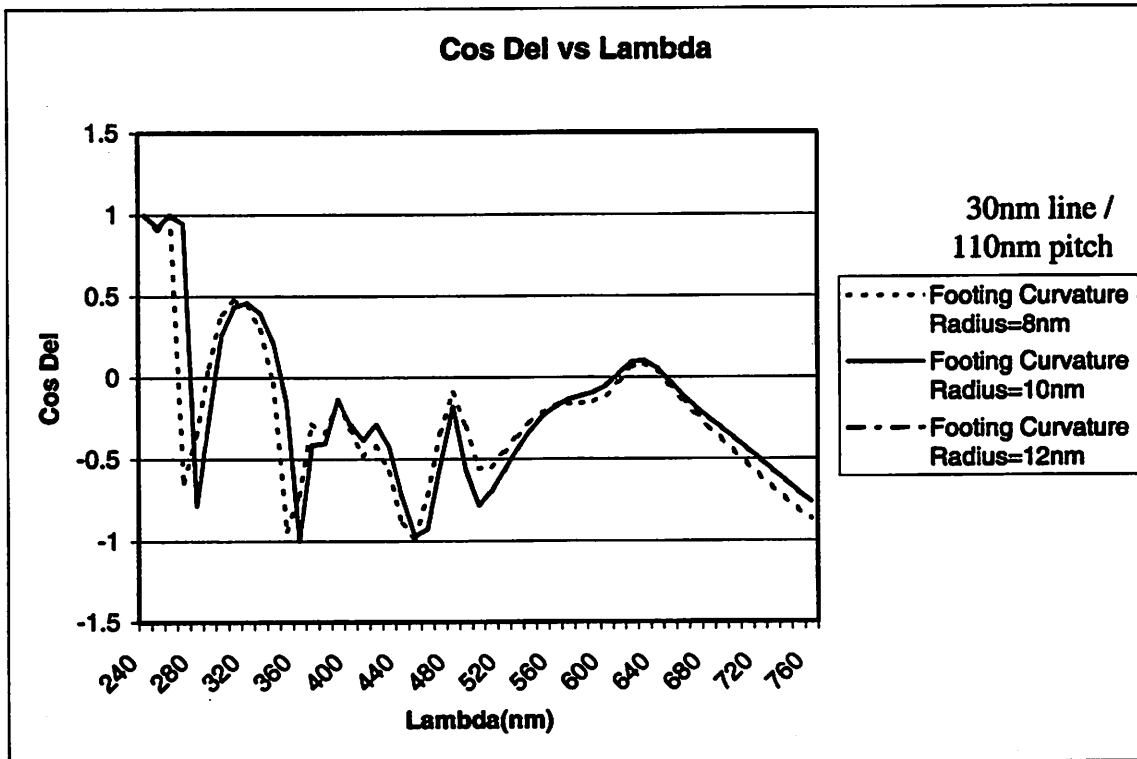
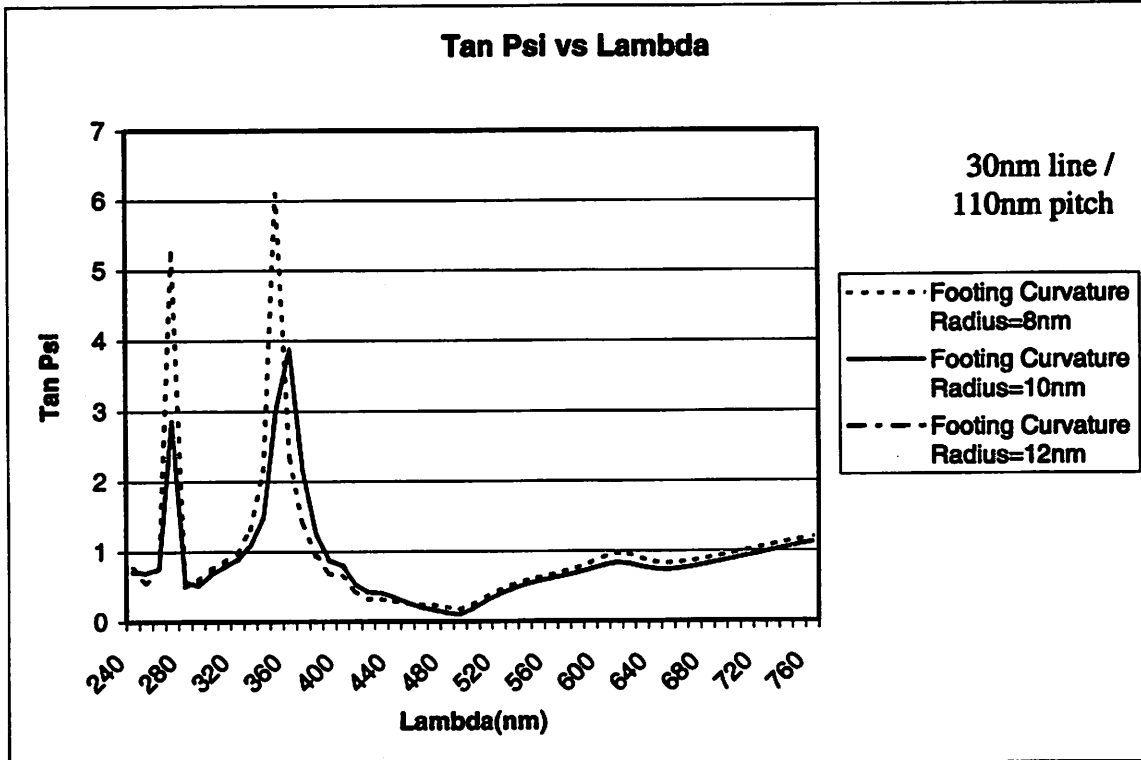
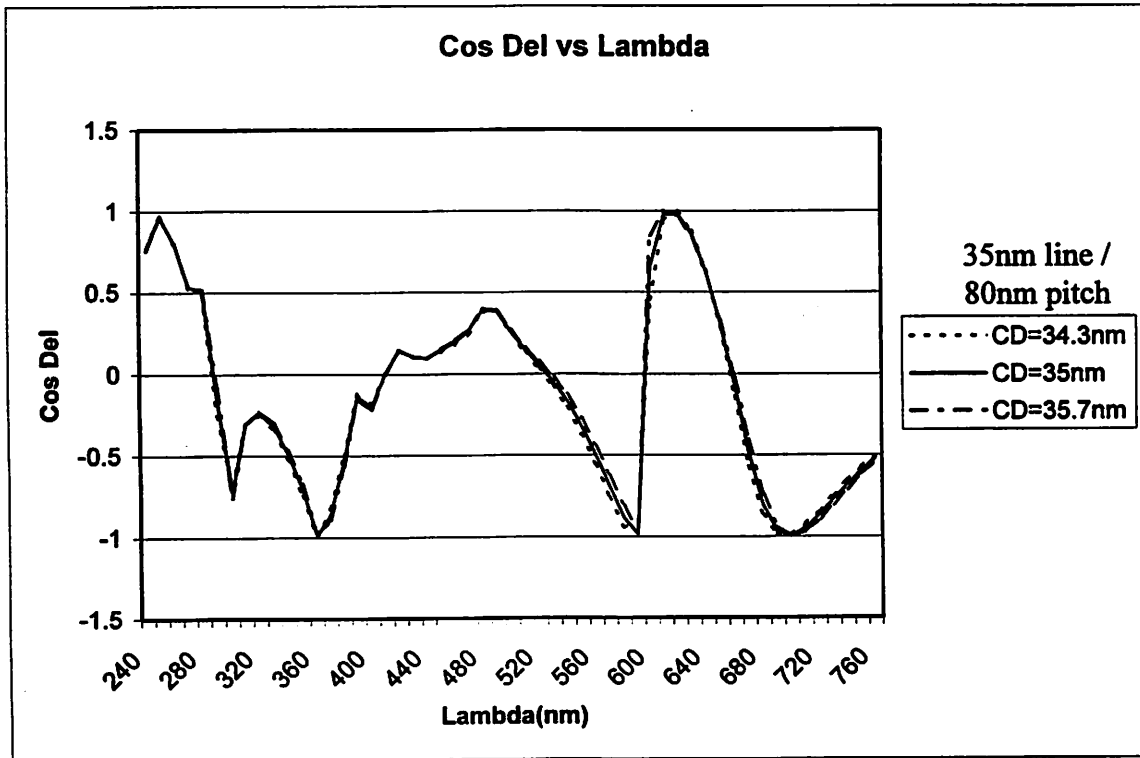
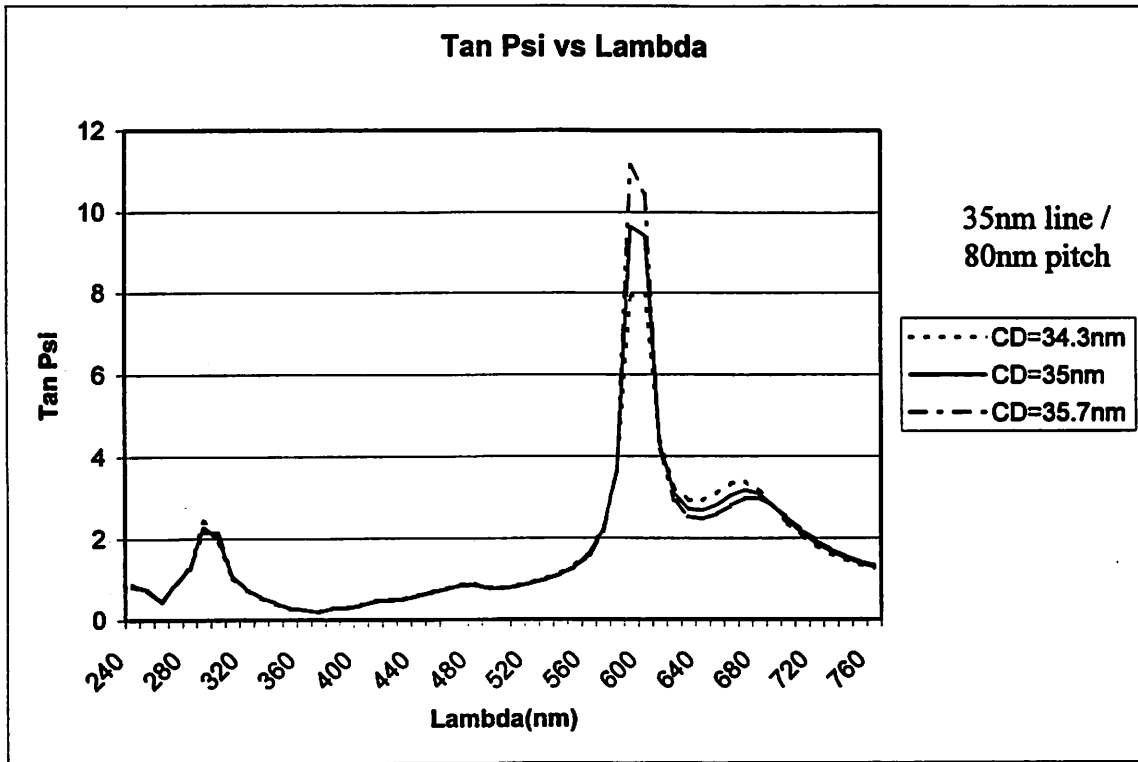
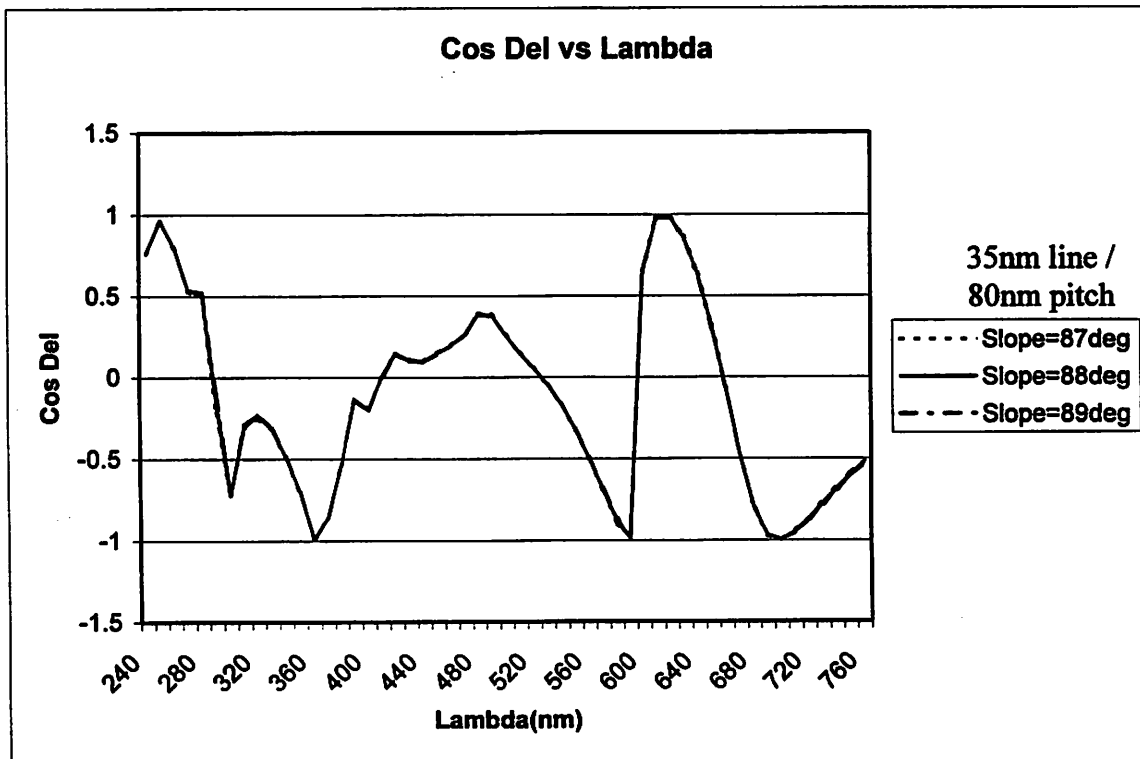
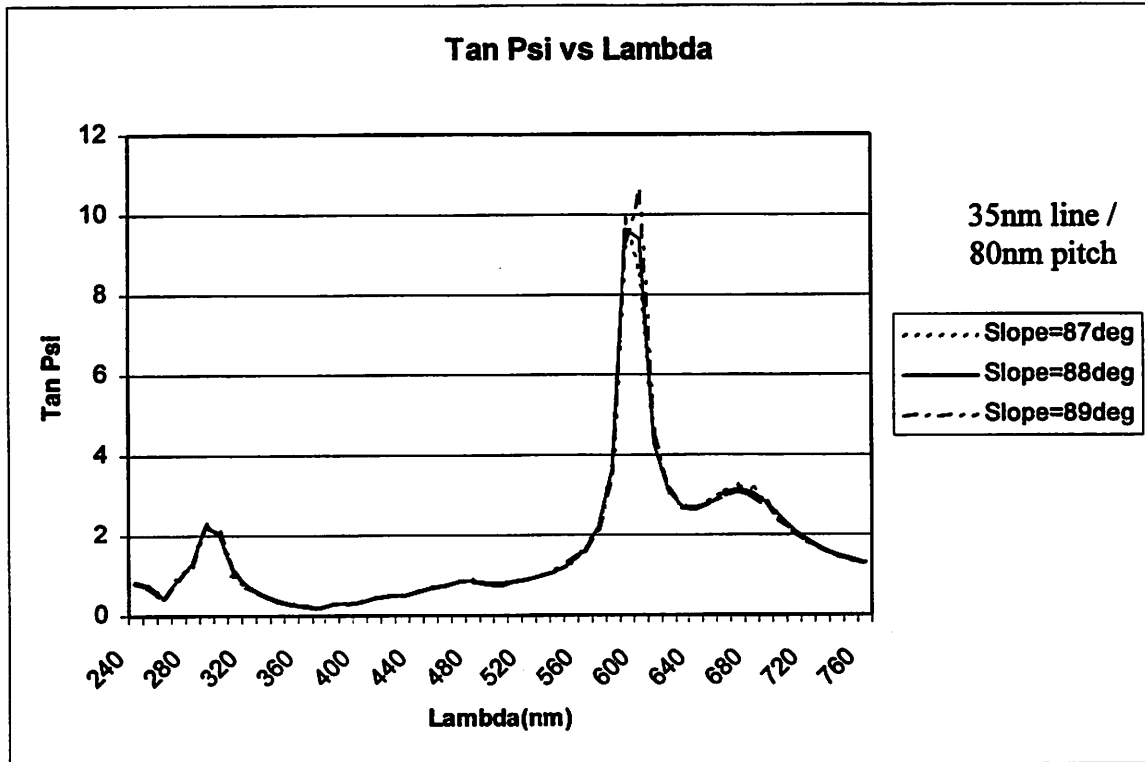
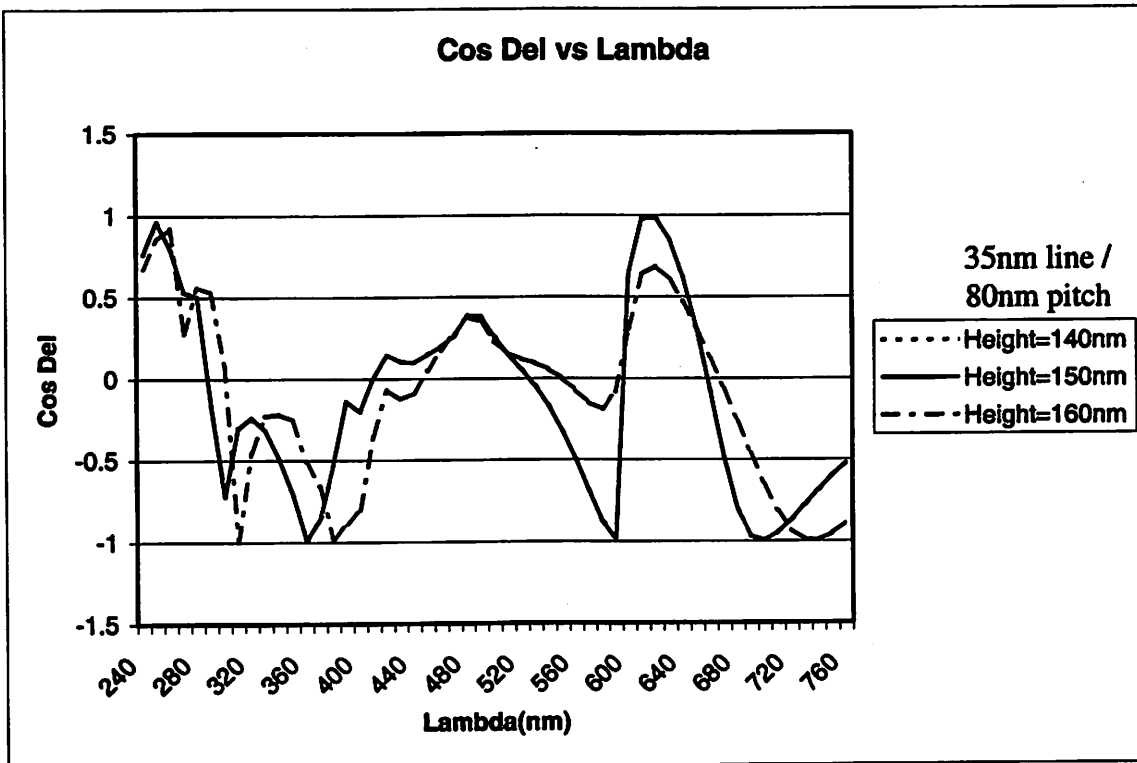
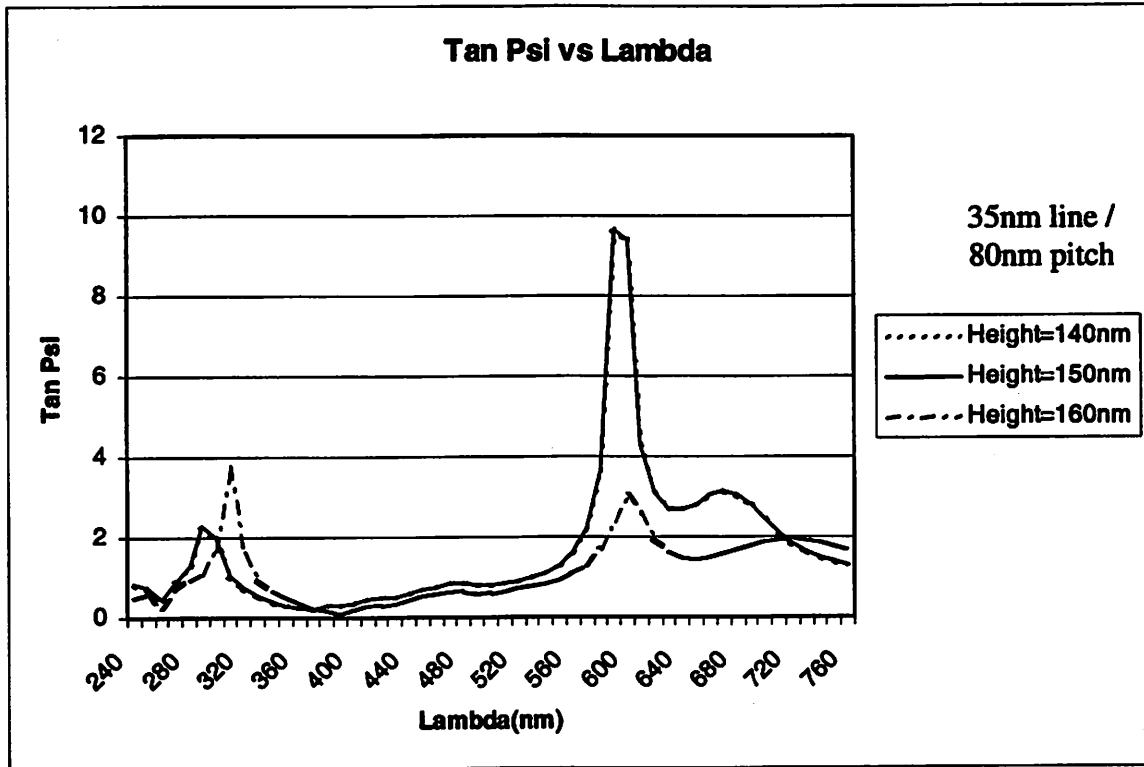
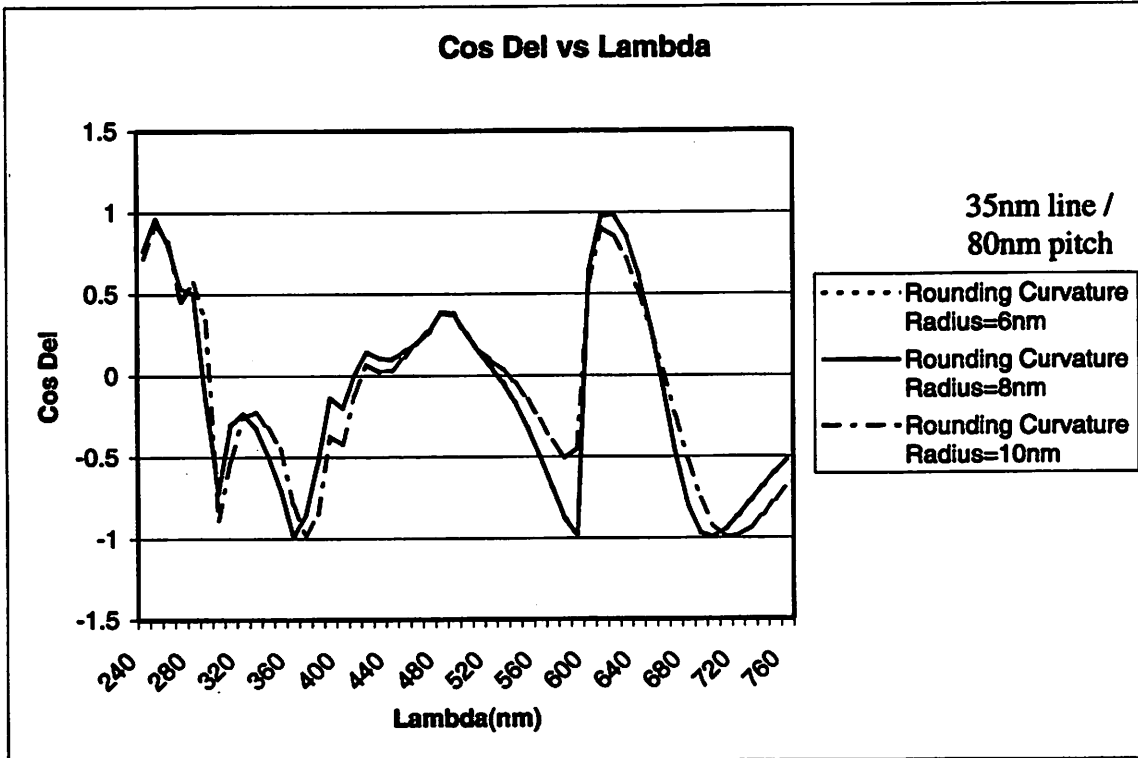
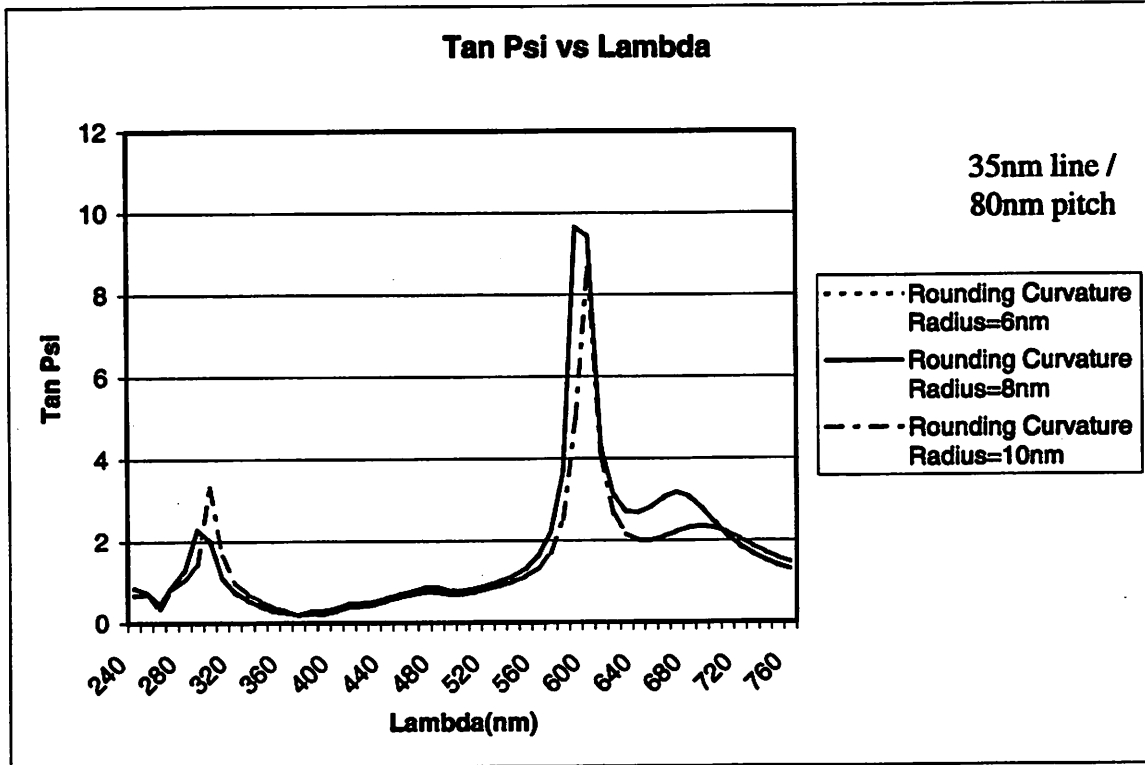


Figure 3.9 (a)-(j) Scatterometric Response for 35nm Line / 80nm Pitch









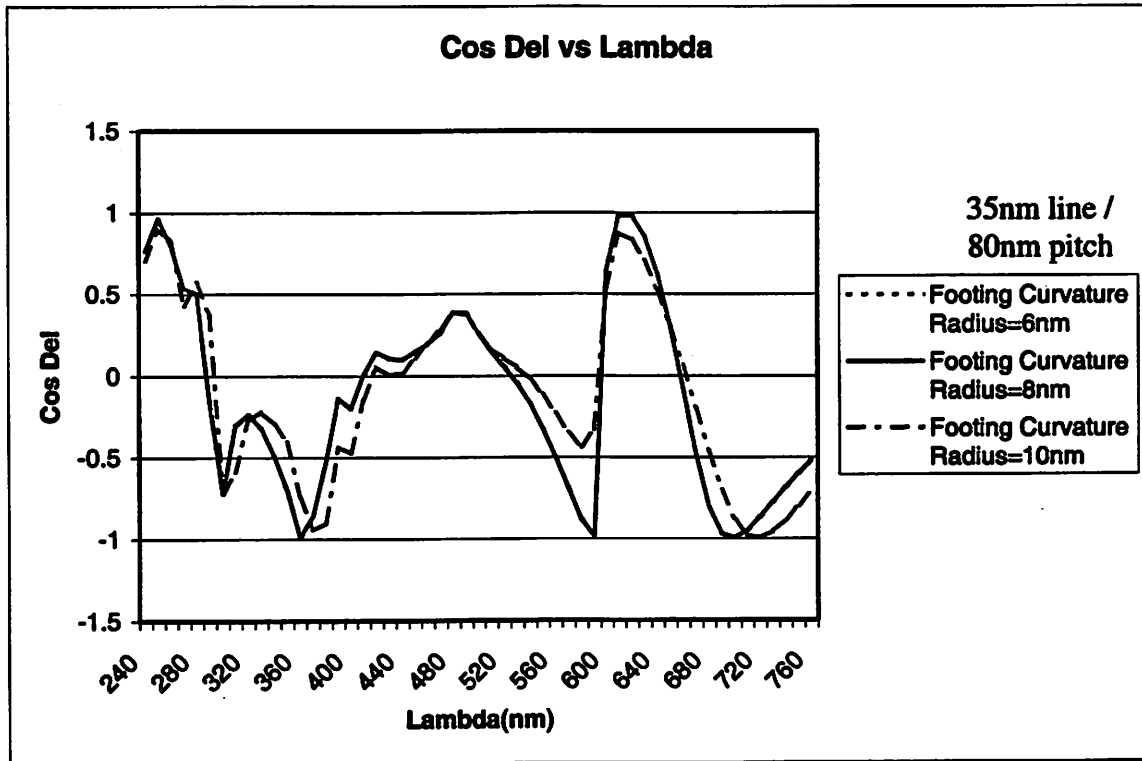
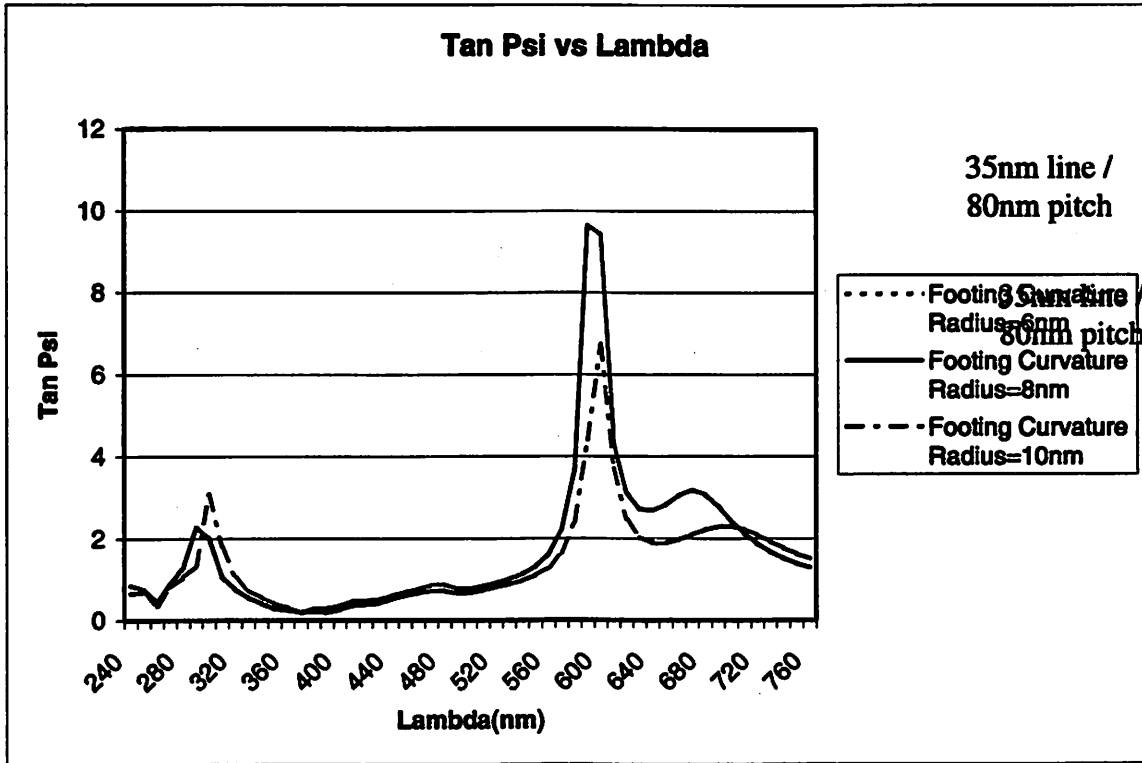
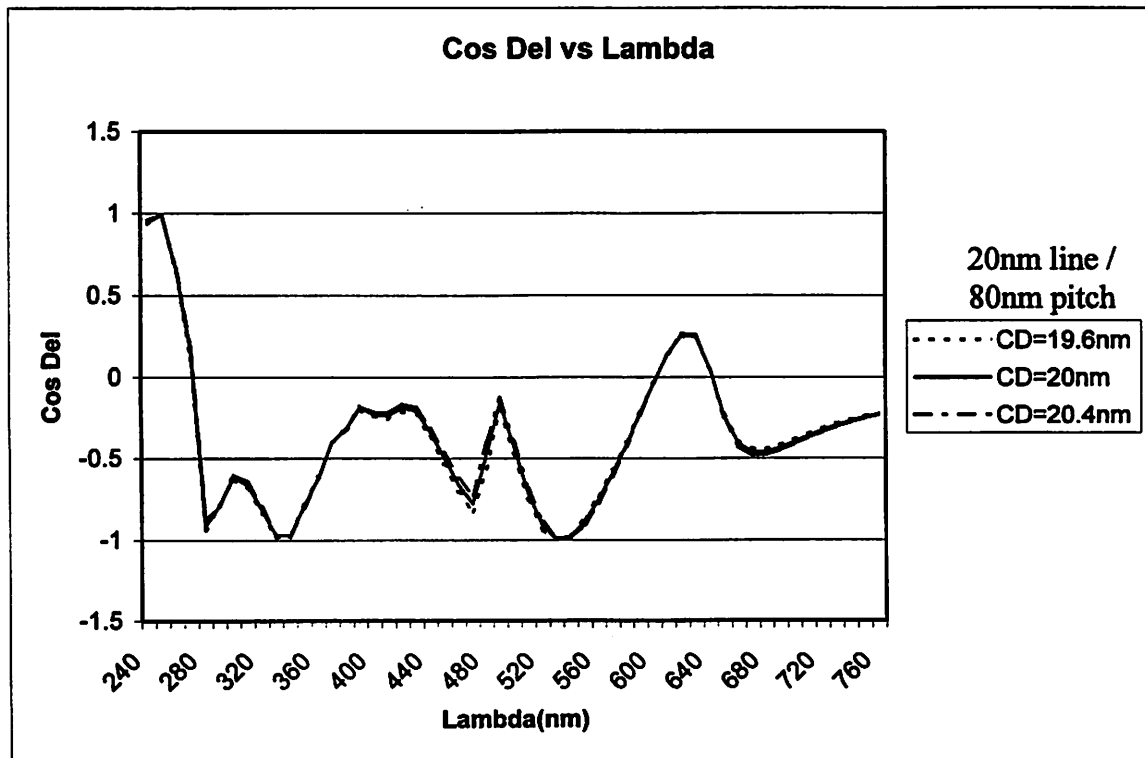
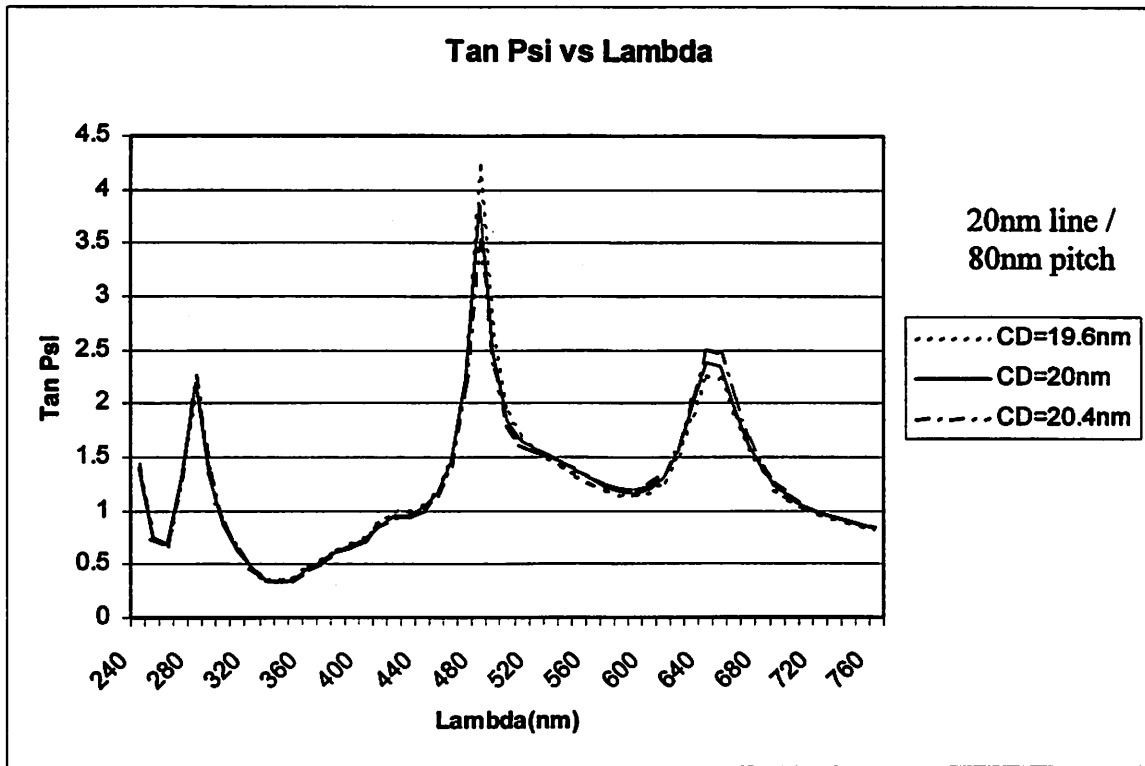
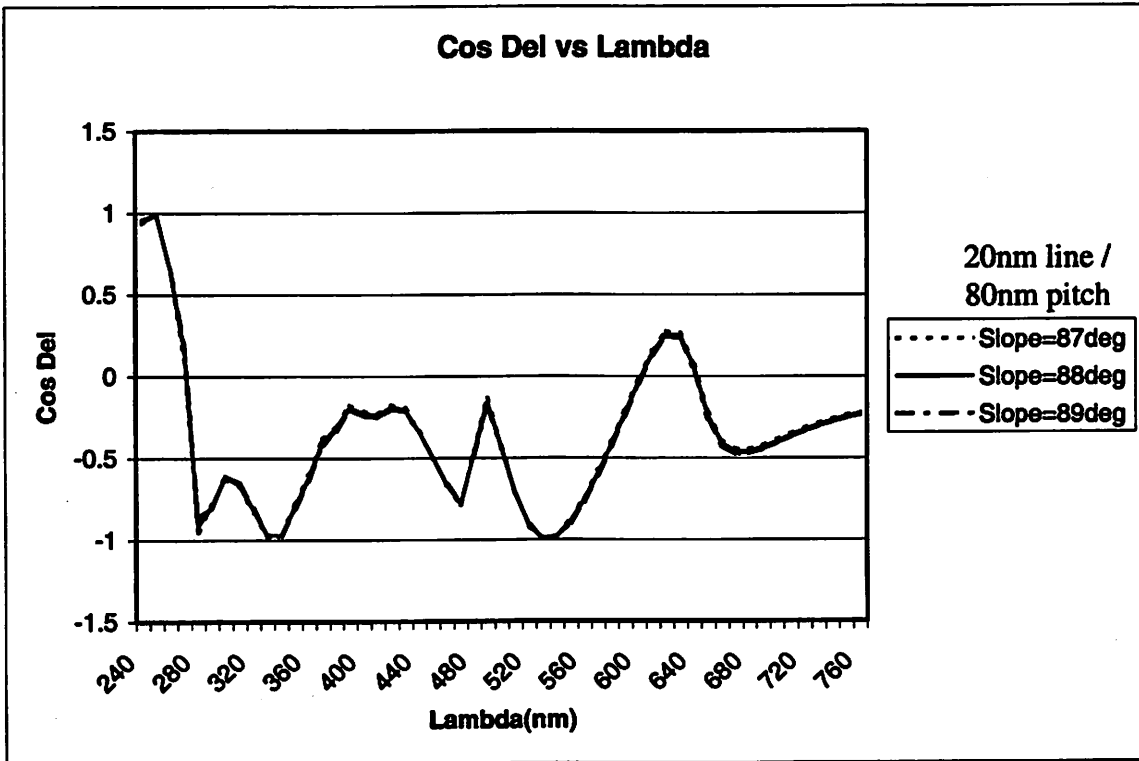
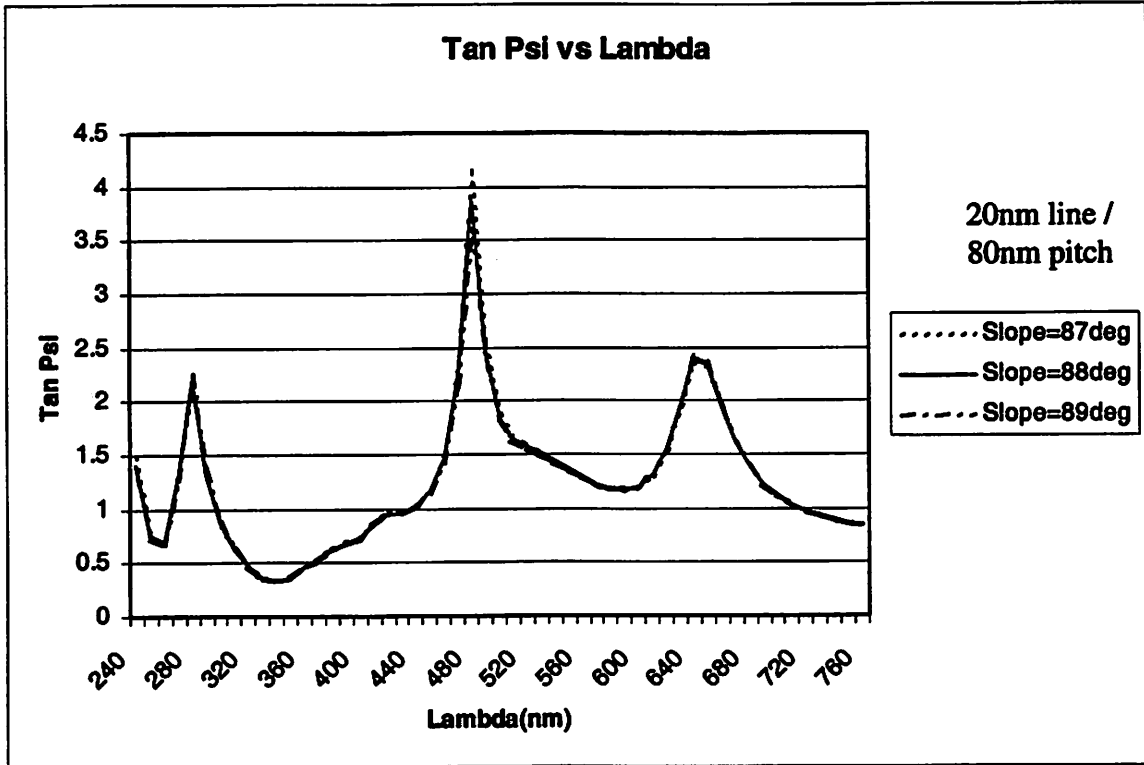
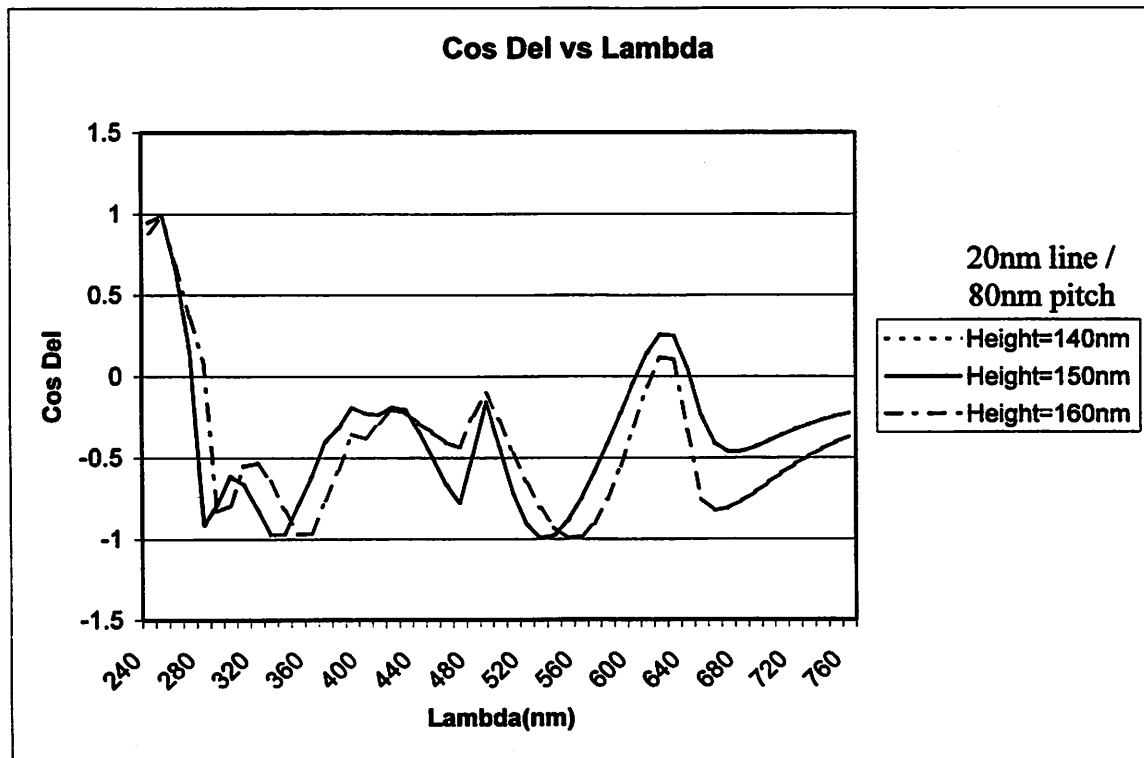
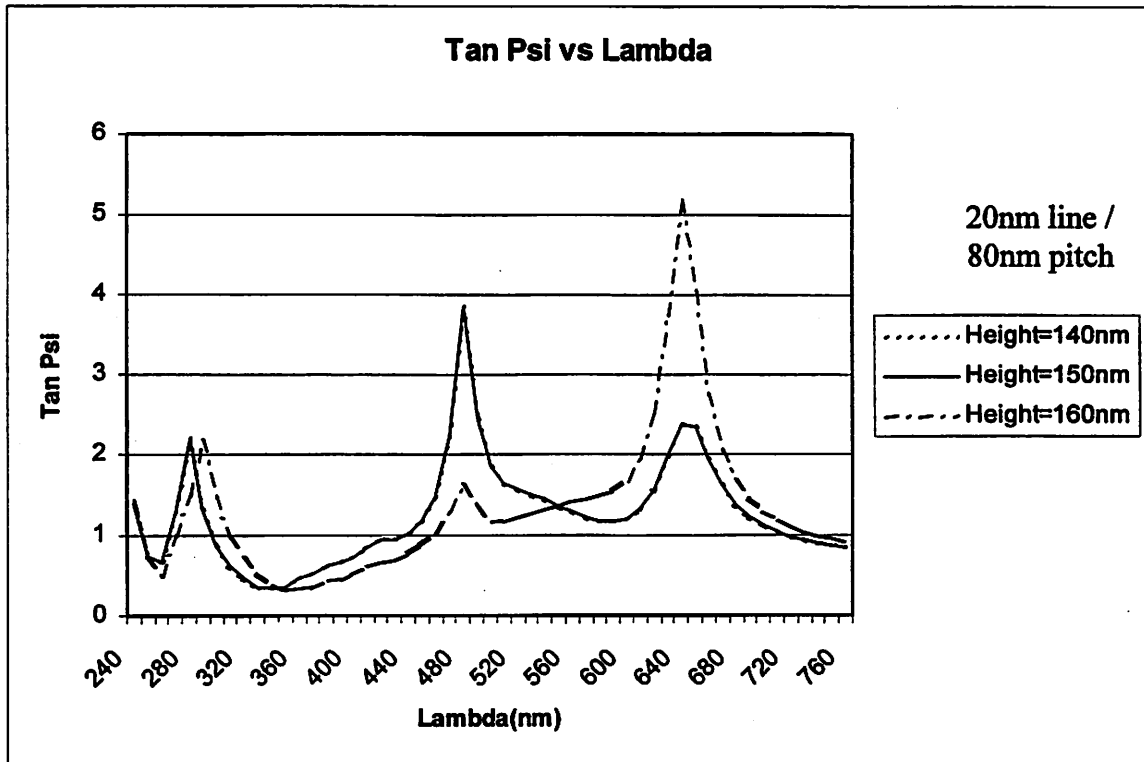
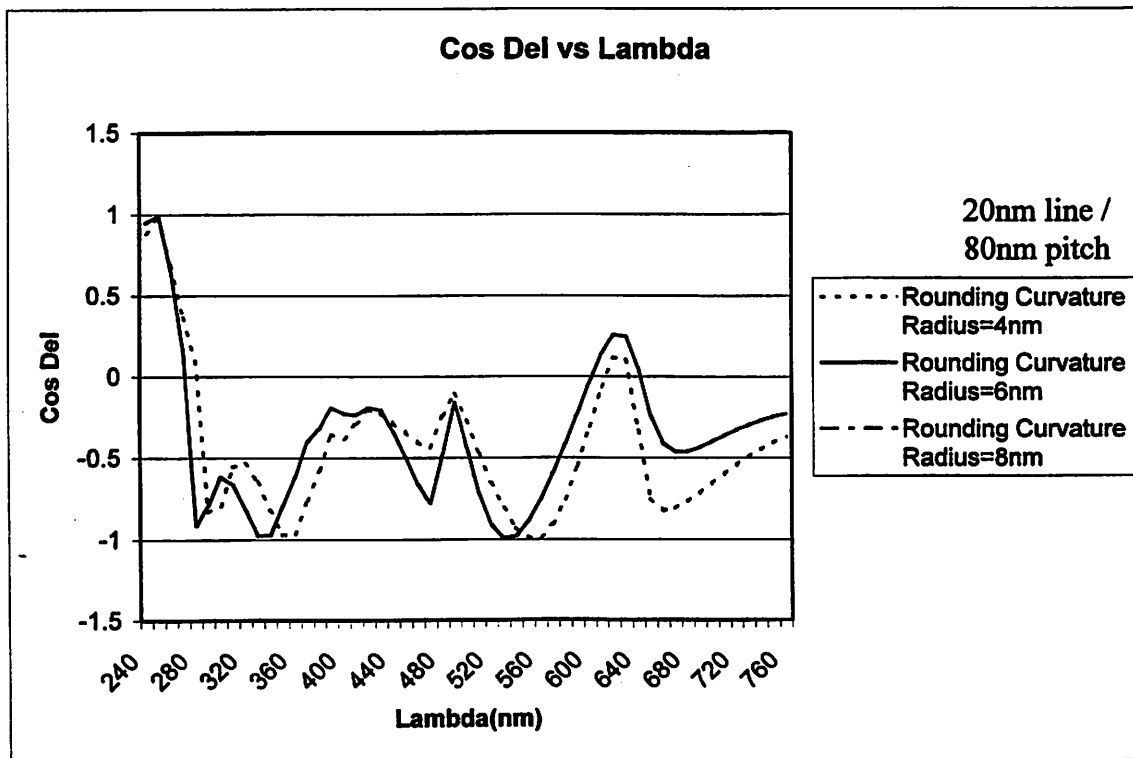
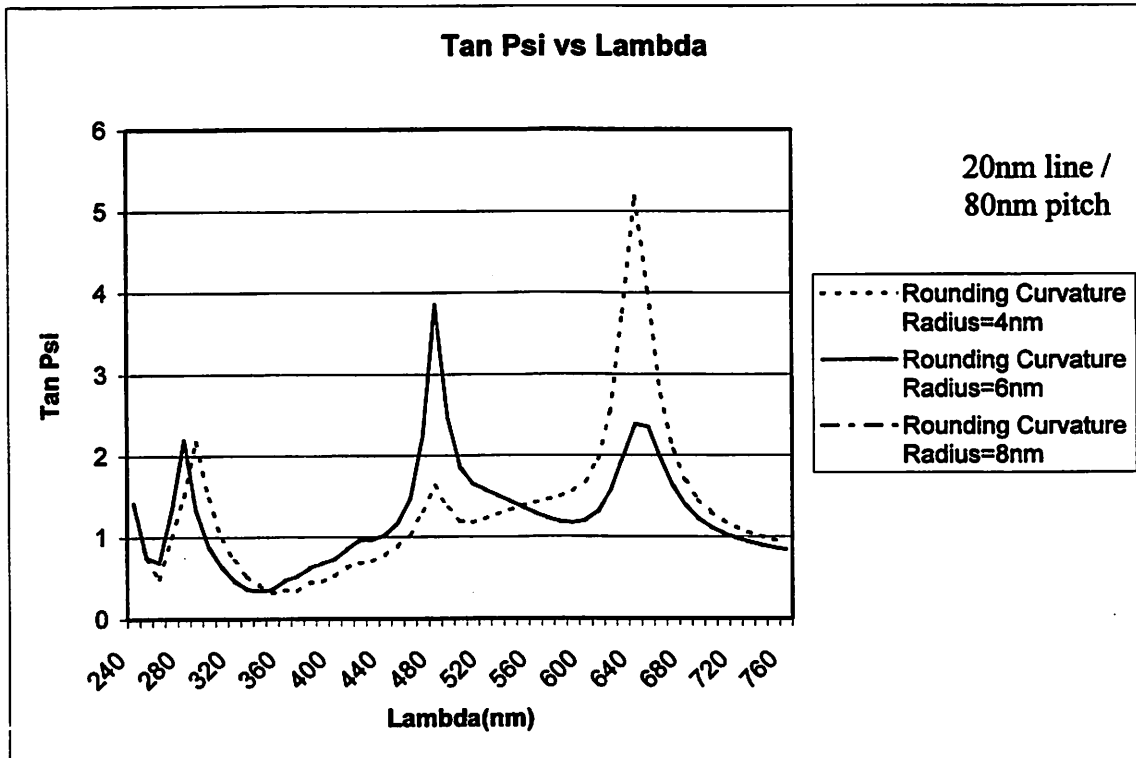


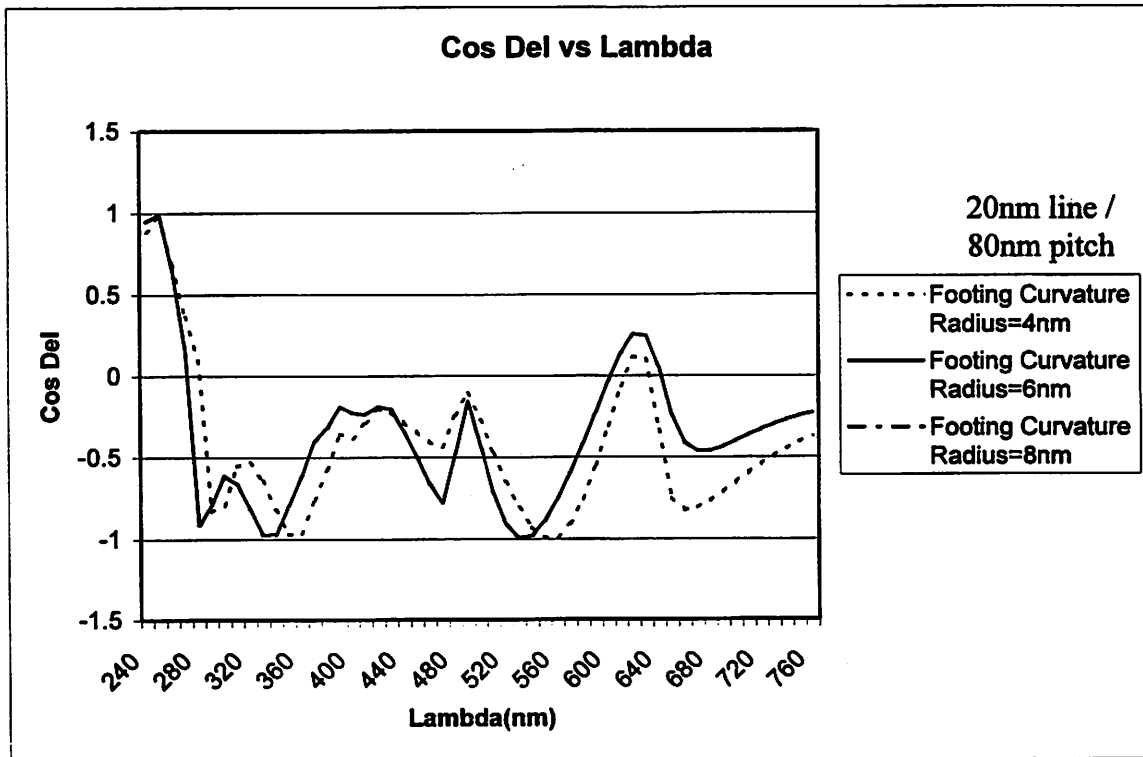
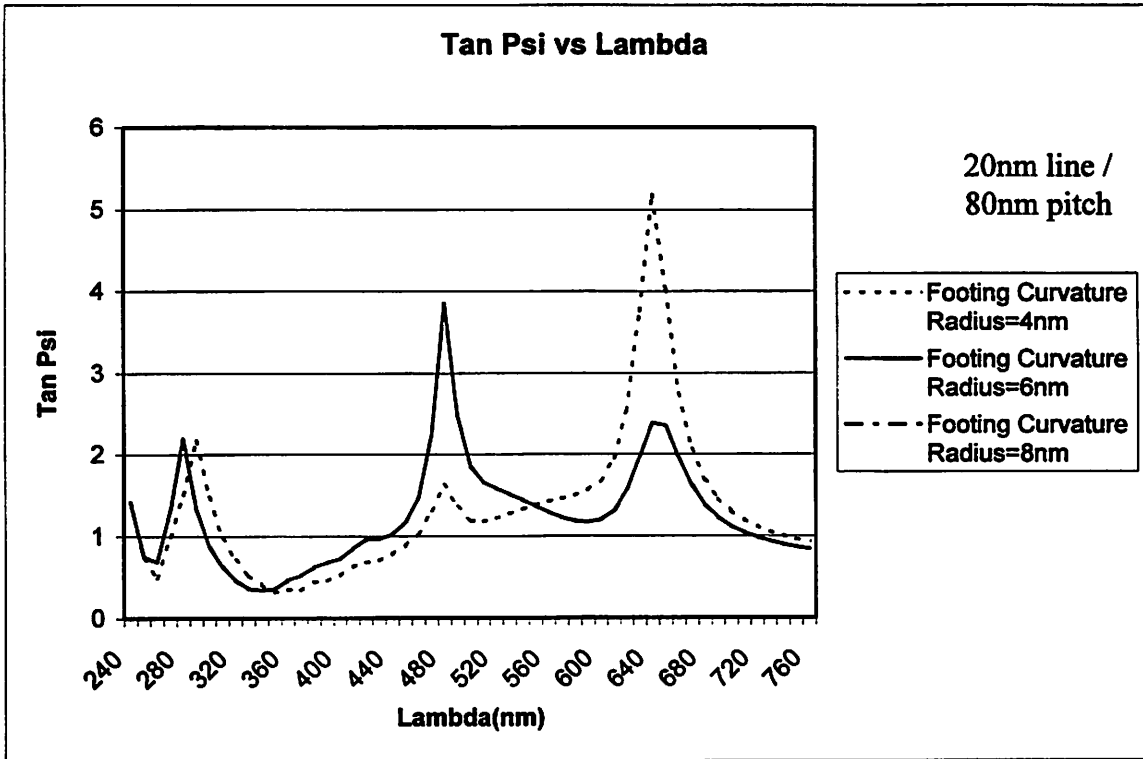
Figure 3.10 (a)-(j) Scatterometric Response for 20nm Line / 80nm Pitch











3.3 Conclusion

The figures show that the sensitivity differs for each profile parameter. For CD variation, in all simulations, there is theoretical variation in simulated electromagnetic response. However, for variation in height, as well as variation in rounding and footing for smaller feature sizes, the difference in simulated response is small in magnitude, which will present itself as a decrease in sensitivity. This could possibly be due to the finite slice thickness inherent in the “construction” of the simulated stacks. The $\tan \Psi$ and $\cos \Delta$ response for each nominal feature is used to determine its associated scatterometric noise when measured using a commercial ellipsometer. This result will then determine the practical sensitivity that can be achieved with spectroscopic scatterometry, which will be discussed in Chapter 4.

References for Chapter 3

- [3.1] “International Technology Roadmap for Semiconductors”, 1999 Edition, Semiconductor Industry Association (SIA).
- [3.2] M.G. Moharam, T.K. Gaylord, “Analysis and applications of optical diffraction by gratings,” Proceedings of IEEE, vol. 73, p. 894-937, 1985.
- [3.3] John K. Ousterhout, “Tcl and the Tk Toolkit,” Addison-Wesley Professional Computing Series, 1994.

Chapter 4

Ellipsometric Detection Limits

In the previous chapter, simulations were shown that a minimum CD variation of 0.4nm for a nominal CD of 20nm could be detected by the difference in the complex reflectance ratio between TM and TE light waves. However, this represents the numerical difference as determined using the RCWA formulation. In order for the sensitivity to be realistically determined, a characterization has to be carried out on the equipment used, in order to take into account uncertainty in measured response caused by the inherent noise of equipment. This overall noise can be attributed to fluctuations in the intensity of the light source; angular uncertainties of the polarizer, compensator and analyzer; as well as the resolution of the detector.

Work has been done to explore the feasibility of variable-angle ellipsometric scatterometry for the metrology of sub-0.1 μm linewidth structures [4.1].

In this chapter, the theory of scatterometric measurements using an ellipsometer will be described. A full understanding of the functioning of an ellipsometer is required in order to fully understand the noise contributions by each element in the ellipsometer. Jones' vectors [4.2] will be used this effect to analyze the transformations for a nulling ellipsometer as well as for the case of modulation by a rotating element.

4.1 Jones vectors

4.1.1 Nulling ellipsometer

The nulling ellipsometer is so described because it uses the detection of a minimum reflected signal to calculate the complex reflectance of a surface profile.

In this setup, the polarizer, compensator and analyzer are rotated such that a zero (or near zero) intensity value is obtained at the detector, apart from noise. The notation for unpolarized or circularly polarized light immediately after passing through the polarizer is given by

$$\begin{pmatrix} B \cos P \\ B \sin P \end{pmatrix}, \quad (4.1)$$

where B is the amplitude of the light emerging from the source and P is the polarizer angle, which is measured from the plane of incidence looking in the opposite direction of the traveling light. The vector can be simplified to become

$$\begin{pmatrix} \cos P \\ \sin P \end{pmatrix}, \quad (4.2)$$

given that we are only interested in the polarization state of the light, as is the case in nulling ellipsometry.

The corresponding Jones matrix for this arrangement is

$$\begin{pmatrix} \tilde{E}_{p,i} \\ \tilde{E}_{s,i} \end{pmatrix} = \begin{pmatrix} \cos Q & -\sin Q \\ \sin Q & \cos Q \end{pmatrix} \begin{pmatrix} 1 & 0 \\ 0 & -i \end{pmatrix} \begin{pmatrix} \cos Q & \sin Q \\ -\sin Q & \cos Q \end{pmatrix} \begin{pmatrix} \cos P \\ \sin P \end{pmatrix} \quad (4.3)$$

or

$$\begin{pmatrix} \tilde{E}_{p,i} \\ \tilde{E}_{s,i} \end{pmatrix} = \begin{pmatrix} \cos Q \cos(P-Q) + i \sin Q \sin(P-Q) \\ \sin Q \cos(P-Q) - i \cos Q \sin(P-Q) \end{pmatrix}, \quad (4.4)$$

where $E_{p,i}$ and $E_{s,i}$ are the components of incident light with its electric vector in the plane and perpendicular to the plane of incidence, respectively; and Q is the angle between the fast-axis of a quarter-wave plate and the plane of incidence.

After reflection from a sample, the polarization state of light is given by

$$\begin{pmatrix} \tilde{E}_{p,r} \\ \tilde{E}_{s,r} \end{pmatrix} = \begin{pmatrix} \tilde{R}_p & 0 \\ 0 & \tilde{R}_s \end{pmatrix} \begin{pmatrix} \tilde{E}_{p,i} \\ \tilde{E}_{s,i} \end{pmatrix}, \quad (4.5)$$

where $E_{p,r}$ and $E_{s,r}$ are the components of the electric field for the reflected light and R_p and R_s are the complex reflection coefficients for incident light with its electric vector in the plane and perpendicular to the plane of incidence, respectively.

In order for the light reflected from the sample to be extinguished completely by the analyzer, then the light incident on the analyzer after reflection has to be linearly polarized. As such, the two components of the Jones vector for the reflected light must be in phase. This implies that the ratio of reflected TM and TE light has to be a real number:

$$\text{Im} \left(\frac{\tilde{E}_{p,r}}{\tilde{E}_{s,r}} \right) = \text{Im} \left(\frac{\tilde{R}_p \tilde{E}_{p,i}}{\tilde{R}_s \tilde{E}_{s,i}} \right) = 0 \quad (4.6)$$

Substituting the term

$$\tilde{\rho} = \left(\frac{\tilde{R}_p}{\tilde{R}_s} \right) \quad (4.7)$$

and rearranging, we can rewrite the equation as

$$\text{Im}(\tilde{\rho} \tilde{E}_{p,i} \tilde{E}_{s,i}^*) = 0, \quad (4.8)$$

where $\tilde{E}_{s,i}^*$ denotes the conjugate of $\tilde{E}_{s,i}$.

$\tilde{\rho}$ can be broken up into its real and imaginary parts by using the relation from Chapter

2:

$$\tilde{\rho} = \tan \Psi \cos \Delta + i \tan \Psi \sin \Delta \quad (4.9)$$

Substituting this relation into the prior equation enables us to find the polarizer angles that could possibly result in linearly polarized light after reflection and hence can produce a null after passing through the analyzer, which will satisfy the following:

$$\tan 2(P - Q) = -\sin 2Q \tan \Delta \quad (4.10)$$

If a null exists after passing through the analyzer on satisfying the equation above, then the resulting Jones vector relation

$$\begin{pmatrix} \cos^2 A & \sin A \cos A \\ \sin A \cos A & \sin^2 A \end{pmatrix} \begin{pmatrix} \tilde{E}_{p,r} \\ \tilde{E}_{s,r} \end{pmatrix} = \begin{pmatrix} 0 \\ 0 \end{pmatrix} \quad (4.11)$$

will give the result of

$$\tan A = -\tilde{\rho} \frac{\tilde{E}_{p,i}}{\tilde{E}_{s,i}} \quad (4.12)$$

Solving this equation gives

$$\tan A = \tan \Psi \frac{\cos(2P - 2Q) \cos \Delta \sin 2Q - \sin(2P - 2Q) \sin \Delta}{\cos(2P - 2Q) \cos 2Q - 1}, \quad (4.13)$$

which is the relation between A and Ψ .

4.1.2 Modulation by Rotating Element

In this method, the light beam incident on the sample is modulated by the rotation of the polarizer, compensator or analyzer. During the course of this research, measurements were conducted using the Sopra GESp5 variable-angle spectroscopic ellipsometer. This ellipsometer uses a rotating polarizer to suppress the effects of parasitic light on measurements.

The associated Jones vector for this technique is given below:

$$\tilde{E}_d = \begin{pmatrix} 1 & 0 \\ 0 & 0 \end{pmatrix} \begin{pmatrix} \cos A & \sin A \\ -\sin A & \cos A \end{pmatrix} \begin{pmatrix} \tilde{R}_p & 0 \\ 0 & \tilde{R}_s \end{pmatrix} \begin{pmatrix} \cos P & \sin P \\ -\sin P & \cos P \end{pmatrix} \begin{pmatrix} 1 & 0 \\ 0 & 0 \end{pmatrix} \begin{pmatrix} E_0 \\ E_0 \end{pmatrix}, \quad (4.14)$$

which gives

$$\tilde{E}_d = E_0 \tilde{R}_s \cos A (\tan \Psi e^{i\Delta} \cos P + \tan A \sin P). \quad (4.15)$$

The resulting intensity seen by the detector can be written as

$$I_d = |\tilde{E}_d|^2 \quad (4.16)$$

which expands into the form of

$$I_d = I_0 (\alpha \cos 2P + \beta \sin 2P + 1), \quad (4.17)$$

where

$$I_0 = \frac{|E_0|^2 |\tilde{R}_s|^2 \cos^2 A (\tan^2 \Psi + \tan^2 A)}{2} \quad (4.18)$$

$$\alpha = \frac{\tan^2 \Psi - \tan^2 A}{\tan^2 \Psi + \tan^2 A} \quad (4.19)$$

$$\beta = \frac{2 \cos \Delta \tan \Psi \tan A}{\tan^2 \Psi + \tan^2 A} \quad (4.20)$$

The intermediate variables α and β are of interest since they are used by the GESp5 to determine $\tan \Psi$ and $\cos \Delta$.

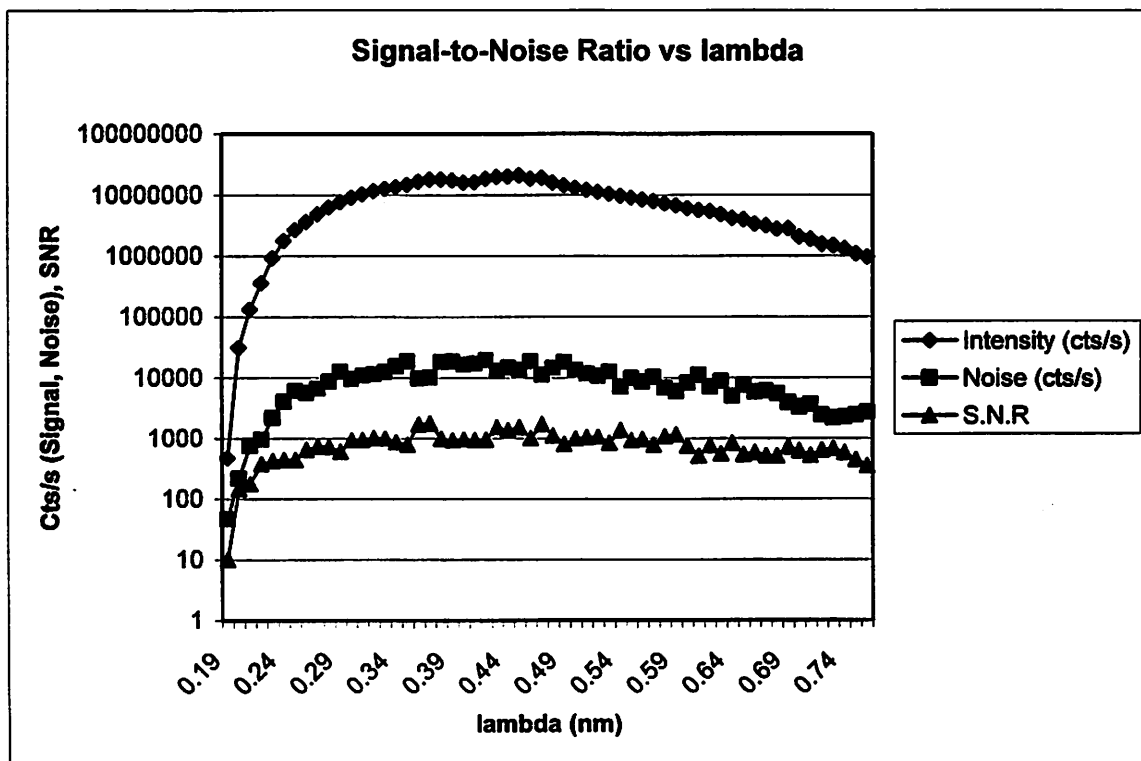
4.2 Signal-to-Noise Ratio for Sopra Ellipsometer

It is important to note that although different ellipsometers utilize different techniques to obtain the values of $\tan \Psi$ and $\cos \Delta$, their errors can be characterized using a general method. Logofatu et al have previously postulated that the more influential sources of measurement errors, such as light source intensity fluctuations and errors from the

polarizer and analyzer are proportional to the intensity of the measured beam [4.3]; if the intensity being measured is low, then the noise floor, caused by factors such as the limited resolution of the detector, figure more importantly.

For this research, signal (intensity)-to-noise ratio (SNR) measurements were taken using the GESp5 over the wavelength spectrum 190nm-760nm. This SNR spectrum, shown in Figure 4.1, is used to determine the noise for each sample, which is a function of wavelength as well as the reflected intensity of the beam.

Figure 4.1 Sopra GESp5 Signal-to-Noise Ratio



4.2.1 Sopra Ellipsometer Measurement Technique

Using the Hadamard method [4.4], the values of $\tan \Psi$ and $\cos \Delta$ can be obtained as functions of direct measurements made by the ellipsometer:

$$\cos \Delta = \frac{\beta}{\sqrt{1-\alpha^2}} \quad (4.21)$$

$$\tan \Psi = \sqrt{\frac{1+\alpha}{1-\alpha}} \tan A \quad (4.22)$$

where

$$\alpha = \frac{1}{2I_0}(S_1 - S_2 - S_3 + S_4) \quad (4.23)$$

$$\beta = \frac{1}{2I_0}(S_1 + S_2 - S_3 - S_4) \quad (4.24)$$

$$I_0 = \frac{1}{\pi}(S_1 + S_2 + S_3 + S_4), \quad (4.25)$$

and

$$S_1 = \int_0^{\pi/4} I(P) dP \quad (4.26)$$

$$S_2 = \int_{\pi/4}^{\pi/2} I(P) dP \quad (4.27)$$

$$S_3 = \int_{\pi/2}^{3\pi/4} I(P) dP \quad (4.28)$$

$$S_4 = \int_{3\pi/4}^{\pi} I(P) dP \quad (4.29)$$

In the calculation of $\tan \Psi$, in order to maximize the SNR value and decrease the sinusoidal contribution of the signal, the analyzer angle A is adjusted so that

$$\tan A = \tan \Psi, \quad (4.30)$$

which is also known as the *tracking* method.

4.2.2 Noise function

Based on the above equations, Taylor's expansion was used to derive the sensitivities of α and β across the wavelength spectrum for different samples.

$$\Delta\alpha = \frac{1}{2I_0^2}(S_1 - S_2 - S_3 + S_4)\Delta I_0 + \frac{1}{2I_0}(\Delta S_1 + \Delta S_2 + \Delta S_3 + \Delta S_4) \quad (4.31)$$

$$\Delta\beta = \frac{1}{2I_0^2}(S_1 + S_2 - S_3 - S_4)\Delta I_0 + \frac{1}{2I_0}(\Delta S_1 + \Delta S_2 + \Delta S_3 + \Delta S_4) \quad (4.32)$$

Given that I_0 is averaged over π and has units of counts per second, while S values are calculated over $\pi/4$ in each instance with units of counts, and the average rotational speed of the polarizer is 60 revolutions/minute or 1 revolution/second, we can qualitatively deduce that

$$\Delta S_n = \sqrt{4} \left(\frac{1}{2\pi} \right) \left(\frac{\pi}{4} \right) \Delta I_0$$

$$\Delta S_n = \frac{\Delta I_0}{4} \quad (4.33)$$

Therefore,

$$\Delta\alpha = \frac{1}{2I_0^2}(S_1 - S_2 - S_3 + S_4)\Delta I_0 + \frac{1}{2I_0}(\Delta I_0) \quad (4.34)$$

$$\Delta\beta = \frac{1}{2I_0^2}(S_1 + S_2 - S_3 - S_4)\Delta I_0 + \frac{1}{2I_0}(\Delta I_0) \quad (4.35)$$

Following this, Taylor's expansion yields sensitivities of $\tan \Psi$ and $\cos \Delta$ of the form:

$$\Delta \tan \Psi = \frac{1}{2} \tan A \left[\sqrt{\frac{1}{(1+\alpha)(1-\alpha)}} + \sqrt{\frac{(1+\alpha)}{(1-\alpha)^3}} \right] \Delta\alpha + \sqrt{\frac{1+\alpha}{1-\alpha}} \frac{1}{\cos^2 A} \Delta A \quad (4.36)$$

$$\Delta \cos \Delta = \frac{1}{\sqrt{(1-\alpha^2)}} \Delta \beta + \frac{1}{2} \beta \left[\sqrt{\frac{1}{(1-\alpha)^3(1+\alpha)}} - \sqrt{\frac{1}{(1+\alpha)^3(1-\alpha)}} \right] \Delta \alpha \quad (4.37)$$

For approximation of the errors, based on the fact that $\alpha = 0$ when $\tan A = \tan \Psi$, we can substitute $\alpha = 0$ into the Taylor's expansions, which simplifies to:

$$\Delta \tan \Psi = \Delta \alpha \tan A + \frac{1}{\cos^2 A} \Delta A \quad (4.38)$$

$$\Delta \cos \Delta = \Delta \beta \quad (4.39)$$

4.2.2.1 Noise vs Integration Time

The derivation of noise in the previous section is for measurements made over a period of π for each wavelength. This noise can be further derived as a function of measurement time as follows.

$$\Delta I_0 = \frac{\Delta I_0}{\sqrt{2t}} \quad (4.40)$$

$$\Delta S_n = \frac{\Delta I_0}{\sqrt{32t}} \quad (4.41)$$

The complete Taylor's expansion on the noise functions of $\tan \Psi$ and $\cos \Delta$ are given below:

$$\begin{aligned} \Delta \tan \Psi = & \sqrt{\frac{1+\alpha}{1-\alpha}} \sec^2 A \Delta A - \frac{\tan A}{4I_0^2} \left[\sqrt{\frac{1+\alpha}{(1-\alpha)^3}} + \sqrt{\frac{1}{(1-\alpha^2)}} \right] \Delta I_0, \\ & + \frac{\tan A}{4I_0} \left[\sqrt{\frac{1+\alpha}{(1-\alpha)^3}} + \sqrt{\frac{1}{(1-\alpha^2)}} \right] \Delta S_1, - \frac{\tan A}{4I_0} \left[\sqrt{\frac{1+\alpha}{(1-\alpha)^3}} + \sqrt{\frac{1}{(1-\alpha^2)}} \right] \Delta S_2, \\ & - \frac{\tan A}{4I_0} \left[\sqrt{\frac{1+\alpha}{(1-\alpha)^3}} + \sqrt{\frac{1}{(1-\alpha^2)}} \right] \Delta S_3, + \frac{\tan A}{4I_0} \left[\sqrt{\frac{1+\alpha}{(1-\alpha)^3}} + \sqrt{\frac{1}{(1-\alpha^2)}} \right] \Delta S_4, \end{aligned} \quad (4.42)$$

$$\begin{aligned}
\Delta \cos \Delta = & -\frac{1}{I_0} \left[\frac{\beta}{\sqrt{(1-\alpha^2)}} + \frac{\alpha^2 \beta}{\sqrt{(1-\alpha^2)^3}} \right] \Delta I_0 + \frac{1}{2I_0} \left[\sqrt{\frac{1}{(1-\alpha^2)}} + \frac{\alpha\beta}{\sqrt{(1-\alpha^2)^3}} \right] \Delta S_1, \\
& + \frac{1}{2I_0} \left[\sqrt{\frac{1}{(1-\alpha^2)}} - \frac{\alpha\beta}{\sqrt{(1-\alpha^2)^3}} \right] \Delta S_2, - \frac{1}{2I_0} \left[\sqrt{\frac{1}{(1-\alpha^2)}} + \frac{\alpha\beta}{\sqrt{(1-\alpha^2)^3}} \right] \Delta S_3, \\
& - \frac{1}{2I_0} \left[\sqrt{\frac{1}{(1-\alpha^2)}} - \frac{\alpha\beta}{\sqrt{(1-\alpha^2)^3}} \right] \Delta S_4, \tag{4.43}
\end{aligned}$$

Given that we are concerned with the magnitude the noise, substituting for $\alpha=0$,

$$\Delta \tan \Psi = \sec^2 A \Delta A - \frac{\tan A}{2I_0^2} \Delta I_0 + \frac{\tan A}{2I_0} \Delta S_1 - \frac{\tan A}{2I_0} \Delta S_2 - \frac{\tan A}{2I_0} \Delta S_3 + \frac{\tan A}{2I_0} \Delta S_4, \tag{4.44}$$

$$\Delta \cos \Delta = -\frac{\beta}{I_0} \Delta I_0 + \frac{1}{2I_0} \Delta S_1 + \frac{1}{2I_0} \Delta S_2 - \frac{1}{2I_0} \Delta S_3 - \frac{1}{2I_0} \Delta S_4, \tag{4.45}$$

$$\begin{aligned}
\sigma^2 \tan \Psi = & \sec^4 A \sigma^2 A + \frac{\tan^2 A}{4I_0^4} \sigma^2 I_0 + \frac{\tan^2 A}{4I_0^2} \sigma^2 S_1 + \frac{\tan^2 A}{4I_0^2} \sigma^2 S_2 + \frac{\tan^2 A}{4I_0^2} \sigma^2 S_3, \\
& + \frac{\tan^2 A}{4I_0^2} \sigma^2 S_4, \\
= & \sec^4 A \sigma^2 A + \frac{\tan^2 A \sigma^2 I_0}{4I_0^4 \cdot 2t} + \frac{\tan^2 A \sigma^2 I_0}{4I_0^2 \cdot 32t} + \frac{\tan^2 A \sigma^2 I_0}{4I_0^2 \cdot 32t} + \frac{\tan^2 A \sigma^2 I_0}{4I_0^2 \cdot 32t} \\
& + \frac{\tan^2 A \sigma^2 I_0}{4I_0^2 \cdot 32t} \\
= & \sec^4 A \sigma^2 A + \frac{\tan^2 A \sigma^2 I_0}{4I_0^4 \cdot 2t} + \frac{\tan^2 A \sigma^2 I_0}{I_0^2 \cdot 32t} \tag{4.46}
\end{aligned}$$

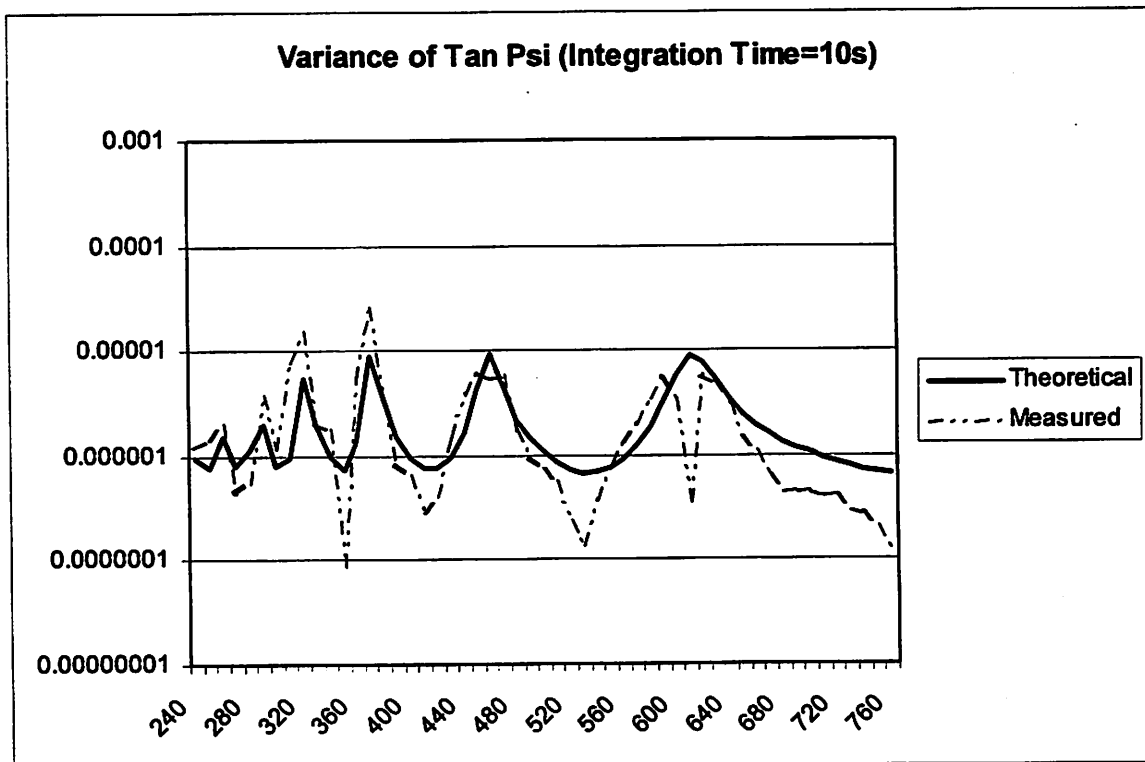
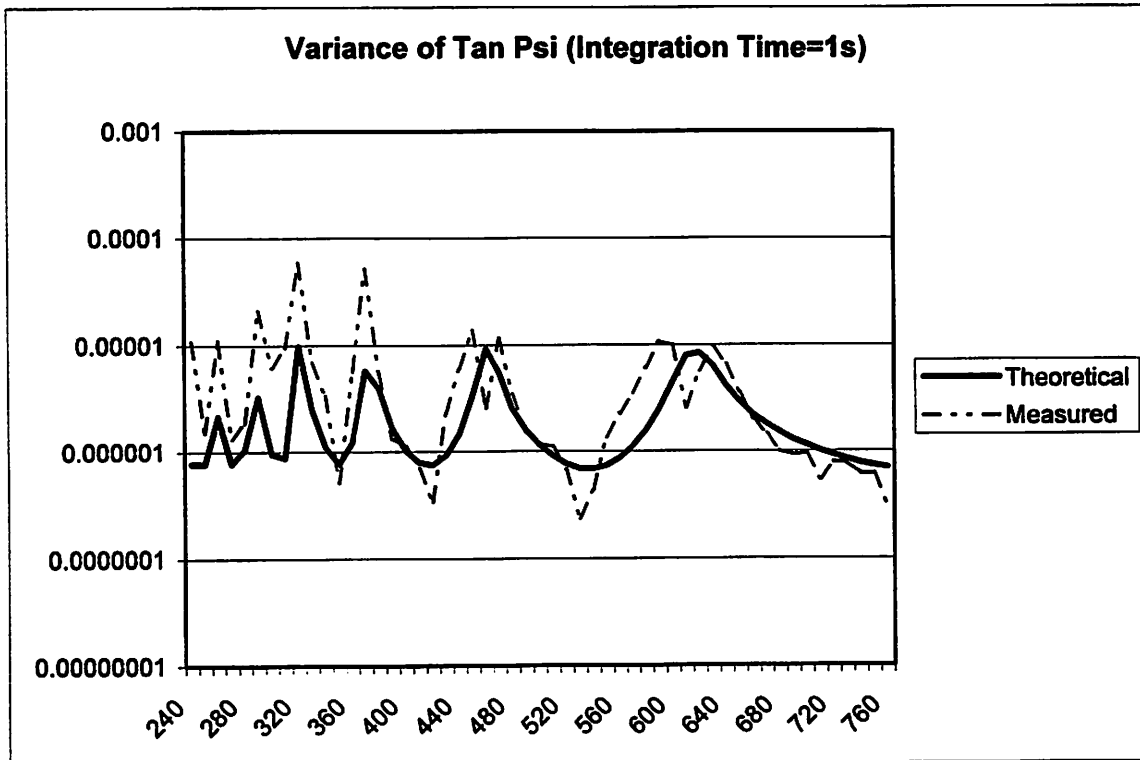
Likewise,

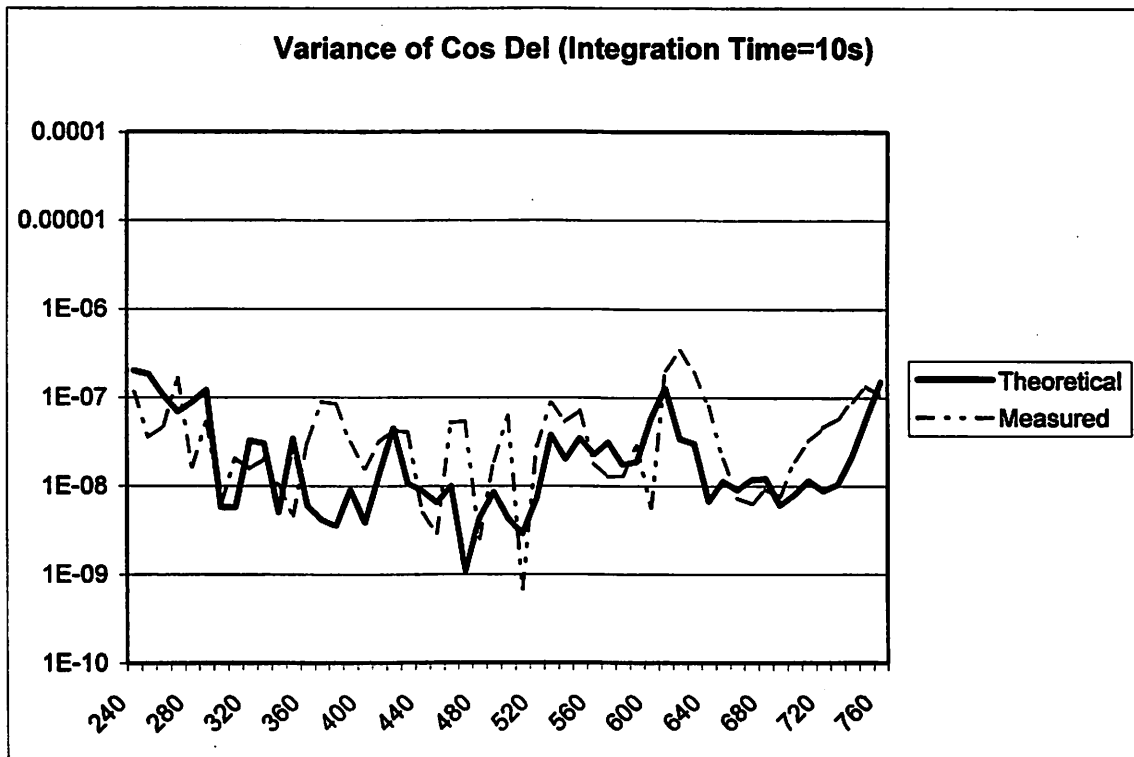
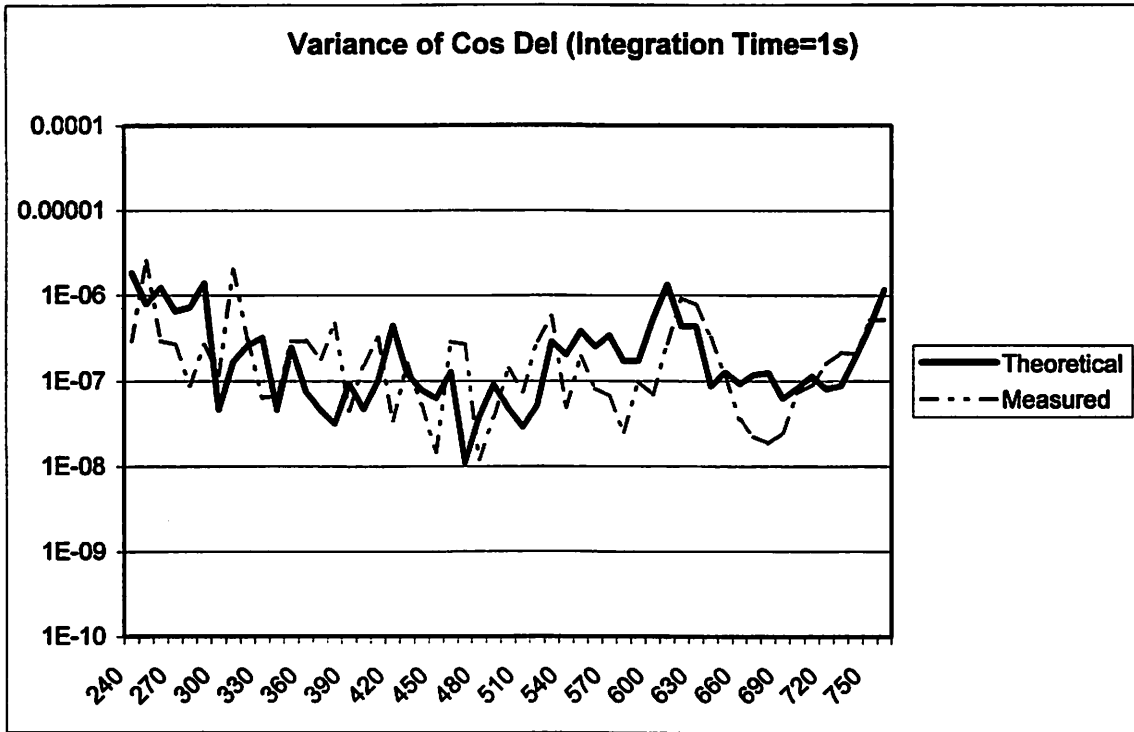
$$\sigma^2 \cos \Delta = \frac{\beta^2}{I_0^2} \sigma^2 I_0 + \frac{1}{4I_0^2} \sigma^2 S_1 + \frac{1}{4I_0^2} \sigma^2 S_2 + \frac{1}{4I_0^2} \sigma^2 S_3 + \frac{1}{4I_0^2} \sigma^2 S_4,$$

$$\begin{aligned}
&= \frac{\beta^2 \sigma^2 I_0}{I_0^2 2t} + \frac{1 \sigma^2 I_0}{4I_0^2 32t} \\
&= \frac{\beta^2 \sigma^2 I_0}{I_0^2 2t} + \frac{1 \sigma^2 I_0}{I_0^2 32t}
\end{aligned}
\tag{4.47}$$

Repeated measurements for different measurement times using the ellipsometer produced results that agree fairly well with this noise function as shown in Figures 4.2(a)-(d) below.

Figure 4.2 (a)-(d) Theoretical and measured scatterometry noise for integration times of 1 second and 10 seconds





From the noise functions, we can observe that the time effect is small for $\tan \Psi$ measurements. However, for $\cos \Delta$, the standard error of measurement decreases with increasing measurement time, which enables detection of smaller profile variations.

4.2.2.2 Incidence Angle Error

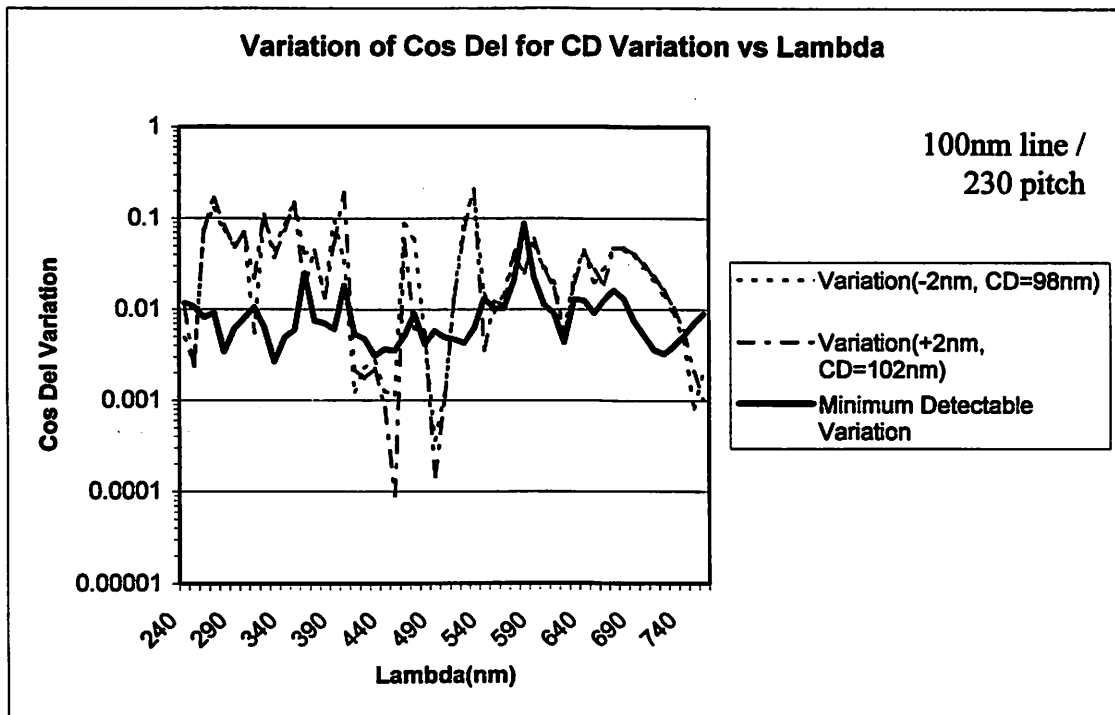
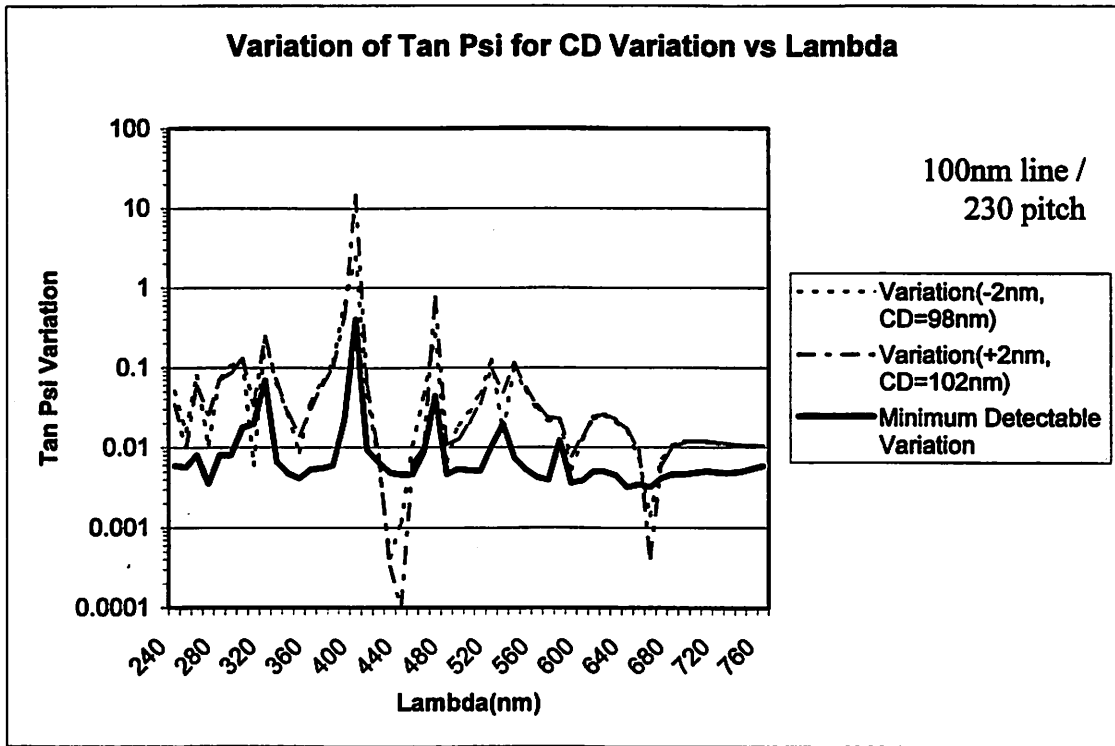
The noise analysis in the previous section applies for measurements made for a single, specific incidence angle. However, for all practical purposes, measurements made using commercial ellipsometers have a spread associated with the incidence angle. This is due to the finite size of the lens used to focus the beam onto the object wafer. The Sopra GESP 5, for instance, has a spread of 1.4 degrees. This results in a measurement that could very well be approximated as an average of all measurements made over that spread of incidence angles. This effect is also taken into account in characterizing measurement noise.

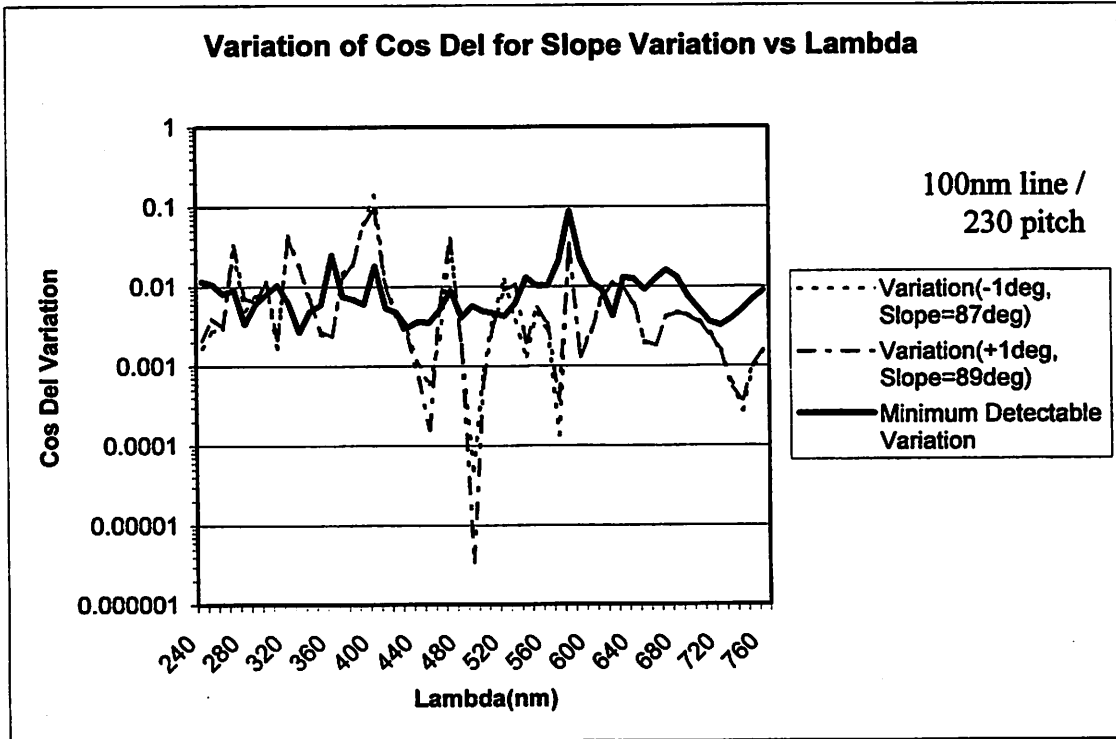
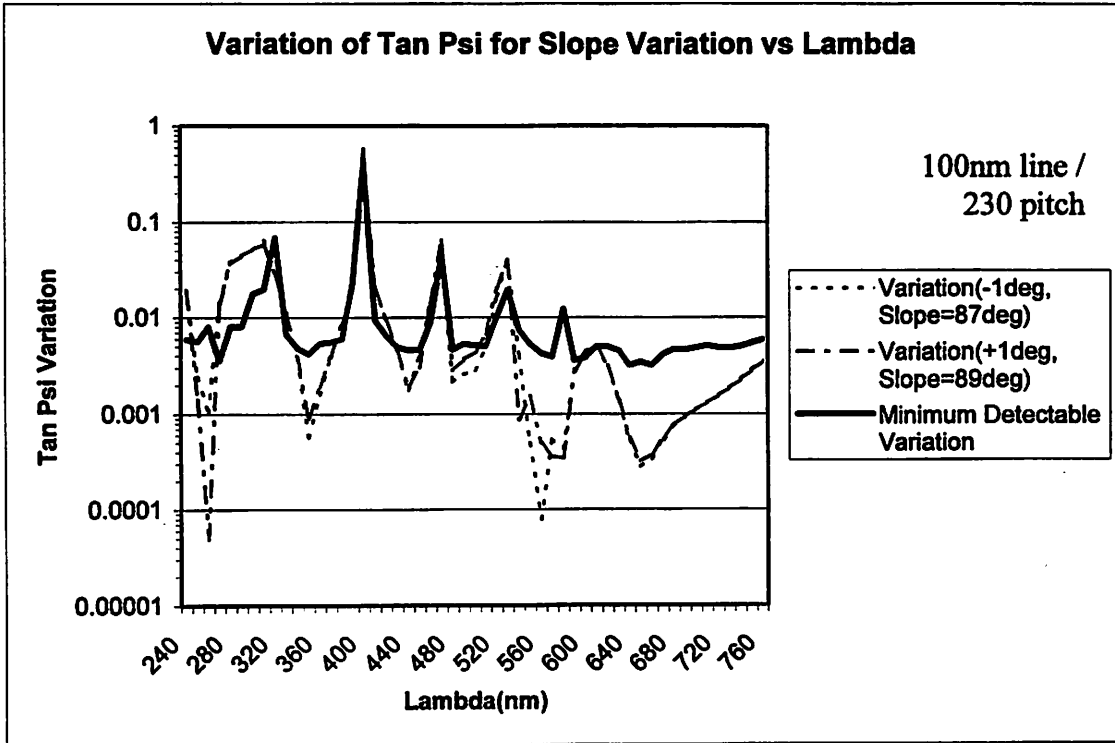
Simulations were done small increments in the incidence angle around the spread of 1.4 degrees. The average of the responses was taken to approximate the response obtained using the ellipsometer.

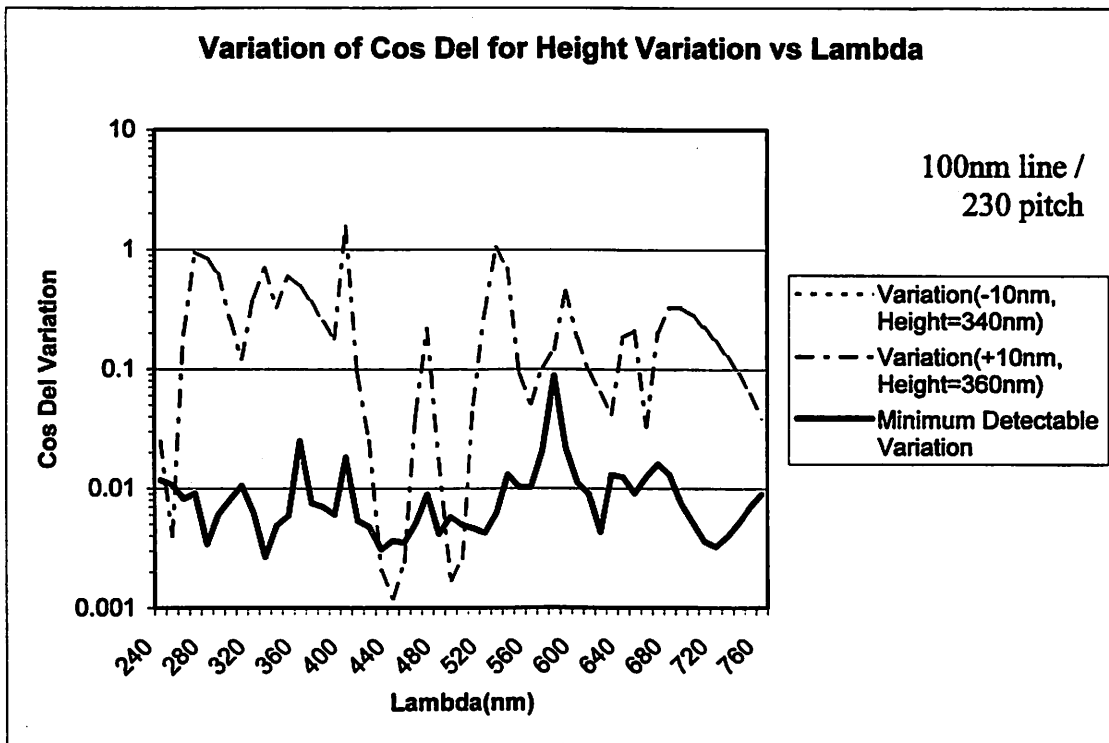
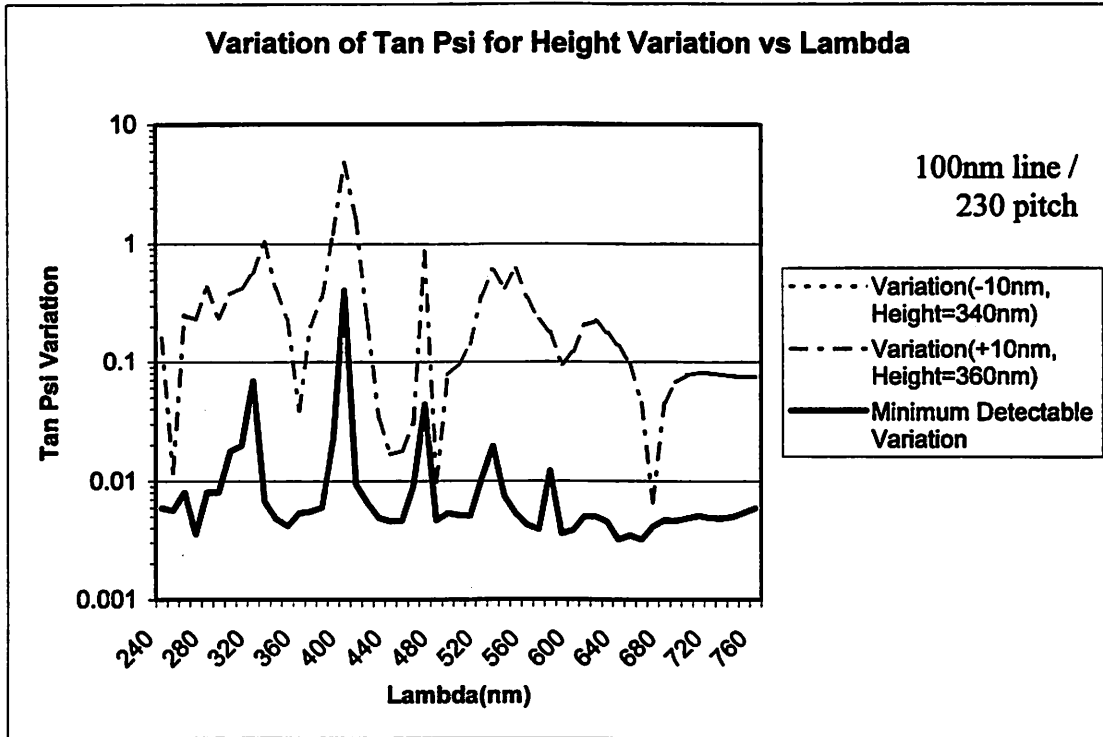
4.3 Sensitivity Analysis for 100nm Technology Node

Based on the theory presented in Section 4.2, sensitivity analysis was conducted for the 100nm technology node using a nominal measurement time of 1 second. Theoretical variation in response is compared to the noise associated with the Sopra ellipsometer to determine the sensitivity of scatterometry in detecting a specific variation. The results are presented below in Figures 4.3-4.4.

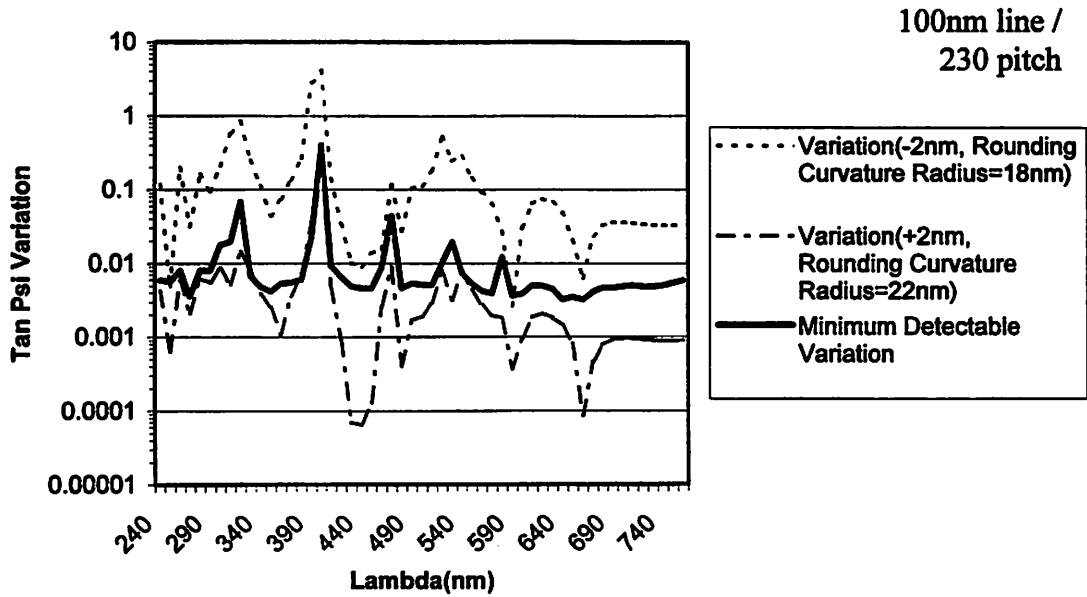
Figure 4.3 (a)-(j) 100nm Linewidth / 230nm Pitch



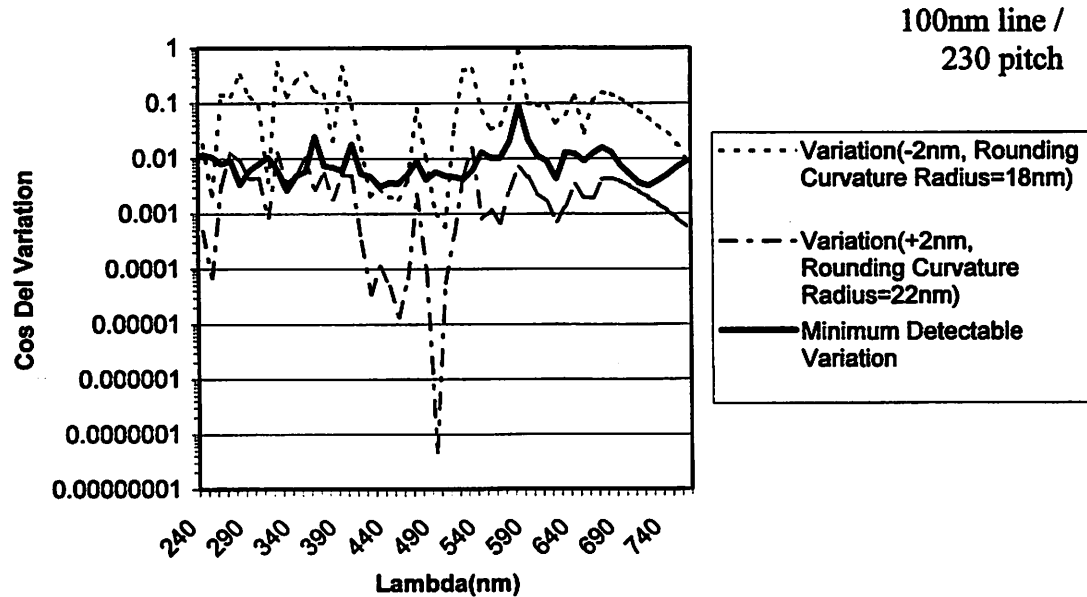




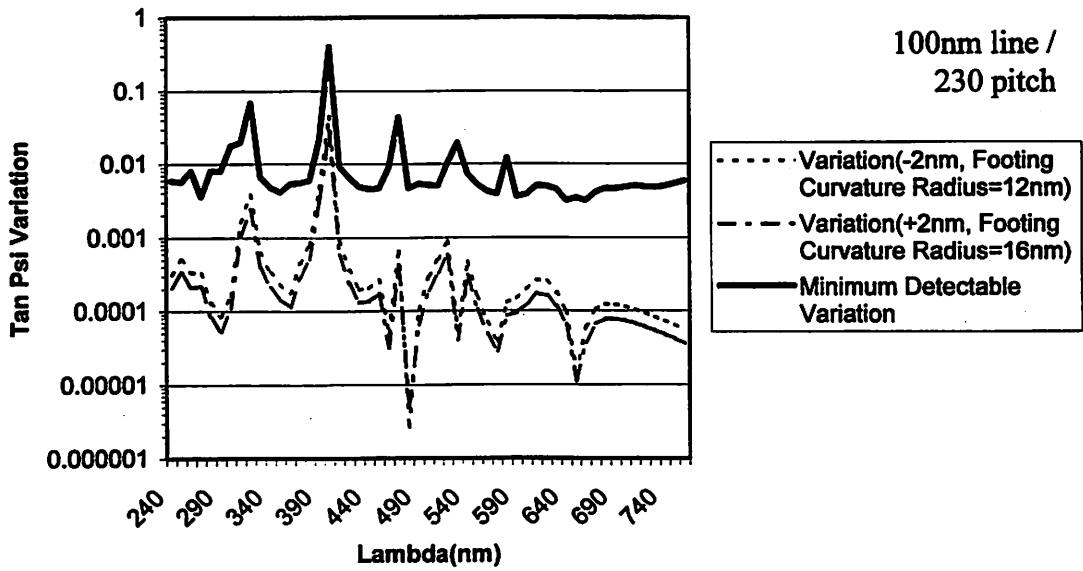
Variation of Tan Psi for Rounding Curvature Variation vs Lambda



Variation of Cos Del for Rounding Curvature Variation vs Lambda



Variation of Tan Psi for Footing Curvature Variation vs Lambda



Variation of Cos Del for Footing Curvature Variation vs Lambda

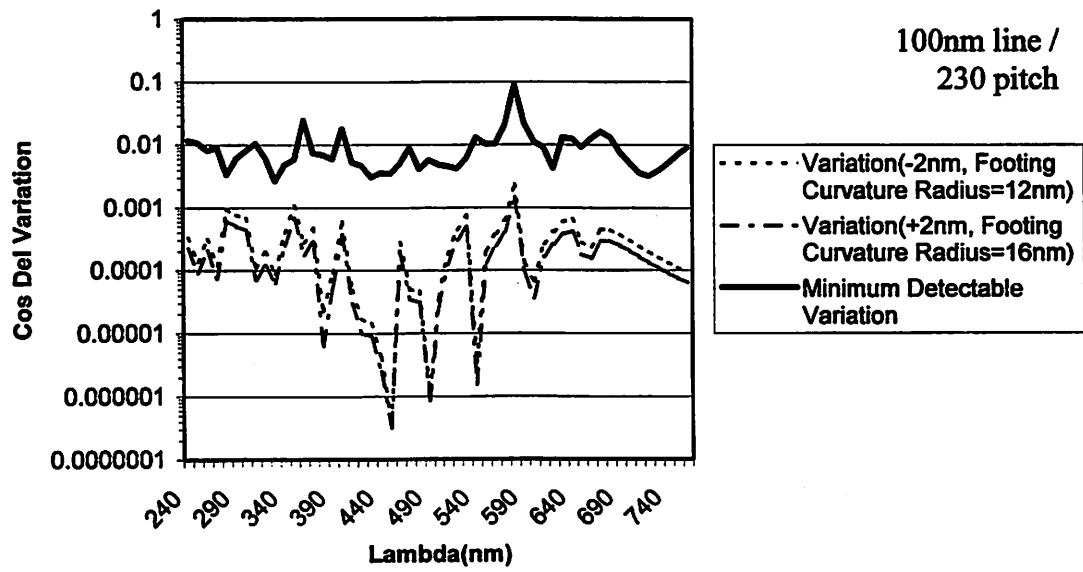
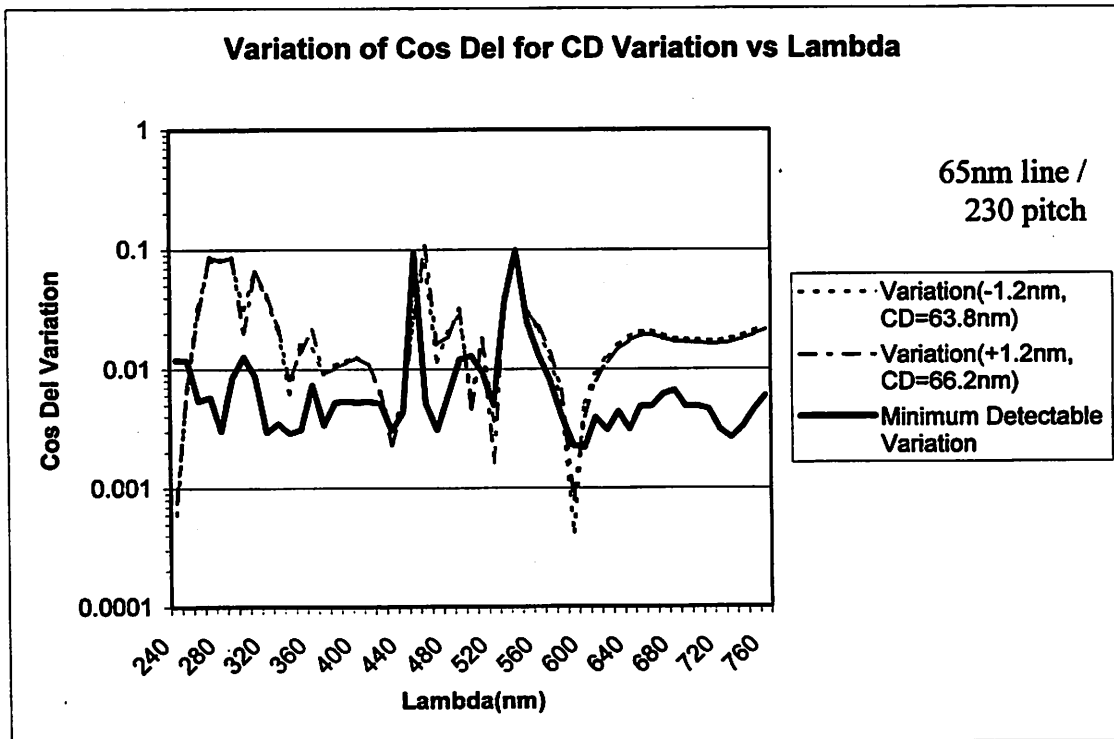
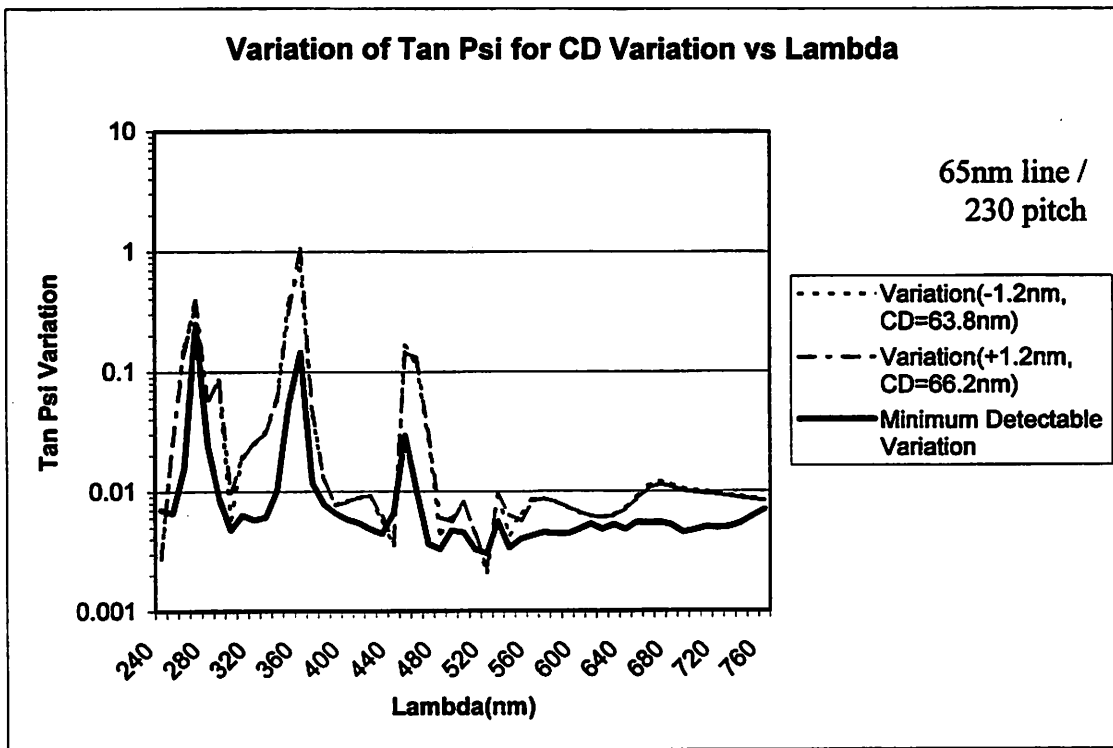
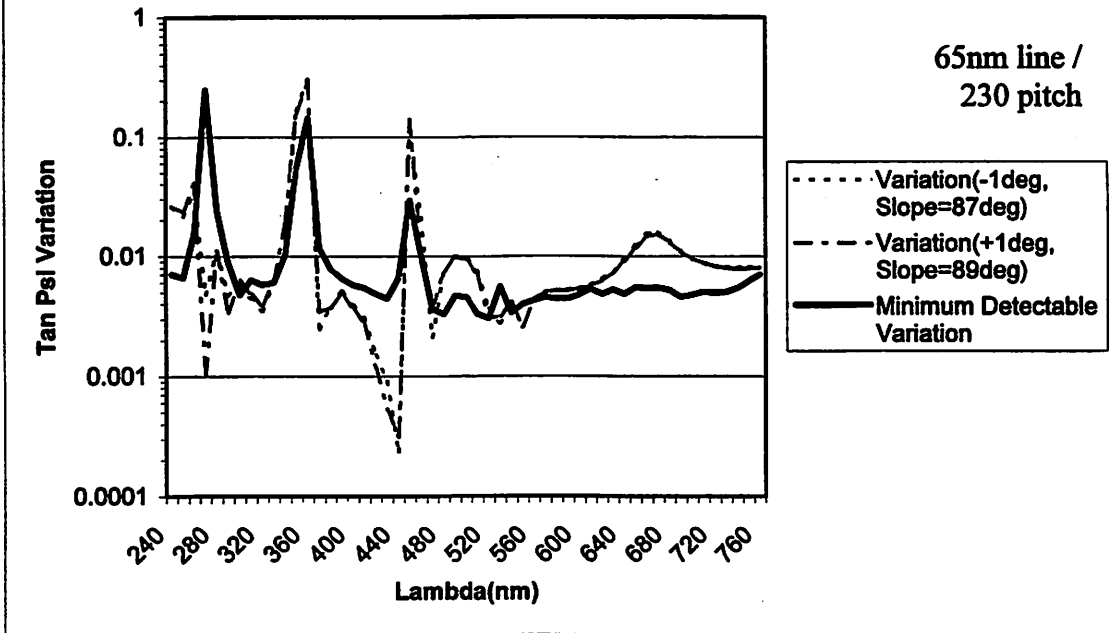


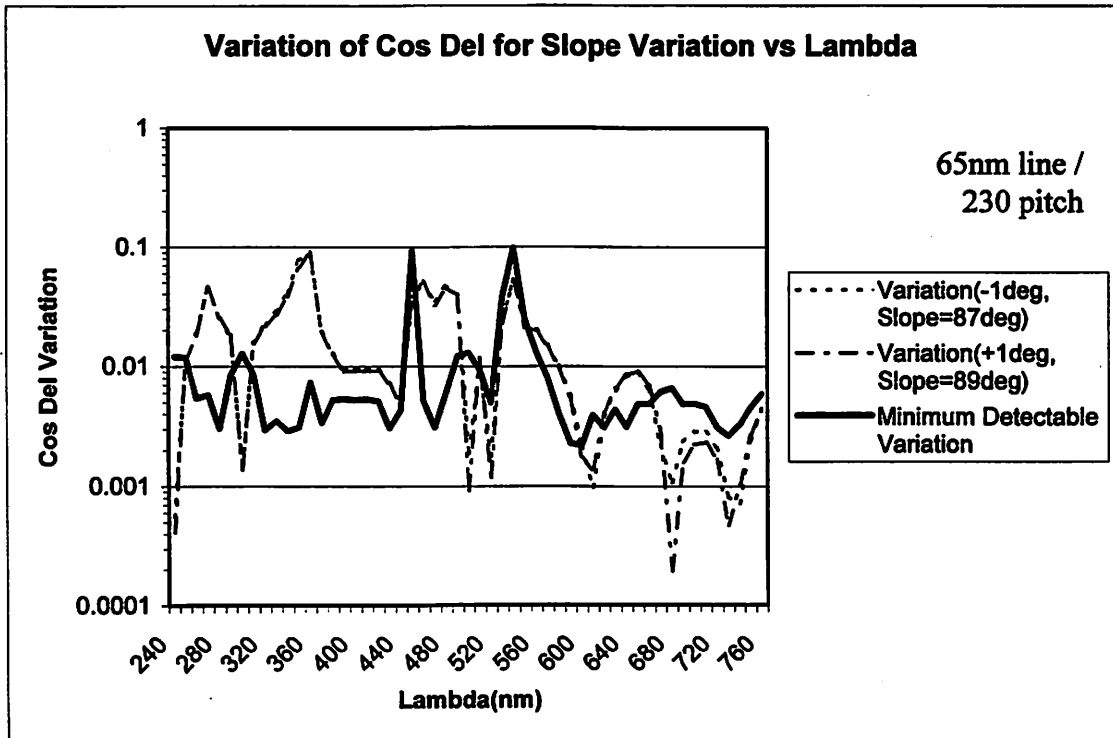
Figure 4.4 (a)-(j) 65nm Linewidth / 230nm Pitch



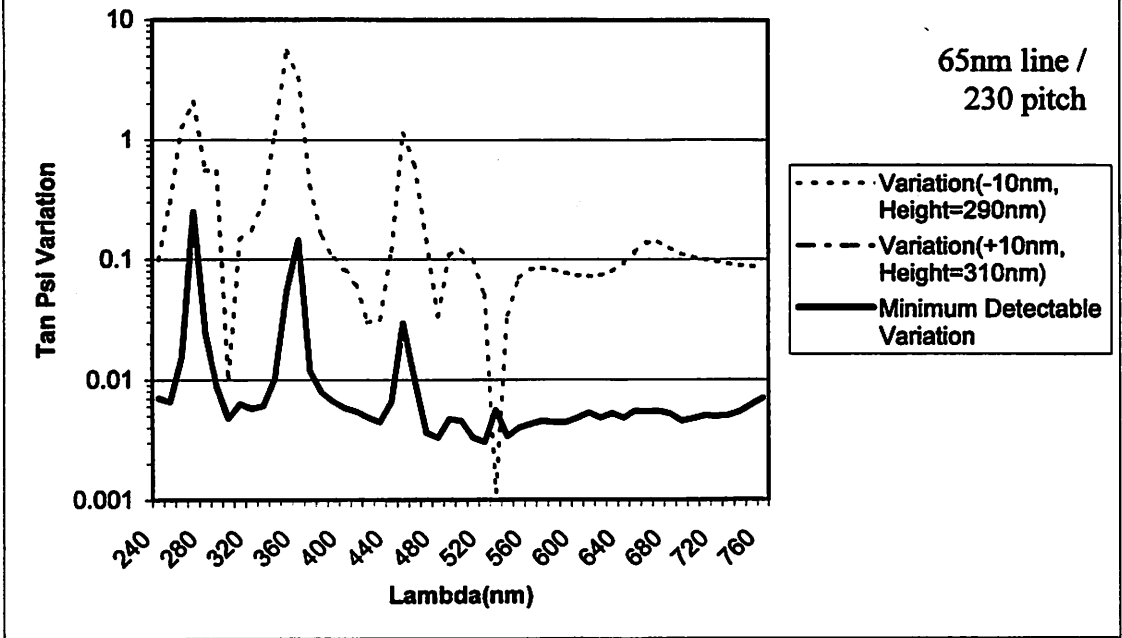
Variation of Tan Psi for Slope Variation vs Lambda



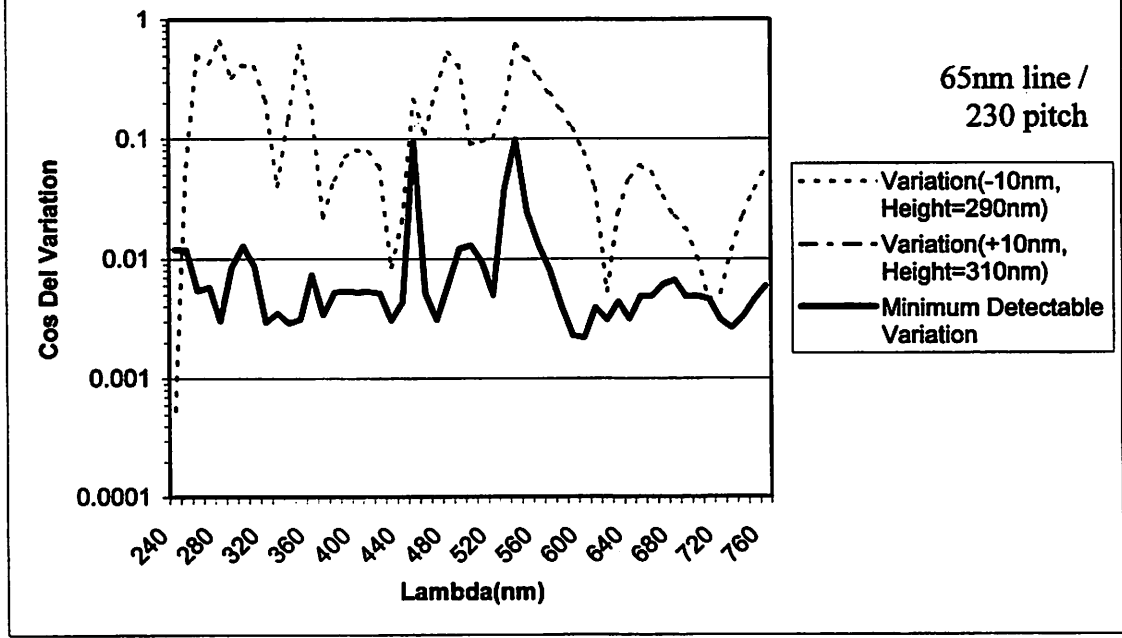
Variation of Cos Del for Slope Variation vs Lambda

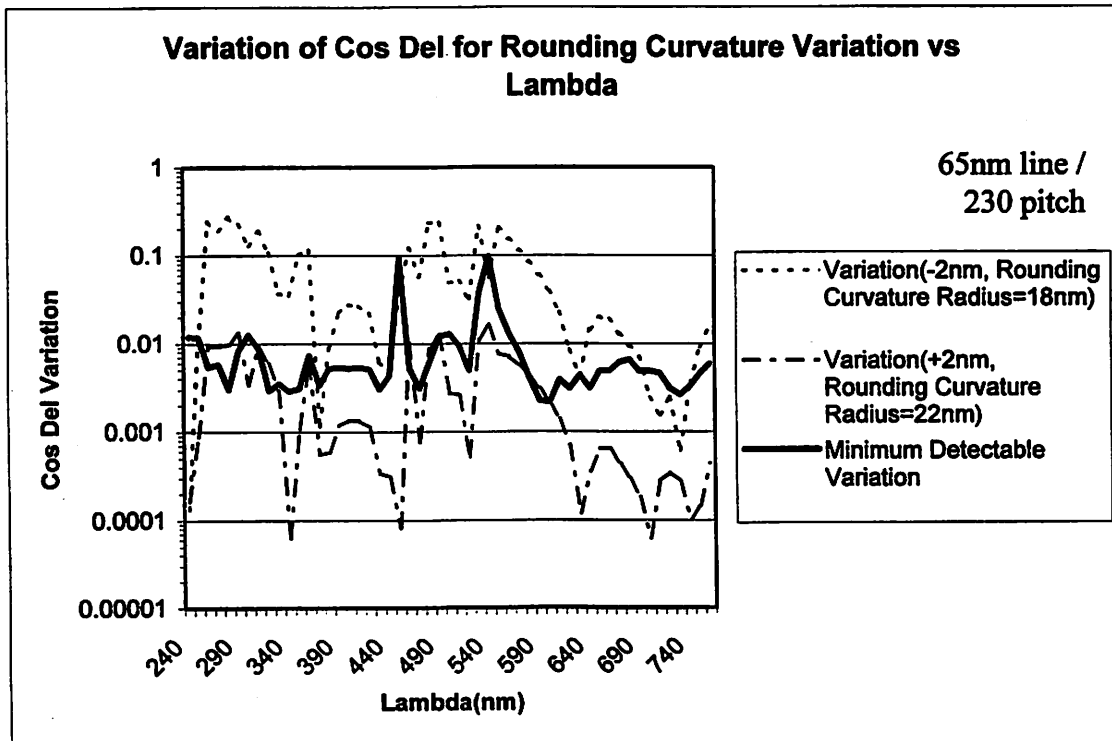
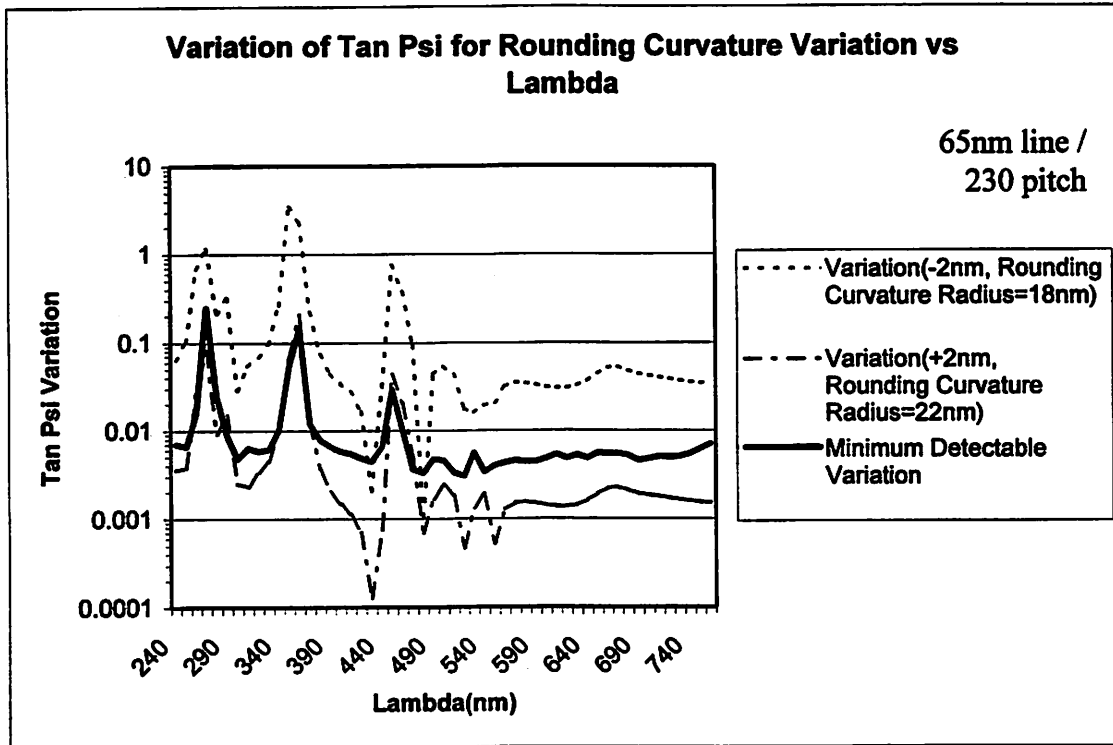


Variation of Tan Psi for Height Variation vs Lambda

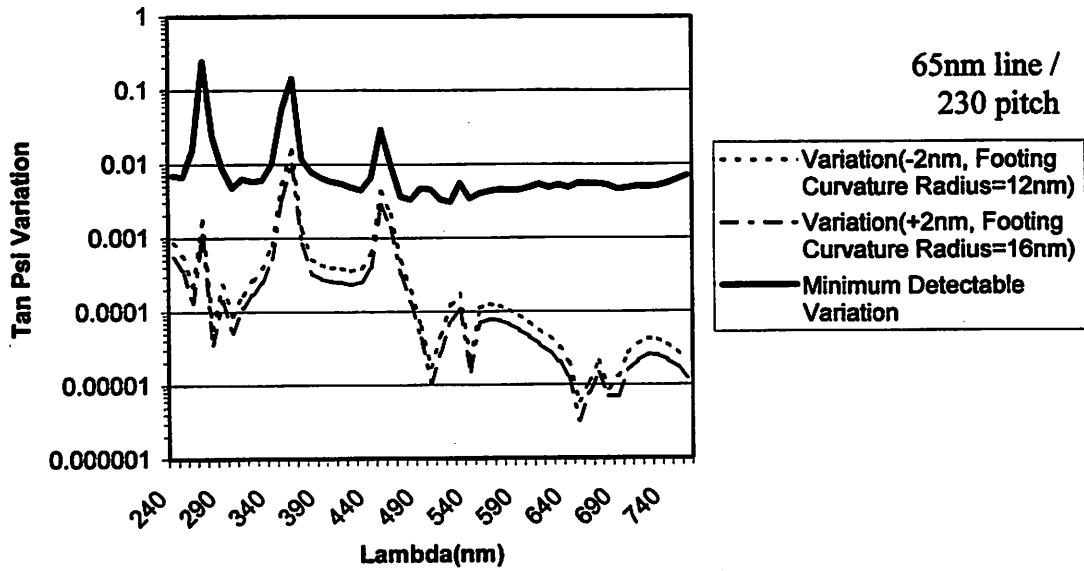


Variation of Cos Del for Height Variation vs Lambda

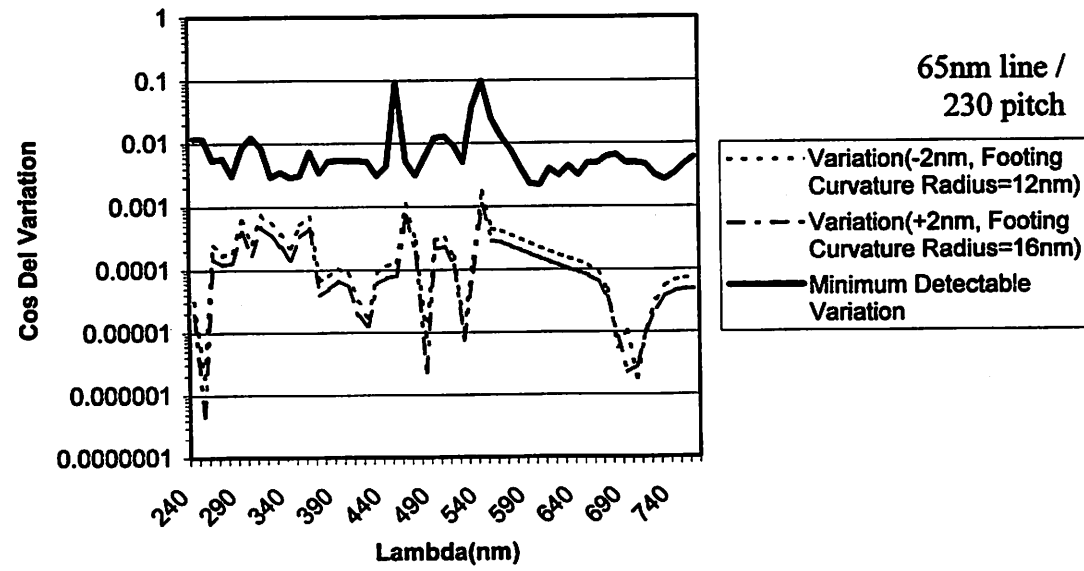




Variation of Tan Psi for Footing Curvature Variation vs Lambda



Variation of Cos Del for Footing Curvature Variation vs Lambda



The figures show that for both 100nm dense lines and 65nm isolated lines, CD variations in line with the technology roadmap's specifications are readily detectable. Slope variations are also readily detectable in both cases. In the case of stack height variation, the complication arises from the fact that because the profiles are constructed piecewise, using rectangular layers of finite thickness to construct rounded profiles, certain variations result in no change $\tan \Psi$ and $\cos \Delta$ response. As such, this would prove to be undetectable.

Simulations were also carried out to determine the effects of interactions of profile variations. The purpose of this experiment was to determine if the different profile variations, ie. CD, height, slope angle, rounding and footing, produce unique changes in the $\tan \Psi$ and $\cos \Delta$ responses, which can thus be easily differentiated.

A total of 3×5^4 simulations each were carried out for the 100nm and 65nm linewidth specifications. This is illustrated in Table 4.1

Table 4.1 Matrix for test of interaction effects of profile variations

Linewidth	100nm	65nm
CD (nm)	98, 100, 102	63.8, 65, 66.2
Slope Angle (°)	82, 85, 88, 91, 94	85, 86.5, 88, 89.5, 91
Height (nm)	340, 345, 350, 355, 360	290, 295, 300, 315, 330
Rounding Curvature (nm)	18, 19, 20, 22, 24	19, 19.5, 20, 22, 24
Footing Curvature (nm)	8, 11, 14, 17, 20	8, 11, 14, 17, 20

The total of 1875 runs for 100nm linewidth profiles including the nominal profile returned 9 undetectable changes excluding the nominal profile. However, upon inspection, these undetectable variations are the result of insufficient sensitivity in detecting height as well as footing changes with respect to the step size, rather than the

result of independently detectable variations canceling each other out. Similar runs for 65nm linewidth profiles also did not demonstrate any interaction effects.

4.4 Conclusion

In this chapter, we have demonstrated the ability of spectroscopic scatterometry to detect the variation in CD as stipulated in the International Technology Roadmap of Semiconductors. Scatterometry has also been demonstrated to have potential to detect variations in other profile parameters such as stack height, side slope angle, rounding and footing, with varying degrees of success. It has also been demonstrated that the various profile variations, due to its spectroscopic nature, produce essentially unique variations in the $\tan \Psi$ and $\cos \Delta$ responses. This is important because it proves that even with the interaction of various profile variations, these variations will not counteract each other to render them undetectable through spectroscopic scatterometry.

More importantly, given that most advanced commercial ellipsometers today employ the modulation-by-rotation method in obtaining measurements, this chapter has demonstrated a systematic way to characterize the noise functions associated with these ellipsometers based on Jones' vectors.

References for Chapter 4

- [4.1] B. K. Minhas, S. A. Coulombe, S. Sohail, H. Naqvi, J. R. McNeil, "Ellipsometric scatterometry for the metrology of sub-0.1 μ m-linewidth structures," *Applied Optics*, vol. 37, no. 22, 1 Aug 1998.
- [4.2] R. C. Jones, "A New Calculus for the Treatment of Optical Systems VIII: Electromagnetic Theory," *Journal of the Optical Society of America*, vol. 46, p. 126-131, 1956.
- [4.3] P. C. Logofatu, J. R. McNeil, "Sensitivity Analysis of Fitting for Scatterometry", *Proceedings of the SPIE - The International Society for Optical Engineering*, vol.3677, p. 177-83, March 1999.
- [4.4] www.sopra-sa.com

Chapter 5

Sub-100nm Scatterometry

Based on the analysis in the Chapter 4, we can conclude that the Sopra GESP5 is indeed capable of operating in the 100nm-technology node. It has sufficient sensitivity in meeting the CD metrology requirement stipulated in the International Technology Roadmap for Semiconductors.

This sensitivity analysis, however, is not perfect. One limitation is that the profiles used in the simulations were constructed by stacking many rectangular layers of different thicknesses and widths, and as such these profiles have defined edges to them, which might provide a stronger reflected signal than what is otherwise possible with a real-life profile.

5.1 Sub-100nm Technology Node

Having confirmed that scatterometry can indeed be employed successfully in the 100nm-technology node, the final part of this work consists of testing its capabilities in sub-100nm nodes. Figures 5.1 through 5.4 below illustrate the variations in $\tan \Psi$ and $\cos \Delta$ responses in response to CD variation for the various sub-100nm technology profiles. Scatterometry noise analysis was carried out for 70nm and 50nm dense lines, as well as 45nm and 30nm isolated lines, with the results included in the plots of CD variation for these lines.

Figure 5.1 70nm Dense Lines

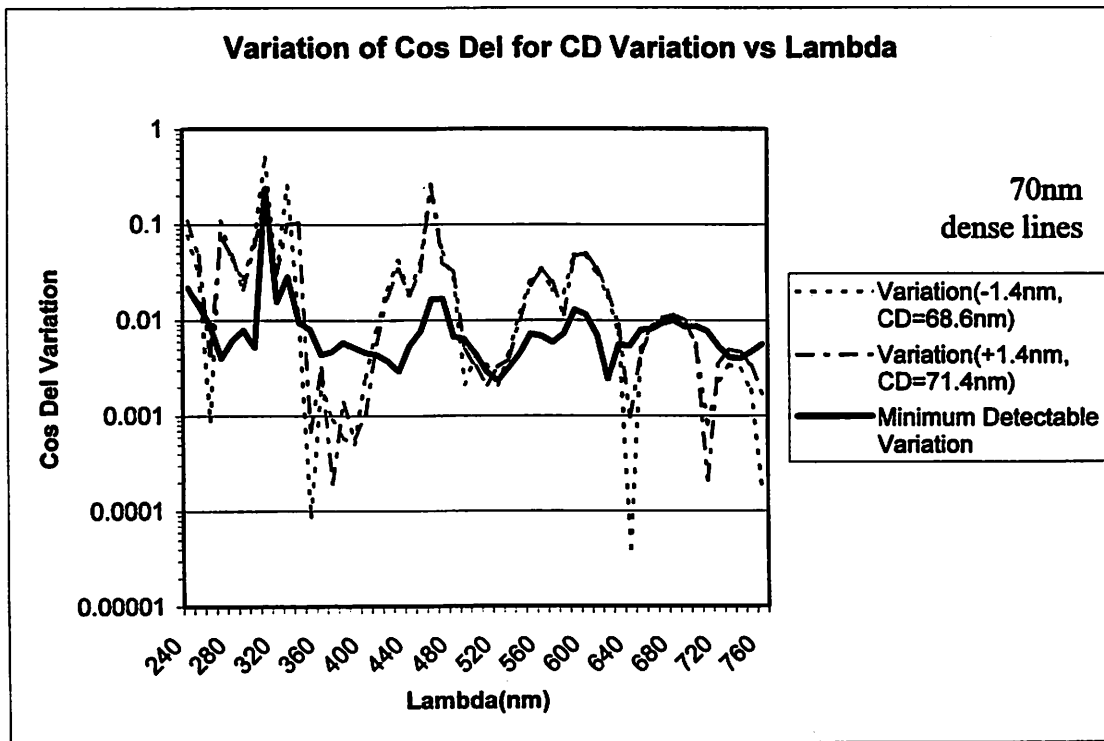
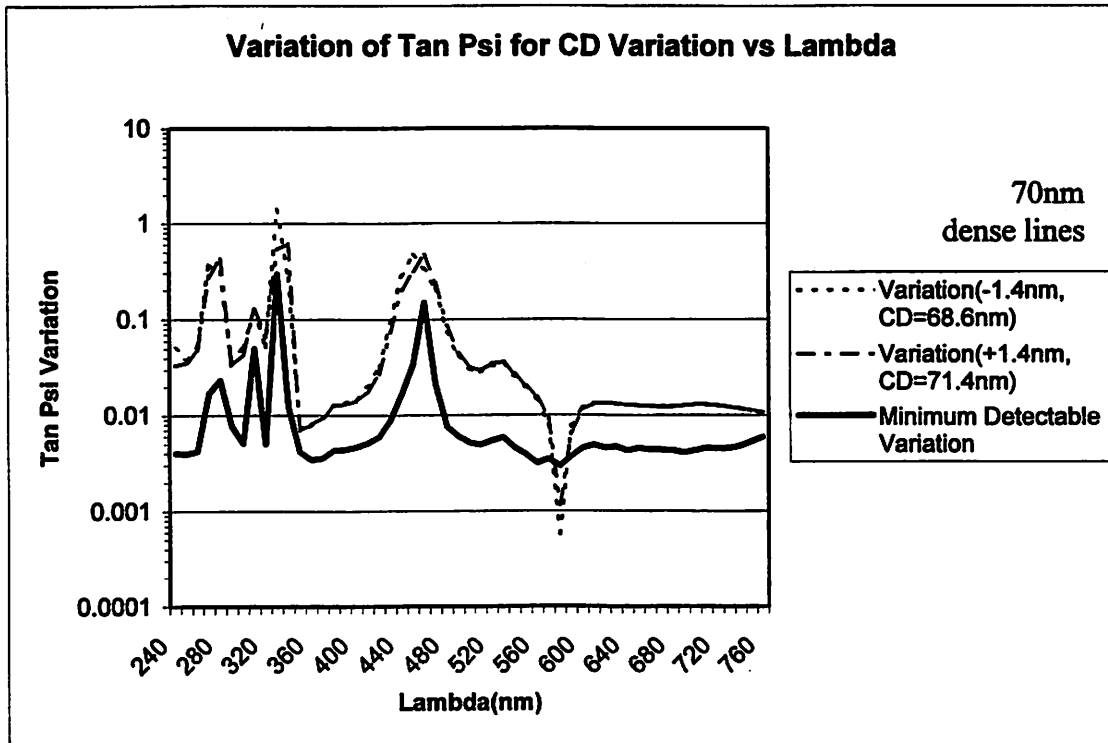


Figure 5.2 50nm Dense Lines

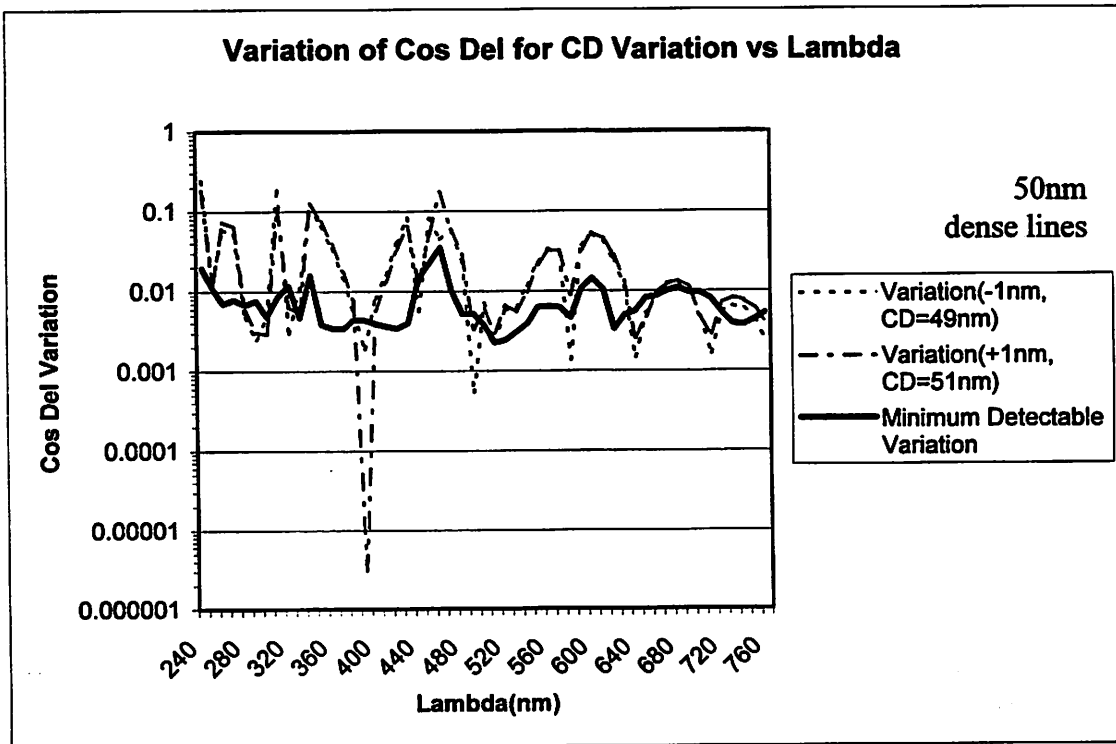
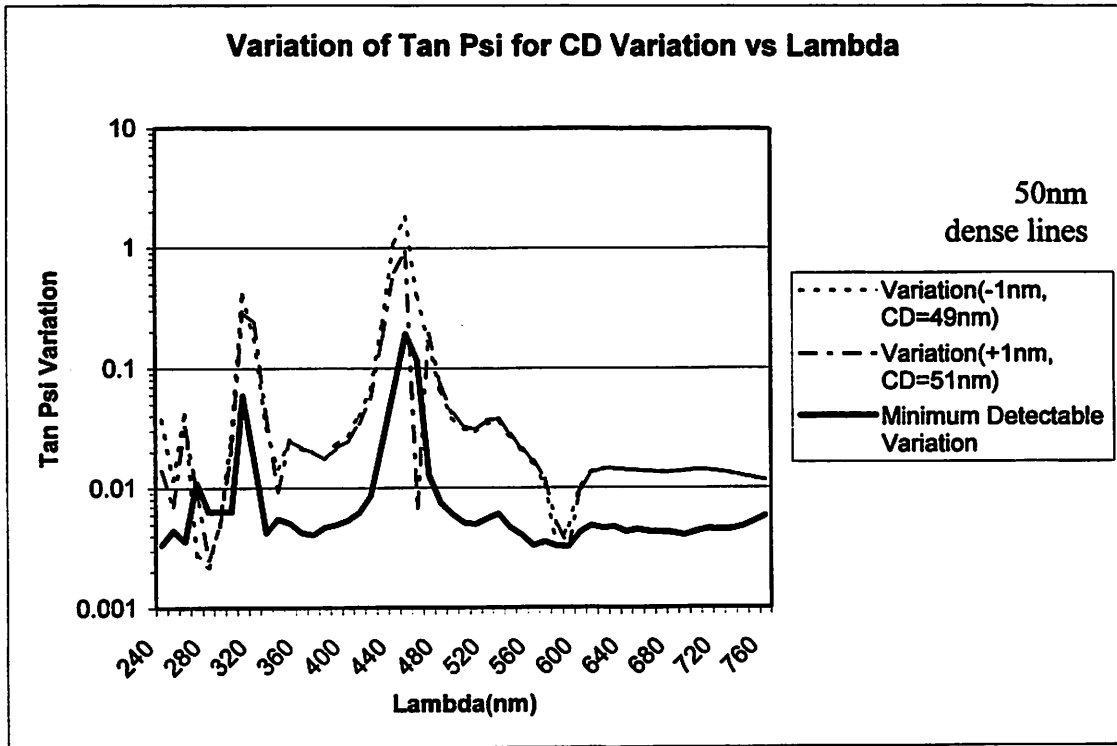


Figure 5.3 45nm Isolated Lines

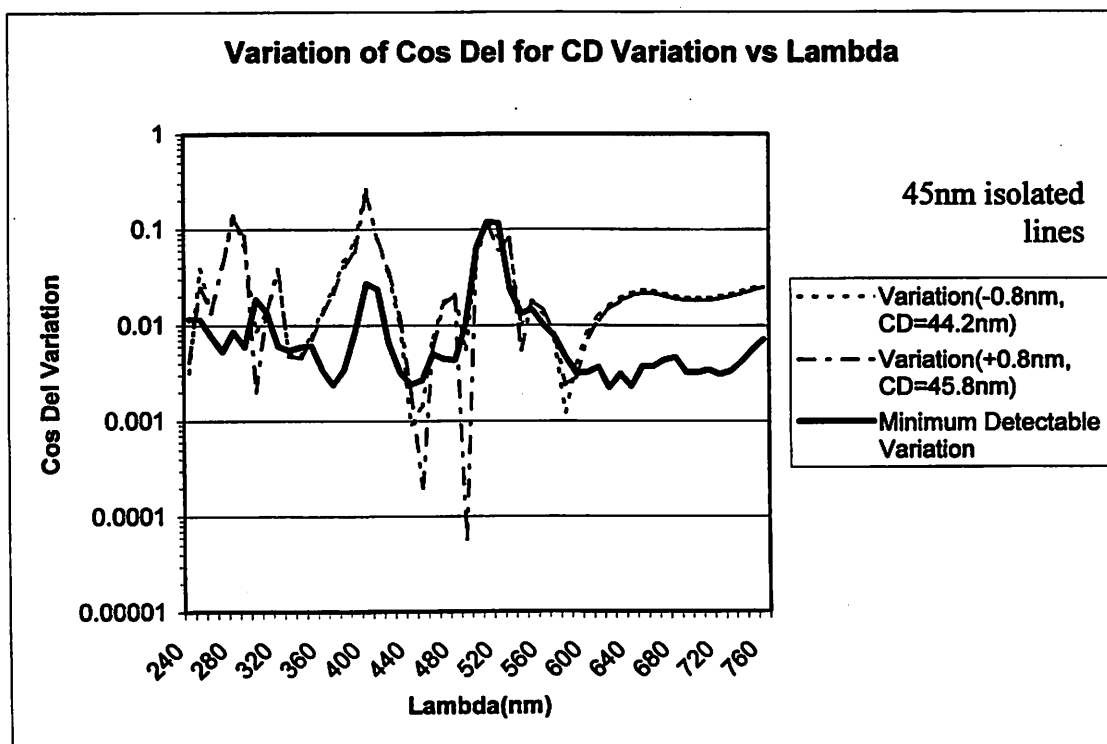
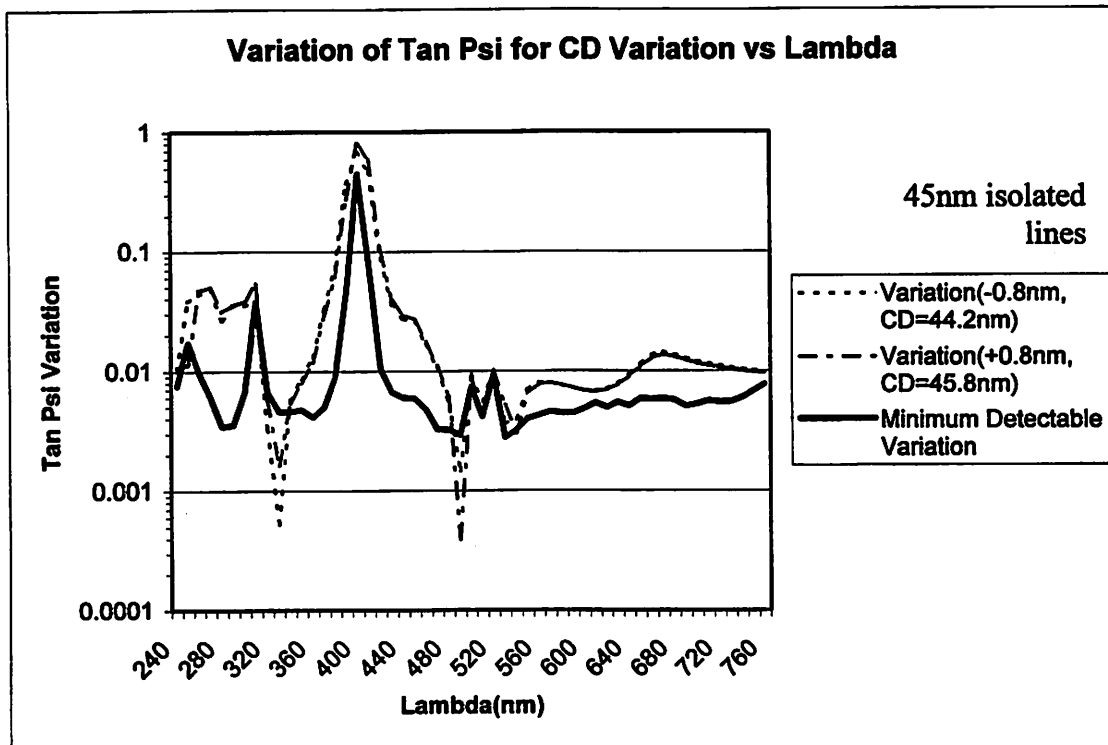
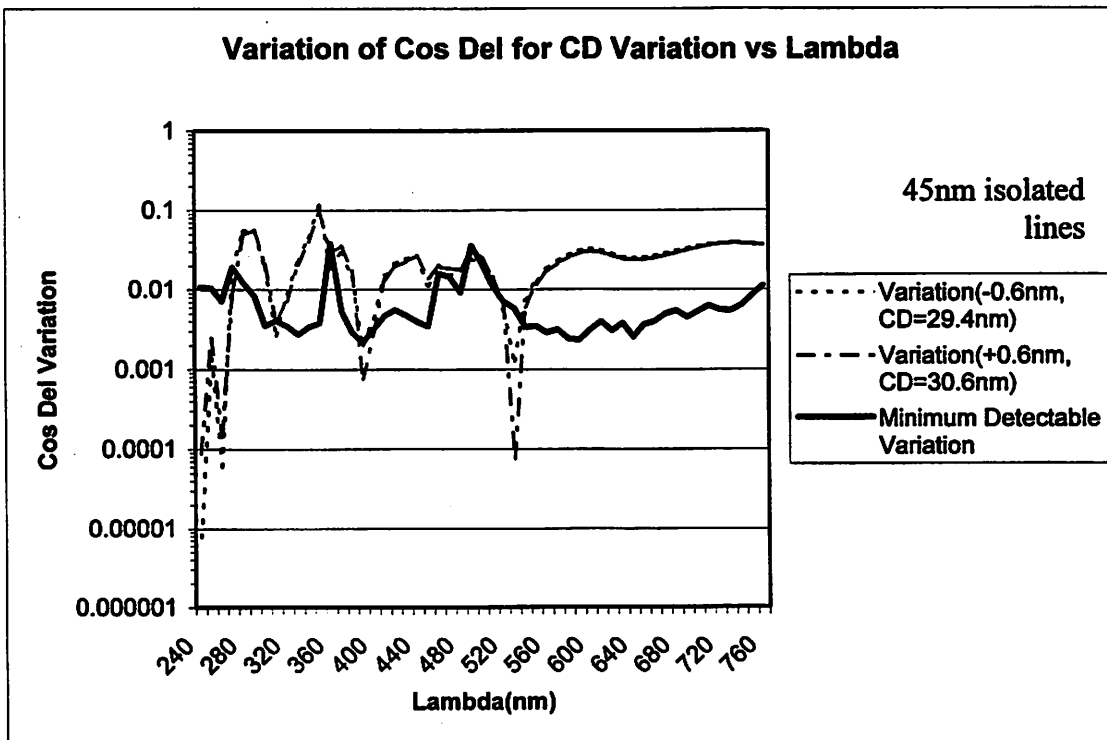
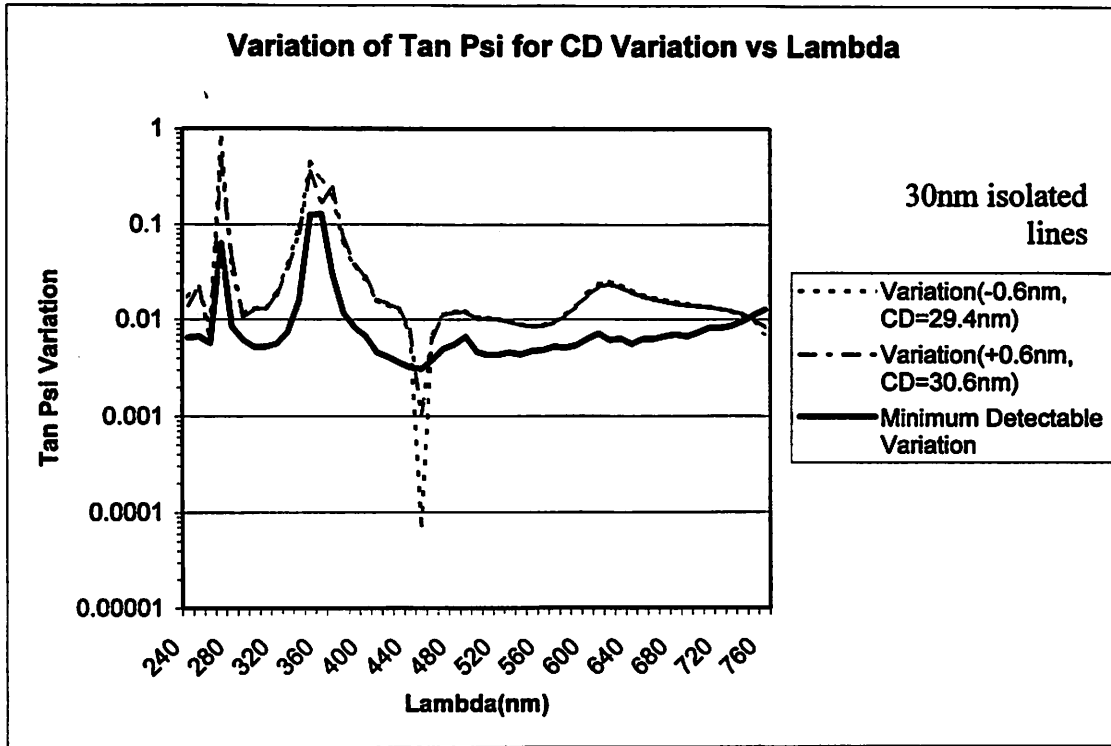


Figure 5.4 30nm Isolated Lines

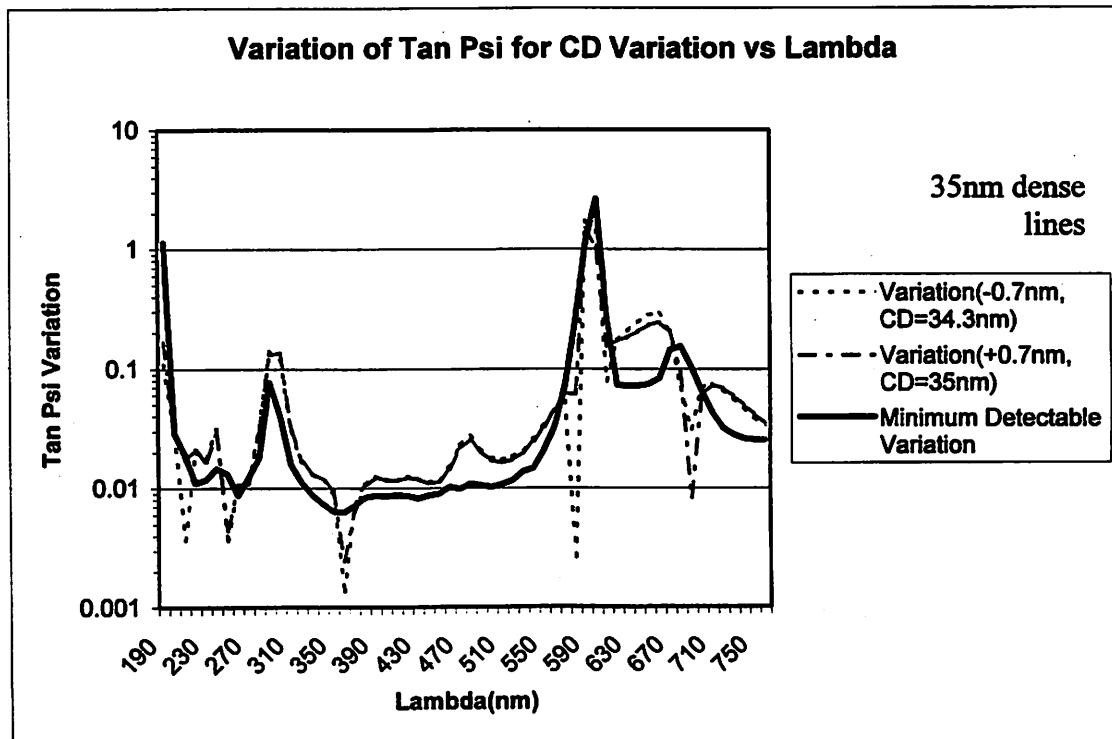


5.2 Sub-240nm Wavelength Analysis

Rayleigh's criterion predicts that as feature sizes decrease, more optical information will be obtained in the shorter wavelength regions. This can be observed from the responses for the 70nm, 50nm, 45nm and 30nm lines.

Additional noise characterization was done for 35nm dense lines as well as 20nm isolated lines. The CD variations for these profiles based on the ITRS roadmap, based on theoretical simulation, will be barely detectable by scatterometry based on current ellipsometer specifications. This section is dedicated to defining specifications required to successfully detect these CD variations. The noise analyses of these profiles are included below.

Figure 5.5 35nm Dense Lines



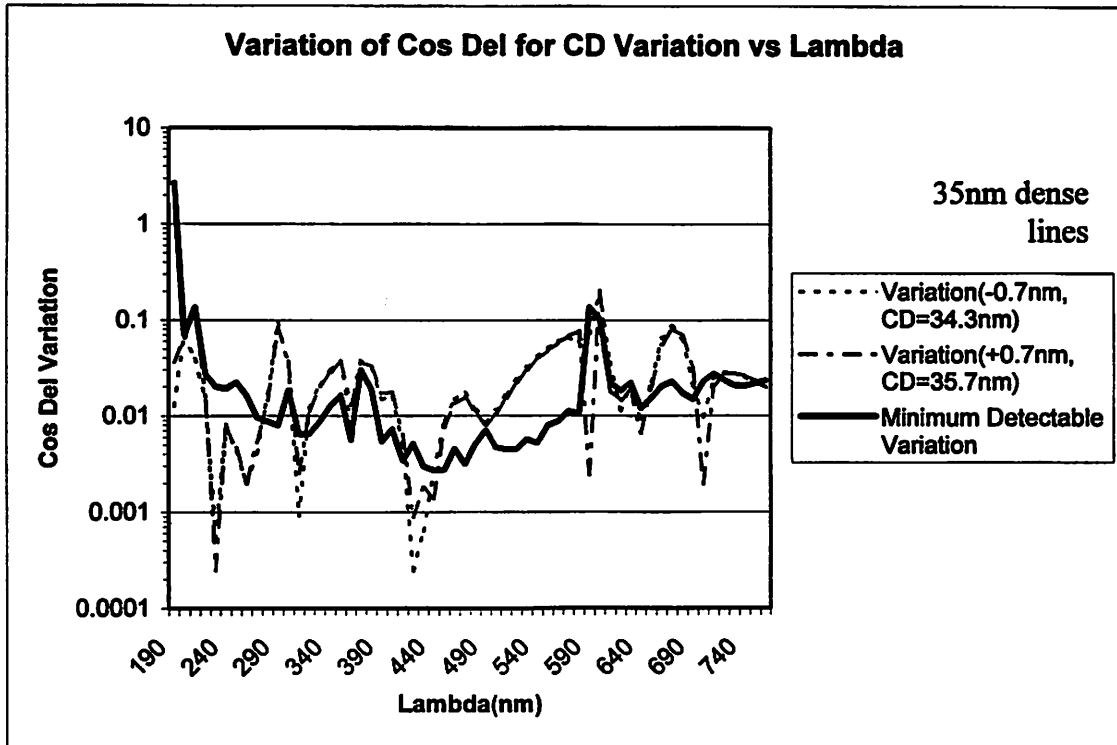
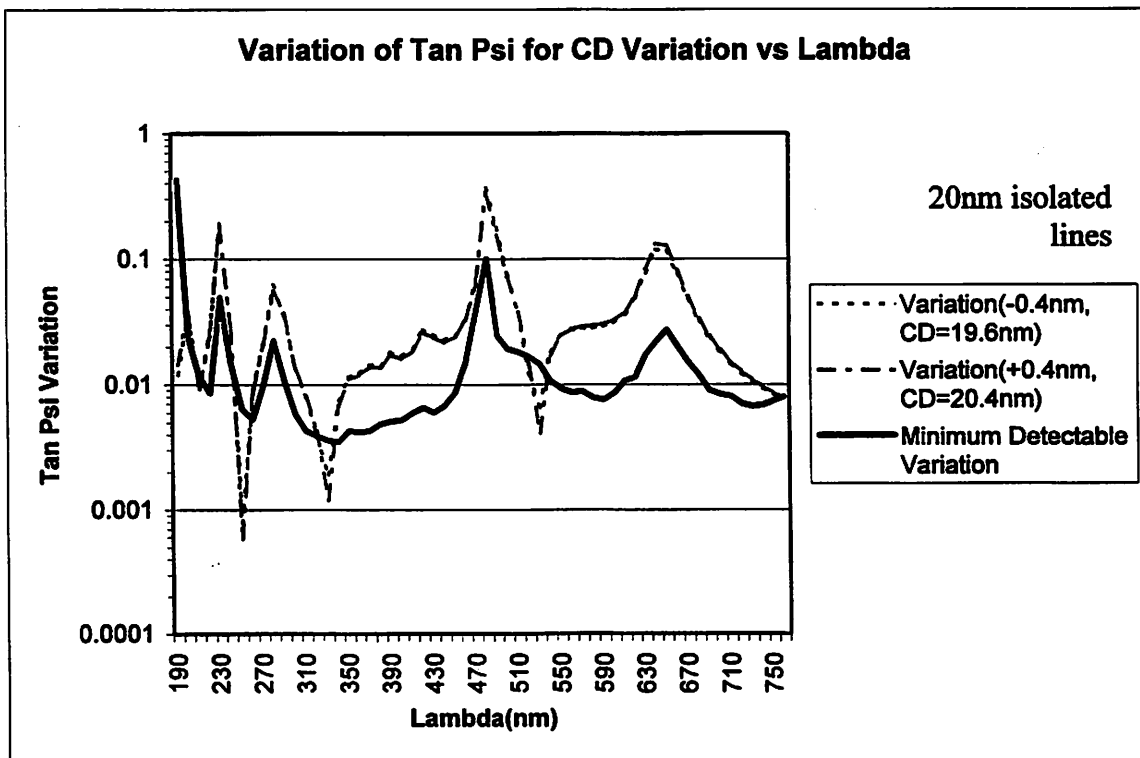
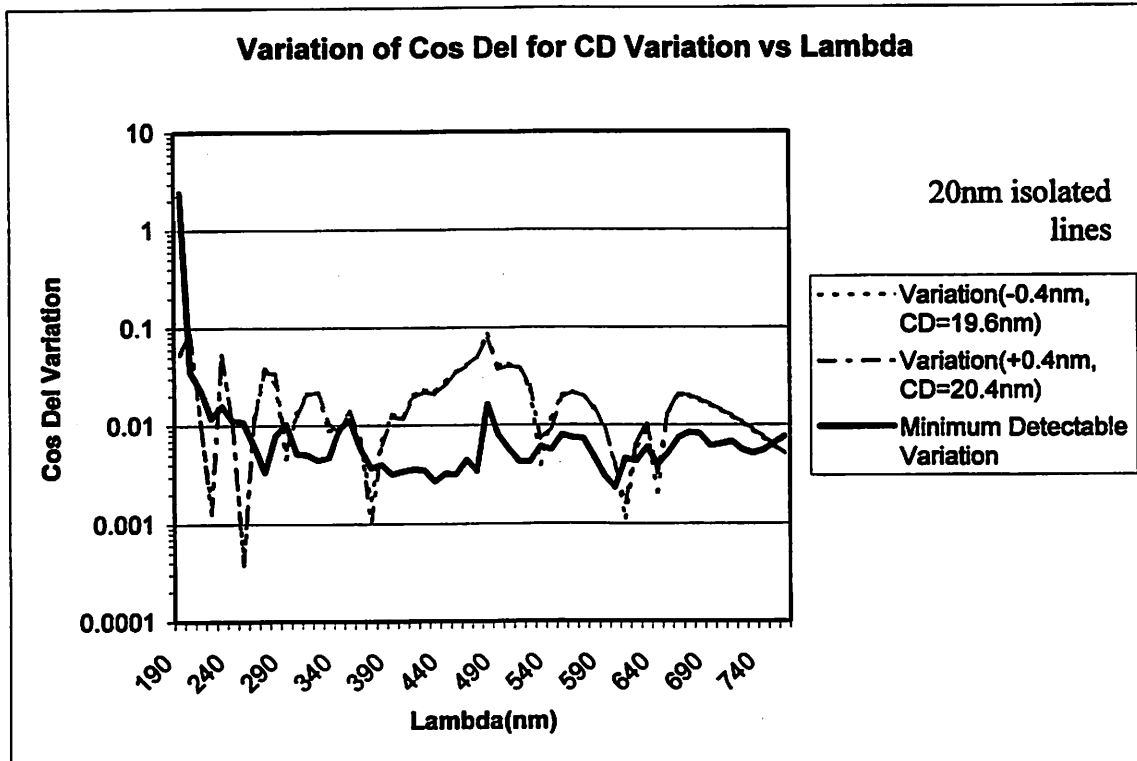


Figure 5.6 20nm Isolated Lines





5.3 Conclusion

In this chapter, we have investigated the ability of scatterometry to operate in the 35nm node. The results are that the CD variations for 35nm dense lines as well as 20nm isolated lines are detectable, but they appear to be approaching the sensitivity limit of scatterometry.

Based on Rayleigh's criterion governing resolution, there is reason to believe that as semiconductor features are scaled down, scatterometric response will move in a similar trend, with more response information being contained in the sub-200nm wavelength region. There is a need to have ellipsometers with high signal-to-noise ratios sufficiently high in this wavelength region to take advantage of the information contained there.

Ellipsometers that operate down to the 157nm wavelength in a purged environment are already available by SOPRA and others.

Secondly, given the complexity of moving parts in an ellipsometric system, there is room for improvement in the precision of the parts. The fact that the variance of $\tan \Psi$ does not decrease significantly with increasing measurement integration time suggests that the angular noise from the analyzer is dominant. As such, motors with more steps per turn could possibly improve the repeatability of measurements and hence the sensitivity of scatterometry.

Future work on this project includes incorporating this information along with other information pertaining to the lithography process in designing and implementing a closed-loop control system. This system will be able to continuously fine-tune the lithography process to produce higher yield and minimize machine downtime.

Chapter 6

Conclusion

6.1 Report Summary

The semiconductor industry is a rapid-moving one, with feature sizes so small that they were once beyond our capabilities, now easily produced. This was best predicted by Gordon Moore, who stated that the logic density of silicon integrated circuits would double approximately every 18 months. Along with this phenomenon, many advances have been made, one of them being the introduction of sophisticated metrology systems, which played a significant role in increasing product yield.

Many different metrology tools have been invented, with the SEM and the AFM being the most prominent tools used for profile metrology to date. However, as device sizes continue to scale down toward the sub-100nm range, new challenges have surfaced due to several reasons. Firstly, tolerance has reduced along with feature size, necessitating metrology tools with higher resolution. Secondly, with the need for more inspections due to lower yield, metrology throughput has become a significant issue. Thirdly, with the complexity of current semiconductor manufacturing processes, wafer destruction for metrology purposes is undesirable.

Scatterometry has recently been proposed to address these issues. In this report, this technique has been explored to determine its ability to operate in the sub-100nm regime. This was conducted in a systematic way, through software simulation using Timbre

Technology's *gtk* engine, hardware experiments with the Sopra GESP5 DUV ellipsometer, as well as quantitative analysis involving Jones' matrices.

The results obtained indicate that scatterometry would indeed be able to operate in the 100, 70 and 50nm technology nodes based on the International Technology Roadmap for Semiconductors.

Possible improvements in ellipsometer specifications have also been discussed in order for scatterometry to be implemented in the sub-35nm nodes.